SELECTIVE FLOCCULATION OF PYRITE AND/OR SILICA IN THE PRESENCE OF COAL

R. Venkatadri, R. Markuszewski, and T. D. Wheelock
Iowa State Mining and Minerals Resources Research Institute
and Chemical Engineering Department
Iowa State University
Ames, Iowa 50011
and
Arden B. Walters
Florida Power & Light Company
Juno Beach, Florida 33408

Abstract

Two cationic surfactants, Arquad T-50 and Duomac T, were investigated as possible selective flocculants or coagulants for iron pyrite or silica particles in the presence of particles of eastern bituminous coal. Although these surfactants were adsorbed by all three materials, they were found to promote the flocculation of pyrite and silica much more than the flocculation of coal when the solid materials were flocculated separately. In subsequent selective flocculation tests involving binary mixtures of the solid components, a good separation of coal and silica was achieved with Duomac T by agitating the flocculating suspension for a prolonged time. However, the separation of coal and pyrite proved more elusive. While some separation was achieved with Arquad T-50 because pyrite was flocculated more extensively than coal, the separation was marginal at best.

Introduction

There is an increasing need for industry to clean ultrafine-size coal, and one of the more promising methods for cleaning such coal is selective flocculation of either the organic material or the mineral matter (1). The principles and various applications of selective flocculation have been reviewed extensively (1-3). Much of the earlier work on this method as well as some of the recent work (4,5) has been based on the use of very long-chain, water-soluble organic polymers which act as bridging flocculants. Examples of such flocculants are polyacrylamide and polyethylene oxide polymers having a molecular weight of 10^6 or more. Recently some success has been achieved with completely hydrophobic, water-insoluble polymers which have a greater affinity for the organic portion of coal than have the water-soluble polymers (6-8). Another class of reagents, which may act as selective flocculants or coagulants, is comprised of ionic surfactants of much lower molecular weight than the polymeric flocculants. When the surfactants are adsorbed, they produce a hydrophobic coating on the coal or mineral particles (2). If the treated particles are brought into very close contact, they can stick together because of hydrophobic interaction. However, since this interaction involves very short-range forces, the effect of longer-range electrostatic repulsive forces may need to be minimized. Achieving rapid flocculation or coagulation of hydrophobic particles smaller than 10 μm in size may require the application of very high shear rates; hence, the term "shear flocculation" has been used to describe such a method (9).

In the work described below an attempt was made to selectively flocculate iron pyrite or silica in the presence of an eastern high volatile bituminous coal by employing a cationic surfactant. Pyrite and silica are two of the most common mineral impurities in coal and their removal has been difficult to achieve when they are finely disseminated. Of the two commercial surfactants selected for this study, Arquad T-50 is an alkyltrimethylammonium chloride in which the alkyl group is derived from tallow, and Duomac T is *N*-tallow derivative of 1,3-propanediamine diacetate. These surfactants were selected because long-chain amines are widely used as selective flotation collectors for quartz and silicate minerals due to their ability to render these materials hydrophobic (10-12). Unfortunately various amines

are also known to be adsorbed by coal, and some have been used as coal flocculants or coagulants (13-16). Therefore, it remained to be seen whether the chosen surfactants would be selective.

In order to see if the flocculants are adsorbed by the different materials, the zeta potential of coal, pyrite, and silica was measured in both the presence and absence of the surfactants. Flocculation tests were conducted with the materials individually using various surfactant concentrations and pH levels. Based on the flocculation characteristics of the individual materials, promising conditions for the selective flocculation of pyrite or silica in the presence of coal were selected and tested.

Experimental

Materials

Materials used in coagulation and flocculation experiments included a specially selected high volatile bituminous coal, iron pyrite, and silica. The coal sample was from the No. 2 gas seam in Raleigh County, West Virginia, and on a dry basis it had a fixed carbon content of 65%, volatile matter content of 33%, ash content of 2-3%, a total sulfur content of 1.0-1.5%, and a pyritic sulfur content of 0.2-0.3%. The coal appeared to be highly hydrophobic and was difficult to wet or disperse in water.

Floated silica powder was obtained from Fisher Scientific Company, and iron pyrite which originated in Huanzala, Peru, was obtained from Ward's Natural Science Establishment. X-ray diffraction analysis showed the silica to be pure quartz with no detectable impurities, and it showed the pyrite to be over 99.5% pure with only traces of silica, calcite, and alumina.

Coarse lumps of coal or pyrite were crushed and then ground. A ball mill containing stainless steel balls was used to grind the pyrite in a dry state. The ground pyrite was analyzed with a Leeds and Northrup Microtrac particle size analyzer which showed that 90% of the material was smaller than 16.6 μm. The coal and silica were ground separately with a high speed impact mill, and the products which passed through a screen with 38 μm openings were used for flocculation.

Arquad T-50 and Duomac T Diacetate were supplied by Armak Chemicals and used as cationic flocculants. Arquad T-50 is a quaternary ammonium compound with the formula $RN(CH_3)_3Cl$ in which R represents alkyl groups of 14 to 18 carbon atoms derived from tallow. Duomac T is an acetic acid salt of an aliphatic diamine and has the formula $RNH(CH_2)_3NH_2 \cdot (HOOCCH_3)_2$ in which R represents alkyl groups of 12 to 18 carbon atoms also derived from tallow. The typical molecular weight of Arquad T-50 is 340 and that of Duomac T is 480. Deionized water having a resistivity of 18 megohm-cm was used in the experimental work; it was prepared by passing steam condensate through a Barnstead NANOpure II deionization system. The pH of the particle suspensions was adjusted by adding either reagent grade ammonium hydroxide or hydrochloric acid.

Methods

A cylindrical Plexiglas vessel having an inside diameter of 6 cm and height of 10 cm was used for coagulation and flocculation tests. The volume of the vessel was 250 ml, and the vessel was fitted with four vertical baffles which projected 0.7 cm into the vessel. An agitator with a variable-speed drive motor and a two-blade impeller having a diameter of 2.8 cm was used for stirring the contents of the vessel.

Flocculation tests were conducted by first dispersing either 1.0 or 2.0 g of material in 200 ml of water. If a single component was to be flocculated, 1.0 g was

used whereas if a two-component mixture was to be flocculated, 2.0 g were used. The slurry was stirred at 1700 rpm for 30 s to obtain a uniform suspension. The pH of the suspension was adjusted with either ammonium hydroxide or hydrochloric acid, and then the particles were redispersed by stirring at 1700 rpm for an additional 10 s. While stirring was continued at 1700 rpm, a dilute solution of the organic flocculant was added rapidly, whereupon the agitator speed was immediately reduced to 300 rpm and stirring was continued for 60 s. After stirring was stopped and the suspension had settled for 60 s, the clear supernatant liquid was decanted, and the remaining solids were recovered by filtration, dried, and weighed to determine the recovery or mass yield of flocculated material.

After treating a two-component mixture by the above procedure, the recovered solids were analyzed to determine the mass recovery of each component. For a coal/pyrite mixture this involved determining the total sulfur content of the flocculated product by means of a Fisher Sulfur Analyzer, and using a sulfur material balance to estimate the distribution of coal and pyrite in the product. For a coal/silica mixture, the ash content of the product was determined and used to estimate the distribution of coal and silica in the product.

For measuring the zeta potential of particles, a concentrated suspension was prepared first by mixing 1 g of material with 50 ml of 0.01 M potassium nitrate and stirring for 1 hr. Twenty drops of the concentrated suspension were subsequently diluted to 100 ml with 0.01 M potassium nitrate. The pH of the suspension was adjusted with either ammonium hydroxide or hydrochloric acid, and the suspension was stirred vigorously for 10 min. If the zeta potential of the material in the presence of a surfactant was to be determined, the requisite amount of surfactant was added and stirring was continued for 1 min. The suspension was allowed to sit overnight without stirring. The particles were resuspended by placing the mixture in an ultrasonic bath and then 20 readings of the zeta potential were made with a Zeta-Meter, system 3.0. The readings were averaged to obtain the reported value. Also the pH of the remaining suspension was redetermined and reported.

The surface of silica was characterized by measuring the induction time or time required for attachment of one or more particles of silica to a small gas bubble when brought into contact. The apparatus and procedure described by Yordan and Yoon (17) were used for this purpose. A short induction time is indicative of a hydrophobic surface, whereas a longer induction time is indicative of a hydrophilic surface.

Results and Discussion

Electrokinetic Properties

The measured zeta potentials of different materials in 0.01 M potassium nitrate are shown as a function of pH in Figure 1. For the bituminous coal the variation in zeta potential with pH was similar in general to that observed for other coals (18-21), and this variation has been attributed to the adsorption of positively charged hydronium ions at low pH and negatively charged hydroxyl ions at high pH (18). The nature of the zeta potential curve for pyrite suggests that the surface of the pyrite was oxidized, since similar curves were reported for oxidized pyrite by others (19,21). The zeta potential curve for unoxidized pyrite was reported to be monotonic with a single isoelectric point between pH 2 and 4. The zeta potential curve for silica was similar to that reported for quartz by Pugh (22).

When the zeta potential of the different materials was determined in a solution containing 20 ppm Arquad T-50, the results shown in Figure 2 were obtained. The large positive values of the zeta potential for coal and silica indicate that surfactant cations were adsorbed strongly by these materials over the pH range from 2 to 10. While results for pyrite were not as dramatic, they still confirm adsorption of the surfactant at both high and low pH where the zeta potential was

reversed because of adsorption. In the pH range from 3 to 10, the zeta potential of pyrite may not have been as high as that of the other materials because of competition for adsorption sites by potassium ions. Since sodium ions are known to be adsorbed by pyrite (23), it is anticipated that potassium ions would be adsorbed as well.

The results in Figure 3 indicate that Duomac T was also adsorbed strongly by the various materials over a wide pH range. The decline in zeta potential of the materials between pH 8 and 10 was probably due to a reduction in the dissociation of the diamine. The dissociation of amines is known to decrease between pH 8 and 10 whereas the dissociation of quaternary ammonium compounds remains high over the entire pH range. This would explain why the zeta potential of the materials declined at high pH in the presence of Duomac T but not in the presence of Arquad T-50.

The zeta potential of silica was found to be greatly affected by the concentration of Duomac T in the suspending medium (see Figure 4). The measurements were made at the natural pH of the suspension and showed that the zeta potential increased markedly as the concentration of Duomac T increased. These results again reflect adsorption of surfactant cations.

Flocculation of Individual Materials

The results of flocculating silica suspensions with different concentrations of Duomac T are presented in Figure 4. The recovery or yield of flocculated product increased with increasing concentrations of Duomac T until a concentration of 3 ppm was employed. At this point the silica recovery was 87% and further increases in flocculant concentration had little effect on the recovery. Interestingly, the zeta potential data for silica in Figure 4 show that silica was close to its isoelectric point when suspended in 3 ppm Duomac T. The correspondence between silica recovery and zeta potential for Duomac T concentrations up to 3 ppm suggest that a charge neutralization mechanism may have accounted for the type of flocculation which took place. On the other hand, when Duomac T concentrations of 20 ppm or more were applied, the zeta potential of silica was so high that electrostatic repulsion would create a formidable barrier to flocculation or coagulation. Nevertheless, a high recovery of silica was achieved which apparently was due to the hydrophobic coating imparted by the surfactant. The hydrophobicity of the treated silica was verified by measuring the induction time of both the treated and untreated material. Thus, the induction time of silica in water was 27.7 ms whereas in 20 ppm Duomac T it was 1.3 ms. This decrease in induction time indicates a large increase in hydrophobicity (17).

The hydrodynamics of the flocculation system may have been such that shear flocculation prevailed, since an increase in agitation time after the surfactant was added produced an increase in silica recovery. Thus with 0.5 ppm Duomac T the recovery increased from 54% for 1 min of agitation to 83% for 5 min of agitation and remained the same for up to 20 min of agitation. This type of behavior is not observed with electrolytic coagulation or polymeric flocculation where the flocs break up with prolonged agitation (9).

The effect of Duomac T concentration on silica recovery is further illustrated by the results presented in Figure 5 which show that the recovery decreased when the concentration was raised above 100 ppm. The same diagram also indicates the effect of Duomac T concentration on the recovery of pyrite and coal when these materials were treated separately at the natural pH of their respective suspensions. The maximum recovery of pyrite was achieved with a surfactant concentration of 20 ppm. Since the recovery of coal never exceeded 10%, little or no flocculation or coagulation of this material took place over the surfactant concentration range of 5 to 80 ppm. The results with coal suggest that adsorption of the surfactant cations may have reduced the hydrophobicity of the coal. This could have occurred if the

hydrophobic tails of the adsorbed cations were directed towards the surface and the hydrophilic head groups were directed away from the surface.

The effect of pH on the recovery of the different materials with 20 ppm Duomac T is shown in Figure 6. Again the materials were treated separately. While the recovery of silica remained high over the entire pH range, the recovery of pyrite was exceptionally large only between pH 4.5 and pH 10 and coal recovery peaked at pH 8-9. The maximum coal recovery was only 53% compared to a maximum recovery of about 90% for the other materials. The results indicated that it might be possible to selectively flocculate either silica or pyrite in the presence of the coal within the pH range from 2 to 6.

Flocculation results achieved when the different materials were flocculated individually with various concentrations of Arquad T-50 are presented in Figure 7. The maximum recovery of silica was obtained with 10-20 ppm Arquad T-50 and the maximum recovery of pyrite with 80 ppm at the natural pH of the suspension. The coal did not appear to be flocculated at any concentration of the surfactant within the range from 10 to 150 ppm.

The effect of pH on the recovery of the materials with 80 ppm Arquad T-50 is indicated by Figure 8. The recovery of silica and pyrite was high above pH 5, and while the recovery of coal never exceeded 25%, the best coal recovery was observed above pH 8. The results indicated that it might be possible to selectively flocculate either silica or pyrite in the presence of coal at pH 5-6.

Flocculation of Binary Mixtures

Mixtures of coal and either pyrite or silica were flocculated using conditions which would favor the selective flocculation of the inorganic material based on the preceding work. In some cases the coal constituted 90% of the mixture by weight whereas in other cases it constituted 50%. The mass recovery or yield of each component which was recovered in the settled material is given in Table 1. The separation efficiency as defined below is also indicated for each test.

$$\text{Separation Eff. (\%)} = \text{Mineral Recovery (\%)} - \text{Coal Recovery (\%)}$$

Although the percentage recovery of pyrite or silica was generally greater than the percentage recovery of coal, the difference in recovery was small so that the separation efficiency was low. The largest separation efficiency for a mixture of pyrite and coal was 26-27% which was achieved with 80 ppm Arquad T-50 at pH 4.6. Also, the highest separation efficiency for a mixture of silica and coal was only 9.7% which was obtained with 10 ppm Arquad T-50 at pH 4.9. Generally the recovery of one component of a binary mixture went hand in hand with the recovery of the other component, suggesting that the two materials underwent a process of mutual coagulation. Furthermore, in the case of silica/coal mixtures it appeared that the overall recovery was controlled by the relative amount of silica present. Thus, when a mixture containing 10% silica was flocculated, the recovery of either silica or coal was only 25-30%, whereas the recovery of each of these was generally over 80% when the initial mixture contained 50% silica. It is unlikely that electrostatic interaction would cause mutual coagulation of the particles since all of the solid components where charged positively in the presence of the cationic surfactants. On the other hand, the coal particles may have been physically entrapped in the pyrite or silica flocs (2). Also, the different solids may have been held together by hydrophobic association.

An interesting result was achieved when the time of agitation was extended after adding Duomac T to a suspension of silica and coal. As the data in Table 2 indicate, the recovery of silica increased while the recovery of coal decreased. Consequently by agitating the suspension for 20 min it was possible to obtain a separation efficiency of over 84%. However, when the same procedure was applied to

Table 1. Results of flocculating binary mixtures of particles with cationic surfactants

Particle mixture		Slurry	Surfactant		Recovery, %		Sepn.
Materials	Ratio	pH	Type	ppm	Mineral	Coal	Eff., %
pyrite/coal	10/90	4.5	Duomac	20	76.0	64.9	11.1
pyrite/coal	50/50	4.5	Duomac	20	87.1	78.9	8.2
pyrite/coal	10/90	5.4	Arquad	10	53.0	36.3	16.7
pyrite/coal	10/90	4.6	Arquad	80	49.7	23.4	26.3
pyrite/coal	50/50	4.6	Arquad	80	54.9	28.1	26.8
pyrite/coal	50/50	6.0	Arquad	10	82.8	73.2	9.6
pyrite/coal	50/50	9.4	Arquad	10	82.0	78.0	4.0
silica/coal	10/90	4.5	Duomac	20	31.5	32.0	-0.5
silica/coal	10/90	1.5	Duomac	20	25.1	29.3	-4.2
silica/coal	50/50	1.5	Duomac	20	83.8	87.6	-4.8
silica/coal	50/50	4.9	Arquad	10	88.3	78.6	9.7
silica/coal	50/50	9.6	Arquad	10	76.0	72.8	3.2
silica/coal	50/50	6.0	Arquad	80	86.3	81.5	4.8
silica/coal	10/90	6.0	Arquad	80	29.6	25.5	4.1

Table 2. Results of flocculating binary mixtures of particles at pH 4-5 with 20 ppm Duomac T

Particle mixture		Agitation	Recovery, %		Sepn.
Materials	Ratio	time, min.	Mineral	Coal	Eff., %
silica/coal	50/50	1	80.0	79.1	0.9
silica/coal	50/50	5	98.8	45.2	53.6
silica/coal	50/50	20	95.7	11.3	84.4
pyrite/coal	50/50	1	87.1	78.9	8.2
pyrite/coal	50/50	5	92.0	82.0	10.0
pyrite/coal	50/50	20	80.2	75.7	4.5

a suspension of pyrite and coal, no benefit was realized. Apparently the interaction between coal and silica particles was weaker than that between coal and pyrite particles. Further work is needed to explain these divergent results and to see whether the method can be extended to the separation of clay or shale and coal.

Conclusions

Two cationic surfactants, Arquad T-50 and Duomac T, were found to strongly promote the flocculation or coagulation of iron pyrite and silica particles while showing only a moderate tendency to promote the flocculation of an eastern bituminous coal. Selective flocculation tests showed that it is possible to achieve a good separation of coal and silica with Duomac T providing the particle suspension is agitated for a prolonged time after introducing the surfactant. However, an

extended treatment time did not benefit the separation of coal and pyrite, and the separation of these materials proved more elusive.

By observing the effect on the zeta potential it was shown that the surfactants were adsorbed by all three solid materials. Adsorption of Duomac T by silica greatly increased the hydrophobicity of this solid as indicated by a corresponding decrease in measured induction time. While charge neutralization could account for coagulation of silica in the presence of small concentrations of Duomac T, it is likely that in the presence of high concentrations hydrophobic interaction between particles plays a leading role in flocculation. The increased silica recovery achieved by prolonging the time of agitation is indicative of shear flocculation of hydrophobic particles. Further research is needed to account for the interaction between coal and silica or between coal and pyrite in the presence of the surfactants.

Acknowledgments

This work was performed for the Iowa State Mining and Mineral Resources Research Institute through funds provided by the Florida Power and Light Company. The laboratory assistance of Mr. D. A. Clark is gratefully acknowledged.

Literature Cited

1. S. V. Krishnan, "Selective Flocculation of Fine Coal", in: Fine Coal Processing, S. K. Mishra and R. R. Klimpel (eds.), Noyes Publications, Park Ridge, New Jersey, 1987, pp. 160-178.

2. J. A. Kitchener, "Flocculation in Mineral Processing", in: The Scientific Basis of Flocculation, K. J. Ives (ed.), Sijthoff & Noordhoff, Aphen aan den Rijn, The Netherlands, 1978, pp. 283-328.

3. Shaning Yu and Y. A. Attia, "Review of Selective Flocculation in Mineral Separations", in: Flocculation in Biotechnology and Separation Systems, Y. A. Attia (ed.), Elsevier, Amsterdam, 1987, pp. 601-637.

4. L. Spencer and G. F. Brookes, "Polyacrylamides and Selective Flocculation of Coal/Shale Mixtures", Coal Preparation, 4, 133-159 (1987).

5. G. Barbery and P. Dauphin, "Selective Flocculation of Coal Fines", in: Flocculation in Biotechnology and Separation Systems, Y. A. Attia (ed.), Elsevier, Amsterdam, 1987, pp. 535-546.

6. Y. A. Attia, "Cleaning and Desulfurization of Coal Suspensions by Selective Flocculation", in: Processing and Utilization of High Sulfur Coals, Y. A. Attia (ed.), Elsevier, Amsterdam, 1985, pp. 267-285.

7. Y. A. Attia, Shaning Yu, and S. Vecci, "Selective Flocculation Cleaning of Upper Freeport Coal with a Totally Hydrophobic Polymeric Flocculant", in: Flocculation in Biotechnology and Separation Systems, Y. A. Attia (ed.), Elsvier, Amsterdam, 1987, pp. 547-564.

8. L. Spencer, S. Thompson, and G. F. Brookes, "Hydrophobic Polymers in Coal Preparation", Proceedings of International Symposium on Innovative Plant and Processes for Minerals Engineering, Doncaster, UK, March 31-April 2, 1987, (The Minerals Engineering Society), pp. 173-193.

9. L. J. Warren, "Shear Flocculation", Chemtech, 11, 180-185 (1981).

10. J. Leja, Surface Chemistry of Froth Flotation, Plenum Press, New York, 1982.

11. R. W. Smith and S. Akhtar, "Cationic Flotation of Oxides and Silicates", in: Flotation, A. M. Gaudin Memorial Volume, Vol. 1, M. C. Fuerstenau (ed.), AIME, New York, 1976, pp. 87-116.

12. A. Bleier, E. D. Goddard, and R. D. Kulkarni, "The Structural Effects of Amine Collectors on the Flotation of Quartz", in: Flotation, A. M. Gaudin Memorial Volume, Vol. 1, M. C. Fuerstenau (ed.), AIME, New York, 1976, pp. 117-147.

13. P. J. Bethel and G. F. Brookes, "Reversibility of Long-chain Alkyl Amine Adsorption at the Coal Surface", Transactions of the Institution of Mining and Metallurgy, Sec. C, 86, C164-C165 (1977).

14. N. J. Miles, "Amines and their Applicability to Coal Flotation", Ph.D. Thesis, University of Nottingham, Nottingham, England, 1983.

15. G. F. Brookes and P. J. Bethel, "Zeta Potential, Contact Angle and the Use of Amines in the Chemical Dewatering of Froth-Floated Coal", Powder Technology, 40, 207-214 (1984).

16. J. R. Field, "Some Development Associated with Flocculants during the Last Decade", Coal Preparation, 4, 79-107 (1987).

17. J. L. Yordan and R. H. Yoon, "Induction Time Measurements for the Quartz-amine Flotation System", Preprint No. 86-105 for SME Annual Meeting, New Orleans, LA, March 2-6, 1986.

18. J. A. L. Campbell and S. C. Sun, "Bituminous Coal Electrokinetics", Transactions of the Society of Mining Engineers of AIME, 247, 111-122 (1970).

19. W. W. Wen and S. C. Sun, "An Electrokinetic Study on the Oil Flotation of Oxidized Coal", Separation Science and Technology, 16, 1491-1521 (1981).

20. D. W. Fuerstenau, J. M. Rosenbaum, and J. Laskowski, "Effect of Surface Functional Groups on the Flotation of Coal", Colloids and Surfaces, 8, 153-173 (1983).

21. S. Kelebek, T. Salman, and G. W. Smith, "An Electrokinetic Study of Three Coals", Canadian Metallurgical Quarterly, 21(2), 205-209 (1982).

22. R. J. Pugh, "Selective Coagulation in Quartz-Hematite and Quartz-Rutile Suspensions", Colloid & Polymer Science, 252, 400-406 (1974).

23. A. M. Gaudin and W. D. Charles, "Adsorption of Calcium and Sodium on Pyrite", Transactions AIME, 196, 195-200 (1953).

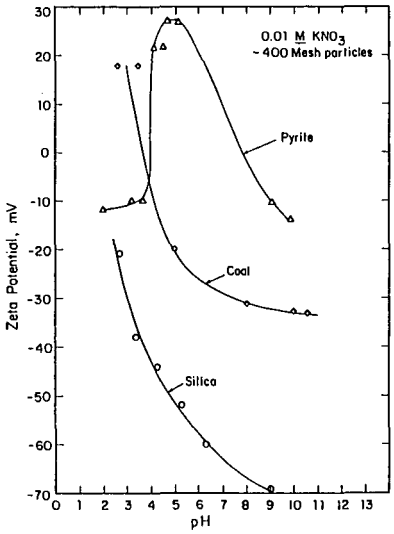

Figure 1. Zeta potential of coal, pyrite, and silica.

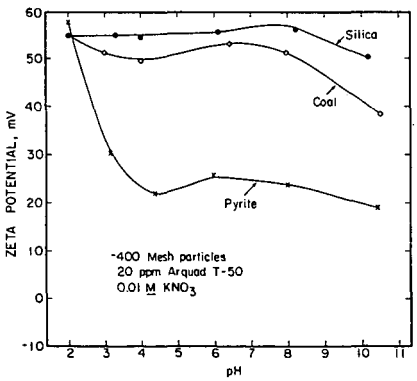

Figure 2. Zeta potential of different materials in the presence of Arquad T-50.

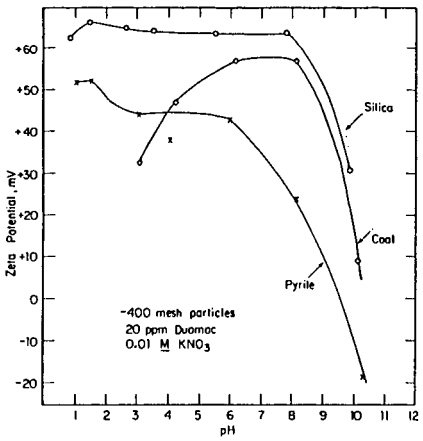

Figure 3. Zeta potential of different materials in the presence of Duomac T.

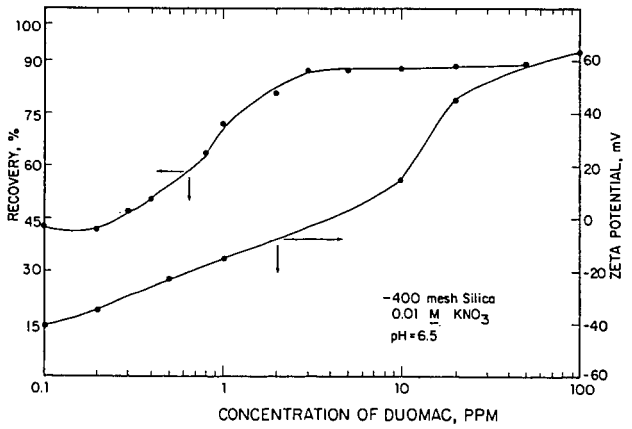

Figure 4. Effect of Duomac T concentration on the zeta potential and recovery of silica.

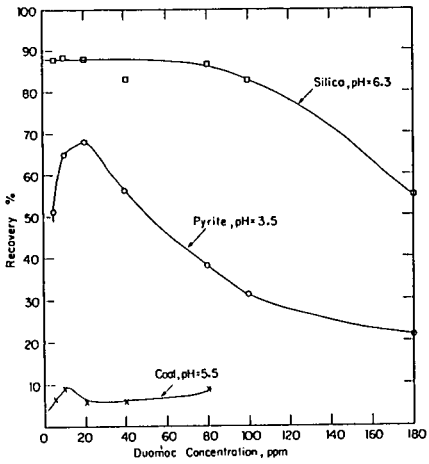

Figure 5. Effect of Duomac T concentration on the flocculation recovery.

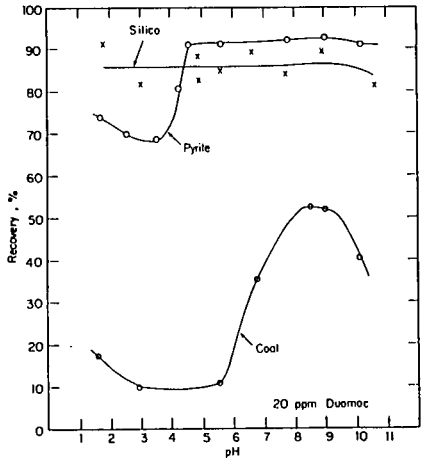

Figure 6. Effect of pH on the recovery of different materials with Duomac T.

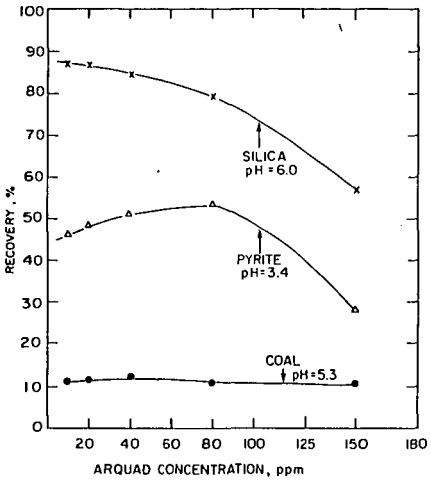

Figure 7. Effect of Arquad T-50 concentration on the flocculation recovery.

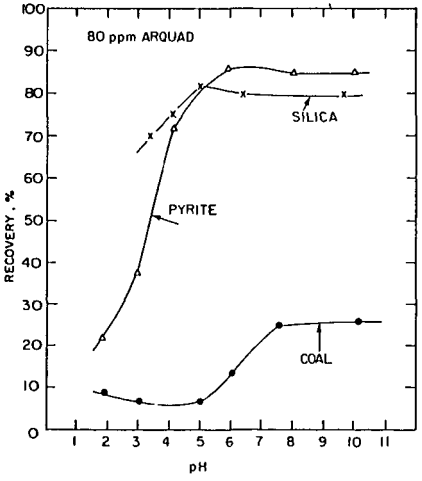

Figure 8. Effect of pH on the recovery of different materials with Arquad T-50.

The Effects of Advanced Physical Coal Cleaning on Mineral Matter and Ash Composition and its Relationship to Boiler Slagging and Fouling Potential

P. J. DeMaris, R. B. Read, and L. R. Camp

Illinois State Geological Survey
615 East Peabody Drive
Champaign, IL 61820

INTRODUCTION

Recent progress in cleaning medium to high-sulfur coals from the Illinois Basin by advanced flotation methods (Read et al., 1987a) has led to the need to evaluate changes in the ash fusion temperatures of deep cleaned coal. Because the alumina- and silica-rich clay minerals and coarse pyrite are more easily removed during coal cleaning than finely disseminated pyrite, it is believed that deeply cleaned coal products may have lower ash fusion temperatures because of altered composition of the remaining ash.

To investigate this question a suite of six coals, cleaned to various degrees, were analyzed for ash chemistry (ASTM method on 750°C Ash), ash fusion temperatures, petrographic variation and mineralogic composition. The samples include the two major mined seams in the Illinois Basin, the Herrin (No. 6) and Springfield (No. 5) Coal Members, as well as the widely used Pittsburgh seam. In this abbreviated paper results for ash chemistry and ash fusion analysis are reported and evaluated.

The coals tested contain a variety of minerals. For a run-of-mine (ROM) or channel sample the typical mineral suite listed in decreasing abundance order is: various clay minerals (kaolinite, illite and expandables), pyrite/marcasite, quartz, calcite and other minerals.

As these coals are cleaned certain components are more easily removed, such as the free clay and quartz (largely from floor and roof materials) and coarse pyrite/marcasite and calcite from the coal seam. While some of the mineral matter can be liberated with minimum crushing and removed by gravity separation without significant Btu loss, the finely dispersed (framboidal) pyrite requires extensive grinding to achieve significant liberation levels (Read et al., 1987B)

Ash minerals remaining in the flotation concentrates are predominantly clay, quartz, and pyrite/marcasite, with only traces of calcite remaining. Ash values for the six samples examined at various stages of cleaning are shown in Table 1. Particle size for the wet tabling step was 6M x 0. The table concentrate was ground to 80% passing 400M for the flotation step. Grinding time was 5 minutes in a stirred ball mill; mean particle size fell between 15 and 20 μm based on particle size analysis. Flotation was not optimized for ash rejection, but was maintained at acceptable (>75%) Btu recoveries.

ASH FUSION TEMPERATURES AND ANALYSIS

Coal cleaning causes significant changes in ash fusion temperature (Table 1). Taking first the changes from the ROM sample to the tabled samples, most temperatures under reducing condition stayed the same or dropped slightly (most less than 50°C) with the largest changes in the initial deformation temperature (IDT) and lesser changes through the fluid temperature (FT). Exceptions to this were the Herrin-SC1 where the IDT dropped 75°, and the Herrin-SW where the FT dropped 75°.

From the ROM sample to tabled sample most temperatures under oxidizing conditions changed only slightly, dropping by less than 50°F; largest changes generally occurred in the FT (Table 1). Exceptions to this are the Springfield-SE sample where the FT increased 60°F and the Herrin-SW samples where the FT increased 115°F.

Examination of the changes between ROM samples and the flotation concentrates points to a wider variation. In general, the reducing temperature increased for the Springfield-SE, but decreased for the three Herrin samples. The Herrin sample with the largest drop (210°F) was the Herrin-SC2. Changes between ROM and flotation concentrate samples in a reducing environment varied considerably; for the Springfield-SE from +45°F to +95°F, for the Herrin-SC1 sample little change (+35°F to -30°F), and for Herrin-SC2 and Herrin-SW significant drops (-65°F to -205°F and +30°F to -180°F, respectively).

For the two samples received as preparation plant products (Herrin-SC3 and Pittsburgh) the flotation concentrate generally had low to moderate increases in ash fusion temperature. Under reducing conditions the Herrin-SC3 increased from +130°F for the IDT to +80°F for the FT. Similarly, the Pittsburgh coal increased 60°F for the IDT and +35°F for the FT. Under oxidizing conditions the IDT for the Herrin-SC3 was increased 210°F while the FT went up only 30°F. The Pittsburgh sample under oxidizing conditions was hardly changed; the IDT was decreased by 5°F and the FT increased 50°F.

No consistent patterns in the changes of ash fusion temperatures emerged from this data, and it was anticipated that chemistry of the ash would also be needed to gain understanding of the variations. Using the work of Winegartner and Rhodes (1975) as a model, statistical correlation analysis for 16 cases was peformed. Significant correlations between a set of variables including various oxide abundance data and derived ratios (See Table 3 for equations) and various ash fusion temperatures and temperature ranges, significant at the 99% confidence level, are reported in Table 2.

For the prediction of reducing ash fusion temperature (reducing), factors involving CaO and base % plus indices involving SiO_2 and Al_2O_3 values had high correlation coefficients (Table 2; Table 3). Best predictors for the initial deformation temperature were FeO*CaO ($r = -.91$) and the R-250 ratio ($r = .90$). Best predictors of the softening temperature were the slagging factor ($r = -.88$) and FeO*CaO ($r = -.78$). Likewise, the best predictors of the hemispherical temperature were the slagging factor ($r = -.91$) and FeO*CaO ($r = -.81$). The fluid temperature was best predicted by the slagging factor ($r = -.91$) and CaO ($r = -.81$). The temperature spread between IT and FT in reducing conditions was less strongly correlated with these variables; the highest correlation ($r = -.84$) was with FeO*Al_2O_3. In general, the slagging factor was the strongest single variable, and it has an inverse relationship with the ash fusion temperature. The second strongest variable for prediction of these ash fusion temperatures is FeO*CaO and it also varies in inverse relationship with the temperature.

The prediction of ash fusion temperature under oxidizing conditions is not as clear cut as those found for the reducing temperatures. The correlation coefficients are generally lower, indicating less precise matches of variation. Best predictors of initial deformation temp. were the base/acid ratio and % base, both inversely correlated ($r = -.72$). Best predictors of the softening temperature are the slagging factor ($r = -.75$) and the base/acid ratio ($r = -.68$). The hemispherical temperature was best predicted by the slagging factor ($r = -.78$) and the Al_2O_3 value ($r = .70$). The fluid temperature was best predicted by the slagging factor ($r = -.80$) and the FeO*CaO value ($r = -.68$). The temperature spread between IT and FT in oxidizing conditions is not well predicted by any of the variables; signifi-

cant but weak positive correlations exist only with the fouling factor (r = .60) and the MgO value (r =.57).

Discussion and Conclusions

In comparing these correlation coefficients to the discussion of coefficients reported in Winegartner and Rhodes (1975) for their eastern data set (which was dominated by Herrin Coal samples) many similarities exist. CaO, % base and the base/acid ratio generally had strong negative correlations with both the reducing and oxidizing ash fusion temperatures in the two studies. The dolomite ratio had a strong correlation (-.72) in our study only with the reducing temperature spread, not with both reducing and oxidizing temperatures as they found.

Winegartner and Rhodes (1975) expected to find FeO well correlated with ash fusion temperature, but were disappointed. In contrast, in our data set FeO*CaO had strong negative correlations with both reducing and oxidizing temperatures, and FeO was also correlated with the initial deformation temperature under reducing conditions. In our data set Al_2O_3 was positively correlated with the ST, HT and FT but not with the RT (Table 2).

Silica ratio values for these 16 samples varied between .76 and .89 and this suggests that high viscosity slags (400 poise) would be produced by this ash (Gibbs and Hill, Inc. 1978). In 4 of 6 cases the flotation concentrates had lower silica ratios than parent feeds, suggesting higher slag viscosities would result. Base/acid ratios for these coals all fell in the 0.13 to 0.28 range, making these coals suitable for dry-bottom furnaces, but unsuitable for slag-tap furnaces.

Analysis of this data set is continuing. We have presented only empirical data on a limited set of coals; broadening of the sample set and running actual combustion tests on selected samples would be most useful.

Bibliography

Gibbs and Hill, Inc., 1978. Coal Preparation for Combustion and Conversion. EPRI Final Report AF-791 Electric Power Research Institute

Harvey et al., 1983. Mineral Matter and Trace Elements in the Herrin and Springfield Coal, Illinois Basin Coal Field. ISGS Contract/Grant Report 1983-4. 162 pp.

Read et al., 1987A Advanced Physical Fine Coal Cleaning: Developments in Pyritic Sulfur and Ash Reduction of Illinois Coal by ISGS Aggregate Flotation in "Processing and Utilization of High Sulfur Coals II". Y. P. Chugh and R. D. Caudle, Eds., pp. 83-93.

Read et al., 1987B The ISGS Aggregate Flotation Fine Coal Cleaning Process, Part A: Development, Characterization and Testing. Final Technical Report to Illinois Coal Development Board, 58 pp.

Winegartner, E. C. and B. T. Rhodes 1975. "An Empirical Study of the Relation of Chemical Properties to Ash Fusion Temperatures". ASME Journal of Engineering for Power . v 97. pp. 395-404.

Table 1. Changes in Ash Fusion Temperatures as a Function of Progressive Ash Reduction

Coal	Condition*	Reducing (°F)**				Oxidizing (°F)**				750°C Ash (wt.%)
		IDT	ST	HT	FT	IDT	ST	HT	FT	
Springfield-SE	ROM	1985	2095	2205	2330	2325	2395	2455	2515	30.8
	Tabled	1970	2150	2250	2350	2295	2385	2485	2575	12.0
	AF Conc	2040	2245	2360	2475	2370	2455	2525	2610	7.3
Herrin-SC1	ROM	2325	2445	2565	2690	2475	2565	2660	2700+	27.7
	Tabled	2250	2390	2520	2655	2480	2550	2620	2670	10.4
	AF Conc	2230	2420	2520	2620	2510	2575	2630	2700+	5.4
Herrin-SC2	ROM	2220	2335	2440	2555	2340	2510	2590	2665	25.5
	Tabled	2210	2330	2440	2550	2365	2465	2560	2665	8.7
	AF Conc	2010	2210	2330	2550	2135	2365	2490	2600	2.5
Herrin-SC3	PPP	2040	2220	2350	2480	2305	2450	2530	2615	5.5
	AF Conc.	2170	2365	2460	2560	2515	2555	2605	2645	4.8
Herrin-SW	ROM	2020	2165	2305	2470	2285	2355	2425	2515	38.6
	Tabled	2045	2140	2270	2395	2285	2370	2460	2630	17.0
	AF Conc	1970	2125	2260	2395	2105	2345	2445	2545	6.4
Pittsburgh	PPP	2015	2345	2445	2550	2490	2550	2610	2650	6.5
	AF Conc	2075	2375	2480	2585	2485	2560	2615	2700+	3.8

* ROM = run of mine; PPP = prep. plant product; AF conc = Aggregate Flotation concentrate
** IDT = intial deformation temp; ST = softening temp.; HT = hemispherical temp.; FT = fluid temp.

Table 2 Correlation matrix of most significant coefficients

Ash Variables	Reducing Temp. (°F) IDT	ST	HT	FT	Temp. Spread	Oxidizing Temp. (°F) IDT	ST	HT	FT	Temp. Sread
SiO_2					-.73					
Al_2O_3		.67	.65	.67			.67	.70	.68	
FeO	-.73				.74					
CaO		-.76	-.79	-.81			-.66	-.66	-.67	
MgO						-.60				.57
K_2O										
Na_2O										
TiO_2										
FeO*SiO_2	-.78				.68					
FeO*Al_2O_3					.84	-.61				
FeO*CaO	-.91	-.78	-.81	-.79		-.72	-.65	-.67	-.68	
% Base	-.87	-.75	-.76	-.68		-.72	-.67	-.67	-.64	
Base/Acid	-.86	-.74	-.76	-.67		.57	-.68	-.67	-.64	
Silica ratio	.86	.61	.64	.58						
Dolomite r.					-.72					
R-250 ratio	.90	.67	.70	.66		.59		.58		
B & W - SF	-.75	-.88	-.91	-.91		-.62	-.75	-.78	-.80	
B & W - FF						.58				.60

* Spread is FT minus IT in °F.

Table 3 Equations for indices*

1.	$FeO*SiO_2$	=	$(FeO)(SiO_2)$
2.	$FeO*Al_2O_3$	=	$(FeO)(Al_2O_3)$
3.	FeO*CaO	=	(FeO)(CaO)
4.	% base	=	Sum of FeO, CaO, MgO, K_2O and Na_2O
5.	Base/acid ratio	=	$\frac{\%\ Base}{100 - \%\ Base}$
6.	Silica value	=	$\frac{SiO_2}{SiO_2 + FeO + CaO + MgO}$
7.	Dolomite ratio	=	$\frac{CaO + MgO}{FeO + CaO + MgO + K_2O + Na_2O}$
8.	R-250 value	=	$\frac{SiO_2 + Al_2O_3}{SiO_2 + Al_2O_3 + FeO + CaO}$
9.	Babcock-Wilcox Slagging Factor	=	$\frac{Na_2O + K_2O + Fe_2O_3 + CaO + MgO}{SiO_2 + Al_2O_3 + TiO_2} \times TS\%$
10.	Babcock-Wilcox Fouling Factor	=	$\frac{Na_2O + K_2O + Fe_2O_3 + CaO + MgO}{SiO_2 + Al_2O_3 + TiO_2} \times Na_2O$

* oxides are expressed as mole percent with iron as FeO, normalized to SO_3 - free basis

BEHAVIOR OF ASH-FORMING MINERAL MATTER IN COAL DURING CHEMICAL CLEANING WITH MOLTEN CAUSTIC

S. M. Kaushik, G. A. Norton, and R. Markuszewski

Ames Laboratory, Iowa State University, Ames, Iowa 50011

ABSTRACT

Coal-derived mineral matter, obtained by low-temperature ashing of Kentucky No. 11 coal, as well as mineral-grade samples of quartz, illite, kaolinite, and pyrite, were treated with various ratios of molten caustic (NaOH, KOH, and 1:1 NaOH-KOH mixtures) at 370°C for 1-2 hours to study the nature of reaction products obtained under the conditions of chemical cleaning of coal by the molten caustic leaching (MCL) process. Under these conditions, most of the reactions of minerals with caustic were very rapid, being complete in less than 10 minutes. The reaction products were characterized by x-ray diffraction, thermogravimetric analysis, atomic absorption spectrophotometry, and chemical analysis. The nature of these products was related to the stoichiometry of the reaction and was useful in explaining the process chemistry and in developing regeneration schemes for the spent caustic.

INTRODUCTION

The reaction of pyrite and coal with molten caustic has been studied first by Masciantonio (1) and then by Meyers and Hart (2) as a potential basis for the chemical cleaning of coal. It became rapidly obvious that molten caustic leaching (MCL) is of unparallelled effectiveness for removing sulfur and ash-forming minerals from coal, leading to the development of the Gravimelt Process by TRW (3-7). The process has been shown to be especially effective for the removal of organic sulfur (7-9).

However, to make this process economical, spent caustic will have to be regenerated for recycling. And to propose and test reactions for the regeneration of caustic, the nature of the reaction products anticipated in the spent caustic needs to be known. Thus, it is important to study the reactions of ash-forming minerals, present in coal, with molten caustic under conditions similar to those of the MCL process. We have undertaken such a study using quartz, kaolinite, illite, and pyrite as the major minerals found in coal and testing coal-derived mineral matter in the form of a low temperature ash.

EXPERIMENTAL

Materials

Quartz (St. Peters sand); kaolinite ($Al_2Si_2O_5(OH)_4$) from Twiggs Company, Georgia; illite ($KAl_2[Si_3AlO_{10}(OH)_2]$, 85% pure, from Ward's Natural Science Establishment, Inc.; and pyrite, both mineral-grade and coal-derived, were used in this study. The low temperature ash (LTA) of a Kentucky No. 11 coal was prepared by using standard procedures. Reagent-grade NaOH and KOH were powdered for easy mixing. Because of

its higher moisture content, the KOH was dried by heating above 410°C for several hours. The powdered NaOH and heated KOH contained 3% and 7% moisture, respectively, as determined by titrimetric assay or TGA.

Procedures and Analyses

Experiments were performed by mixing 1.5 g of quartz with powdered NaOH, KOH, or a 1:1 NaOH + KOH mixture using caustic-to-quartz mole ratios of 2:1, 4:1, 6:1, and 8:1. Similarly, 2 to 3 g each of kaolinite and illite were mixed with appropriate amounts of the above caustics to obtain caustic-to-clay mole ratios of 5:1, 10:1, 15:1, and 20:1. The mixtures of caustic and minerals were heated in an Inconel crucible at 370°C for 2 hours under a slow purge of helium. The reaction products were removed from the crucible while hot and then transferred to a glove box for cooling. The reaction mixture was powdered in an inert atmosphere of a glove box, and the powders were analyzed by x-ray diffraction (XRD) with a Picker x-ray diffractometer using Mo K_α radiation. All the time, the samples were protected from moisture during the analysis by purging the sample holder with nitrogen.

Products from the reaction of quartz with 1:1 NaOH + KOH were also washed with methanol to remove excess caustic. The residues were then dissolved in water and analyzed for Na and K by ion chromatography (IC). These data were used to calculate the Na_2SiO_3 and K_2SiO_3 mole fractions in the reaction products as a function of caustic-to-quartz mole ratio in the original mixture.

In addition, the reactions of quartz, kaolinite, illite, pyrite, and the low temperature coal ash with NaOH, KOH, or 1:1 NaOH + KOH mixtures were studied by thermogravimetric analysis (TGA) using a DuPont 951 Thermogravimetric Analyzer. The samples were prepared by mixing the appropriate amount of caustic with mineral matter or coal ash to achieve the desired caustic-to-mineral mole ratio (6:1 for quartz, 20:1 for kaolinite and illite, 10:1 for pyrite, and 2:1 for the LTA). For a typical TGA experiment, 30-50 mg of the sample mixture (mineral plus caustic) was transferred to the TGA pan and heated continuously, or isothermally at 370°C, under a nitrogen purge (50 mL/min.). The reaction products were subsequently washed with methanol or water, and the washed products were analyzed by chemical methods and by XRD.

RESULTS AND DISCUSSION

Reactions of Caustic with Quartz

An x-ray diffraction pattern of the reaction product obtained by heating a 2:1 NaOH-to-quartz mixture at 370°C for 2 hours is shown in Figure 1. The main product has been identified as sodium metasilicate (Na_2SiO_3). A small amount of unreacted quartz was also present. At higher NaOH-to-quartz ratios, the reaction product was mostly sodium orthosilicate, Na_4SiO_4 (a representative XRD pattern of this product is shown in Figure 2). Also, unreacted NaOH was present at the higher NaOH-to-quartz mole ratios. The reactions can be described by the following equations:

$$SiO_2 + 2\ NaOH \xrightarrow{370°C} Na_2SiO_3 + H_2O\uparrow \qquad \text{(Eq. 1)}$$

$$SiO_2 + 6\ NaOH \xrightarrow{370°C} Na_4SiO_4 + 2\ NaOH + 2\ H_2O\uparrow \qquad \text{(Eq. 2)}$$

where 2 or 4 moles of NaOH react with 1 mole of quartz to form Na_2SiO_3 or Na_4SiO_4, respectively, and water is also one of the products. The products are consistent with the equilibrium diagram of the Na_2O - SiO_2 system which shows the formation of Na_2SiO_3 and Na_4SiO_4 with a richer Na_2O content in the reaction mixture (10). Although Kautz et al. (11) have found Na_4SiO_4 and $Na_6Si_2O_7$ as products in the NaOH - Na_2SiO_3 - SiO_2 reaction system, the absence of $Na_6Si_2O_7$ in our study is probably due to our lower temperature.

When KOH was used as the caustic, potassium metasilicate, K_2SiO_3, was the main reaction product at all KOH-to-quartz mole ratios. A representative XRD pattern of the reaction product obtained at the 6:1 KOH-to-quartz ratio is shown in Figure 3. This reaction can be shown by the following equation, in which only 2 moles of KOH are used for each mole of quartz to result in K_2SiO_3, water, and unreacted KOH:

$$SiO_2 + 6\ KOH \xrightarrow{370°C} K_2SiO_3 + 4\ KOH + H_2O\uparrow \qquad \text{(Eq. 3)}$$

The other potential product, potassium orthosilicate (K_4SiO_4), was not found. It is also not listed in the powder diffraction file.

When the 1:1 NaOH + KOH mixture was employed in the reactions with quartz, the products were a mixture of only Na_2SiO_3 and K_2SiO_3. Surprisingly, no Na_4SiO_4 was found in the reaction products when both NaOH and KOH were present, even at higher caustic-to-quartz ratios. Thus, 2 moles of the mixed caustic were always used up in the reaction for each mole of quartz.

From the IC results for Na and K, obtained during the analysis of the reaction products from treating quartz with various amounts of the 1:1 NaOH + KOH mixtures, the relative amounts of Na_2SiO_3 and K_2SiO_3 were calculated. The data for Na and K, converted to Na_2SiO_3 and K_2SiO_3, respectively, are shown in Figure 4 as a function of the amount of caustic. As can be seen, the ratio of Na_2SiO_3 to K_2SiO_3 increased with increasing caustic-to-quartz mole ratio, indicating that under these conditions quartz forms preferentially Na_2SiO_3. This unforeseen result has implications for chemical coal cleaning by MCL, since the spent caustic will be enriched in KOH, thus requiring less makeup KOH to maintain the 1:1 NaOH-KOH ratio in the mixed caustic used for leaching.

Reactions of Caustic with Clays

The clay minerals kaolinite and illite reacted with molten NaOH to form $NaAlO_2$ and Na_2SiO_3 at all NaOH-to-clay mineral ratios, i.e., 5:1, 10:1, 15:1, and 20:1. A representative XRD pattern of the NaOH-kaolinite reaction product at the 20:1 ratio is presented in Figure 5. Unreacted kaolinite, or illite, was observed in the product when reaction mixture contained 5:1 NaOH-to-clay ratio, and unreacted NaOH was found at 15:1 and 20:1 NaOH-to-clay ratios.

The reactions of excess NaOH with kaolinite and with illite can be shown by equations 4 and 5, respectively:

$$Al_2Si_2O_5(OH)_4 + 20\ NaOH \xrightarrow{370°C} 2\ NaAlO_2 + 2\ Na_2SiO_3 + 14\ NaOH + 5\ H_2O\uparrow \quad \text{(Eq. 4)}$$

$$KAl_2[Si_3AlO_{10}(OH)_2] + 20\ NaOH \xrightarrow{370°C} 3\ NaAlO_2 + 3\ Na_2SiO_3 + 11\ NaOH + 5\ H_2O \quad \text{(Eq. 5)}$$

Similarly, kaolinite and illite reacted with molten KOH to form the analogous products $KAlO_2$ and K_2SiO_3 at all caustic-to-clay ratios. A representative XRD pattern of the products of the KOH-illite reaction at a 20:1 KOH-to-clay ratio is shown in Figure 6.

Reactions of Caustic with Pyrite and LTA

The reaction of pyrite with molten NaOH has been studied by Chiotti and Markuszewski (12). They have proposed equation 6 under reducing and equation 7 under non-reducing conditions:

$$2\ FeS_2 + 11\ NaOH + 1/2\ C \longrightarrow 4\ Na_2S + 2\ NaFeO_2 + 1/2\ Na_2CO_3 + 5\ 1/2\ H_2O \quad \text{(Eq. 6)}$$

$$FeS_2 + 5\ NaOH \longrightarrow 1\ 5/6\ Na_2S + 1/6\ Na_2SO_3 + 2\ 1/2\ H_2O \quad \text{(Eq. 7)}$$

In both cases, Na_2S and $NaFeO_2$ were the main reaction products, and approximately 5 moles of NaOH were used for the reaction with 1 mole of pyrite.

The mineral matter in the low temperature ash (LTA) of coal is composed mostly of quartz, pyrite, and clay minerals. Therefore, the anticipated products from molten caustic reaction with low temperature ash are Na_2SiO_3, $NaAlO_2$, Na_2S, and $NaFeO_2$, and the analogous potassium salts K_2SiO_3, $KAlO_2$, K_2S, and $KFeO_2$. No XRD patterns were obtained, however, since the amount of LTA sample was too small.

TGA Studies

The mineral-caustic reactions were also studied by TGA. For the reaction of quartz with caustic, the TGA in Figure 7 shows an incipient reaction at about 240°C, a more vigorous reaction at 310°C, and completion at 340°C. The TGA curves for the caustic reactions with other minerals were comparable. The isothermal plot (wt. % vs. time) at 370°C indicated that the reaction at this temperature was very fast and was completed in less than 10 minutes. The amount of weight loss, due to water evolved in this reaction, also supports the formation of Na_4SiO_4 and K_2SiO_3 as the main products of reactions with NaOH and with KOH, respectively, at 6:1 caustic-to-quartz ratios.

Figure 7 shows the isothermal TGA plots of the reactions of NaOH with low temperature ash (Kentucky No. 11 coal) and with mineral-grade pyrite. Both reactions were also very fast and were completed within 10 minutes.

Similarly, the clay minerals kaolinite and illite and a coal-derived pyrite reacted very fast with molten NaOH. Again, the reactions were completed in less than 10 minutes. Comparable results were obtained using KOH and the 1:1 NaOH + KOH mixture as the caustic.

CONCLUSIONS

This study shows that coal mineral matter can react with fused or molten caustic at 370°C in a much shorter time of heating than that commonly used in the MCL process for chemical cleaning of coal. The reaction products are mostly Na_2SiO_3, $NaAlO_2$, Na_2S and $NaFeO_2$ plus the analogous potassium compounds when a 1:1 NaOH + KOH mixture is employed as the molten caustic. It is, therefore, possible to calculate the amount of caustic that will be used up in reactions with mineral matter in a particular coal.

These reaction products are water-soluble, but they can form insoluble complex aluminosilicates when present together. Such insoluble aluminosilicates are expected to form during the countercurrent washing with water, and they will probably stay with the coal and the sodium carbonate (13). Fortunately, these are soluble in acid (aqueous H_2SO_4 or HCl) and, therefore, can be removed during the subsequent acid-washing step. Soluble silicates could then be removed from the waste streams by liming to form the insoluble calcium silicate.

ACKNOWLEDGMENTS

Ames Laboratory is operated for the U. S. Department of Energy by Iowa State University under Contract No. W-7405-ENG-82. This work was supported by the Assistant Secretary for Fossil Energy through the Pittsburgh Energy Technology Center. We gratefully acknowledge some experimental assistance from John Finn and helpful discussions with Dr. Premo Chiotti, Dr. Colin Chriswell, and Dr. Kenneth Windom.

LITERATURE CITED

1. P. X. Masciantonio, "The Effect of Molten Caustic on Pyritic Sulphur in Bituminous Coal," Fuel 44, 269-275 (1975).

2. R. A. Meyers and W. D. Hart, "Chemical Removal of Organic Sulfur from Coal," presented at the Amer. Chem. Soc. Meeting, Houston, TX, March 23-28, 1980.

3. TRW Energy Development Group, "Gravimelt Process Development," Final Report No. DOE/PC/42295-T7, June 1983.

4. B. Maijgren and W. Hubner, "Coal Cleaning by Molten Caustics," Proc. International Conf. on Coal Science, 1983, pp. 256-259.

5. R. A. Meyers, "Gravimelt Process Applications and Economics, Proc. 1st Annual Pittsburgh Coal Conf., 1984, pp. 381-384.

6. R. Markuszewski, D. R. Mroch, G. A. Norton, and W. E. Straszheim, "Coal Desulfurization and Demineralization by Molten Caustic Mixtures," in Fossil Fuels Utilization: Environmental Concerns, R. Markuszewski and B. D. Blaustein, eds., Am. Chem. Soc., Washington, D. C., 1986, pp. 42-50.

7. R. A. Meyers, W. D. Hart, J. F. Jones, L. C. McClanathan, J. L. Anastasi, and E. M. Barrish, "Gravimelt Process Modular Circuit Test Results," Proc. 3rd Annual Pittsburgh Coal Conf., 1986, pp. 115-129.

8. G. A. Norton, D. R. Mroch, C. D. Chriswell, and R. Markuszewski, "Chemical Cleaning of Coals with High Organic Sulfur Using Fused Caustic," in Processing and Utilization of High Sulfur Coals - II, Y. P. Chugh and R. D. Caudle, eds., Elsevier, 1987, pp. 213-223.

9. M. A. Nowak, B. R. Utz, D. J. Fauth, and S. Friedman, "Fused Salt Reactions of Organosulfur Compounds," Am. Chem. Soc. Div. Fuel Chem. Preprints, 32(4), 46-52 (1987).

10. F. C. Kracek, "The System Sodium Oxide-Silica," J. Phys. Chem. 34, 1583-1598 (1930).

11. K. Von Kautz, G. Muller, and W. Schneider, "Determination of the Cell Constants and Space Groups of Sodium Orthosilicate (Na_4SiO_4) and Sodium Pyrosilicate ($Na_6Si_2O_7$) and Investigation of their Regions of Stability by Using a High-Temperature Camera," Glastechn. Ber., 43, 377-381 (1970).

12. P. Chiotti and R. Markuszewski, "Reaction of Pyrite with Fused NaOH," Ind. Eng. Chem. Process Des. Dev., 24, 1137-1140 (1985).

13. N. D. Shah, C. D. Chriswell, and R. Markuszewski, "Separation by Countercurrent Washing of Coal-Caustic Mixtures During Chemical Cleaning of Coal," submitted to Separation Science and Technology, 1988.

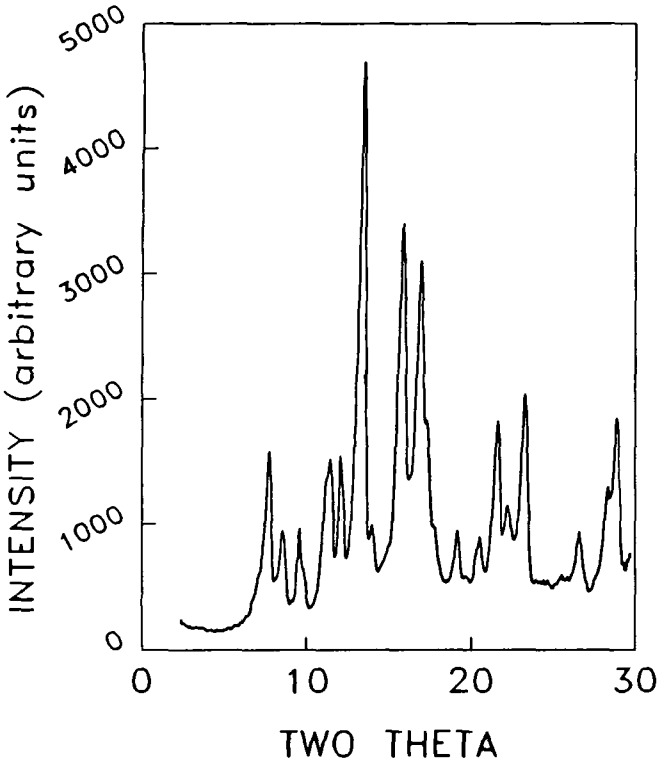

Figure 1. Typical XRD pattern for products from the reaction of SiO_2 with NaOH.

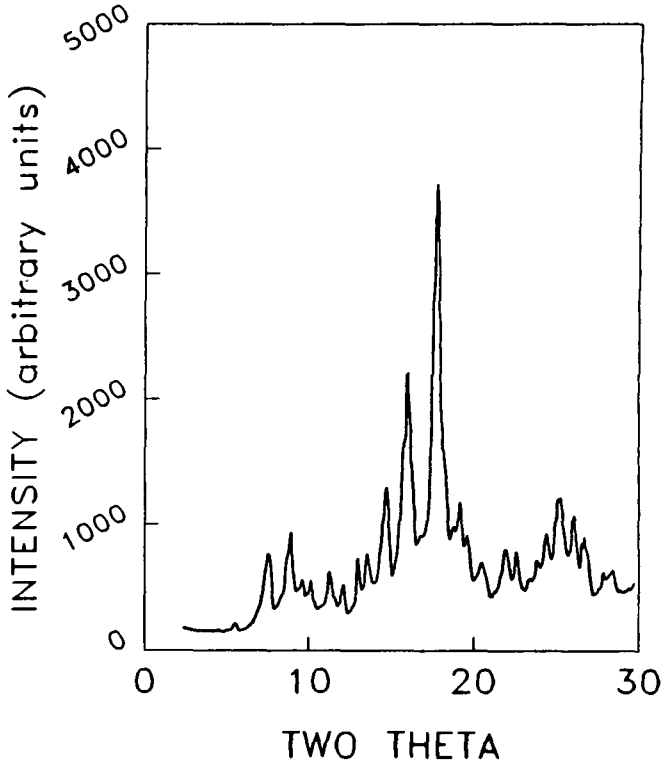

Figure 2. Typical XRD pattern for products from the reaction of SiO_2 with excess NaOH.

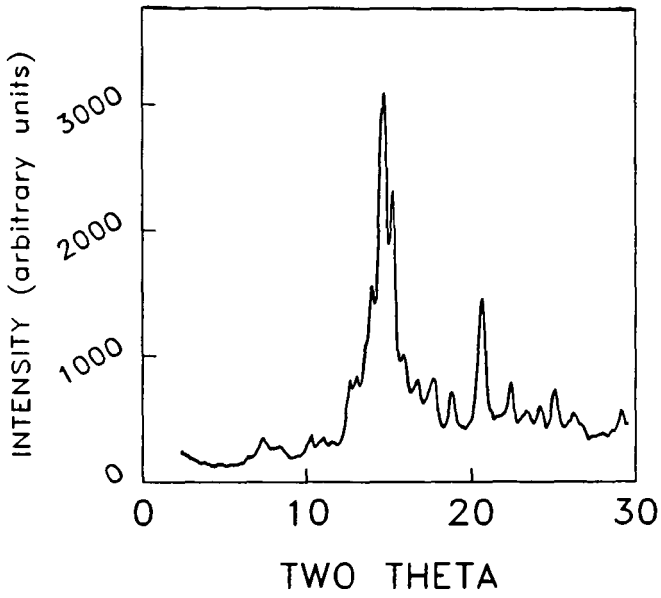

Figure 3. Typical XRD pattern for products from the reaction of SiO_2 with excess KOH.

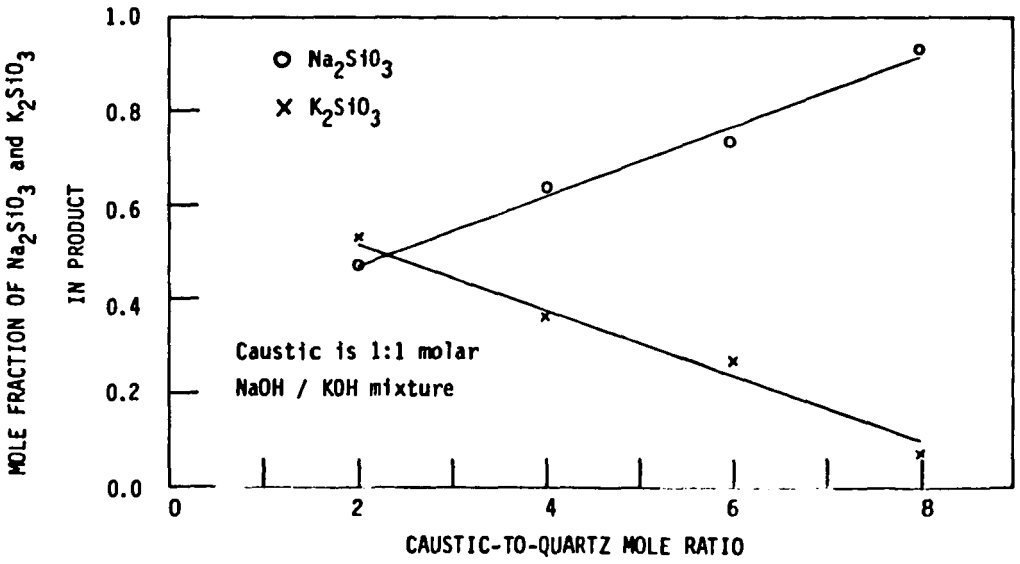

Figure 4. Mole fraction of Na_2SiO_3 and K_2SiO_3 in the product from the reaction of caustic with quartz.

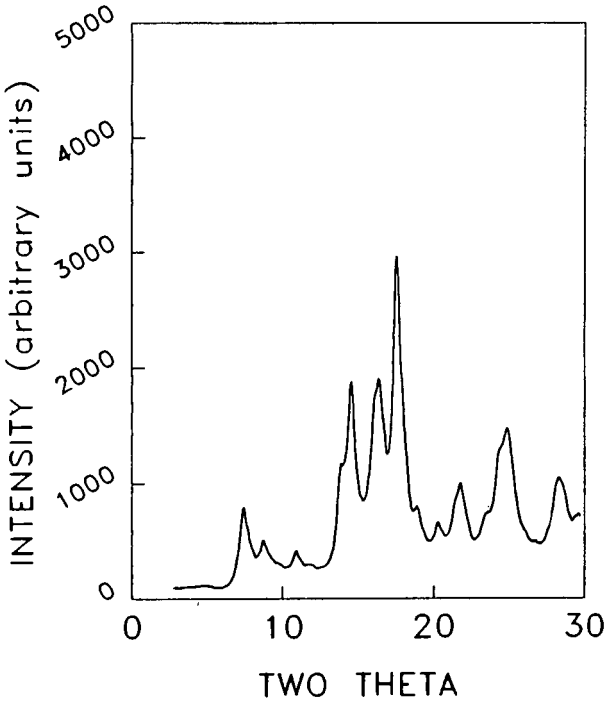

Figure 5. Typical XRD pattern for products from the reaction of kaolinite with excess NaOH.

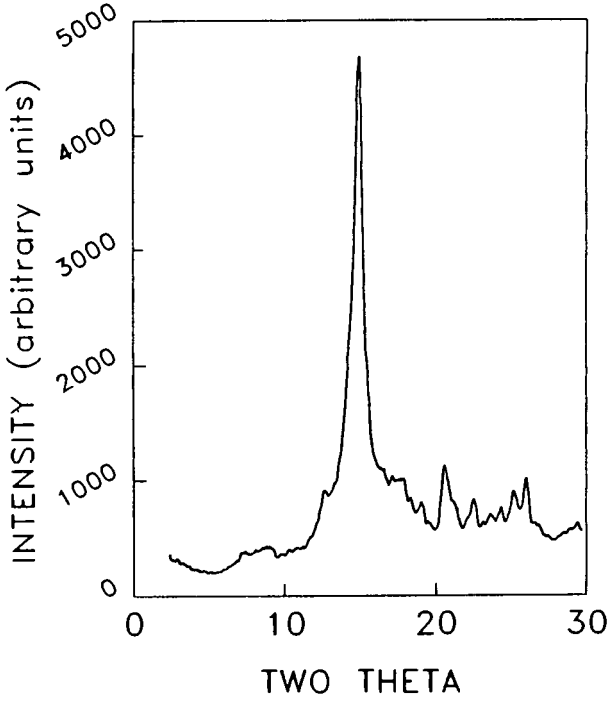

Figure 6. Typical XRD pattern for products from the reaction of illite with excess KOH.

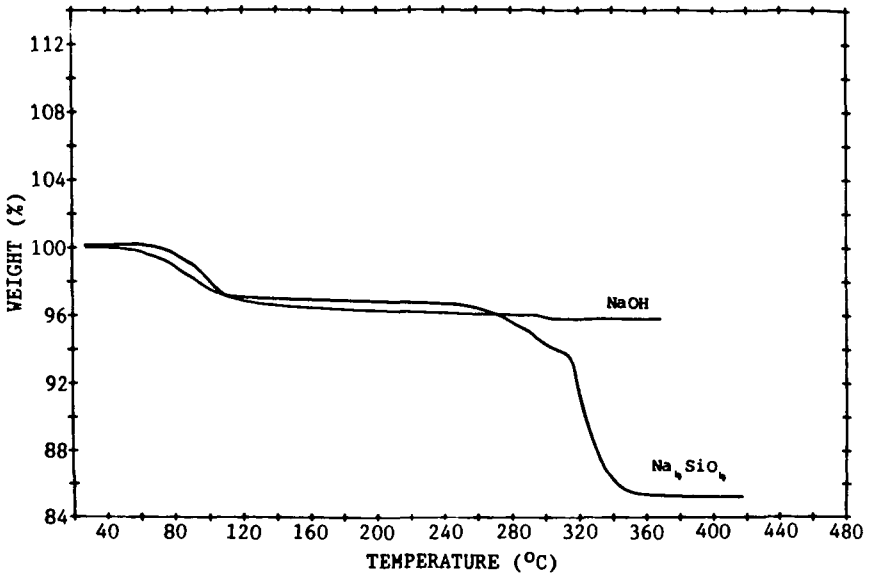

Figure 7. TGA results for the reaction of quartz with NaOH.

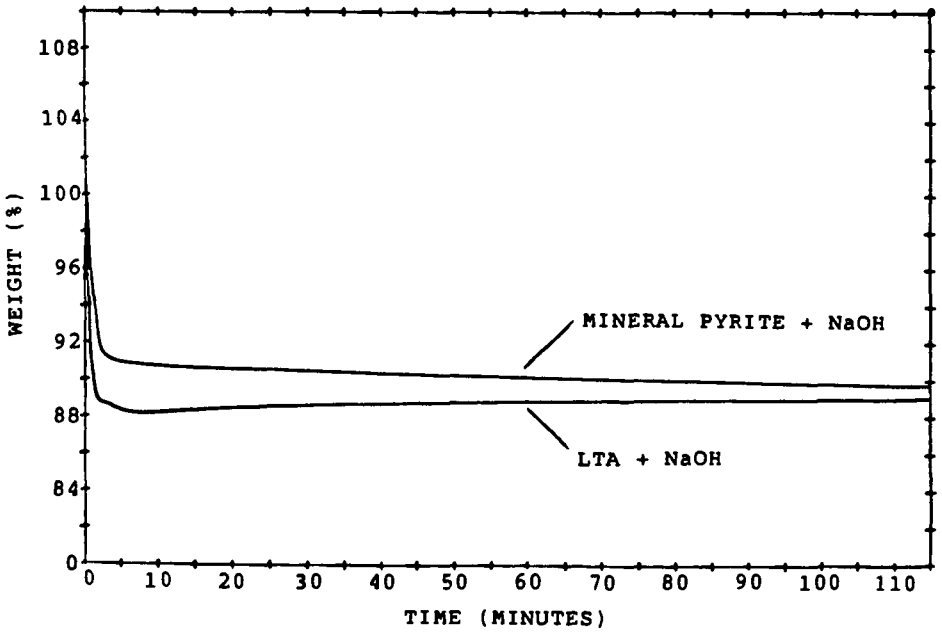

Figure 8. Isothermal TGA curves for the reaction of NaOH with mineral-grade pyrite and a low-temperature coal ash.

THERMODYNAMIC AND RHEOLOGICAL MODELING OF COAL ASH BEHAVIOR

Harold H. Schobert and Bong-Jin Jung
Fuel Science Program
Department of Materials Science and Engineering
The Pennsylvania State University
University Park, PA 16802

INTRODUCTION

This paper describes some recent results attained in modelling the behavior of coal ash and slags derived from it. This work is part of a larger effort which seeks to develop a unified model of ash behavior in combustion or gasification systems. A detailed description of the modelling effort has recently been published (1). Briefly, the focus of the model is on the effects of increasing temperature on coal ash and the recognition that ash will undergo a series of transformations which are specified by the composition and temperature of the ash but which may be independent of the configuration of the processing hardware in which the coal is being consumed.

The feature common to all combustion and gasification systems is that the inorganic components of the coal are exposed to temperatures high enough to induce chemical reactions, phase changes, or both. At low temperatures, dehydration reactions and thermally induced structural rearrangements occur, and are particularly important for clays. In low-rank coals, decarboxylation of the coal structure liberates alkali and alkaline earth cations for reaction elsewhere, such as substitution into the clays (2). At higher temperatures carbonate decomposition can occur.

As the temperature continues to increase, a point is eventually reached at which one or more of the low-melting components of the ash will melt. The formation of a liquid phase often marks the onset of troublesome ash behavior, such as clinkering on grates, agglomeration in fluidized beds, and deposition on steam tubes. In each of these instances, the liquid phase acts as a glue to bond solid particles together. The sintering is governed by the Frenkel equation, which relates the interparticle bonding to the viscosity and surface tension of the liquid phase (3).

At a given temperature, the viscosity and surface tension of the liquid phase will be determined by the liquid composition. However, in cases of partial melting (or of a liquid phase remaining after partial crystallization of a melt) it is unlikely that the composition of the liquid phase is the same as the bulk composition as customarily determined by analysis of the ash produced by the standard ASTM ashing procedures. Consequently, before one can apply a model to calculate the viscosity or surface tension, it is first necessary to determine the actual composition of the liquid.

Our approach to calculating liquid phase composition is the thermodynamic model SOLGASMIX (4,5,6). This program is based on minimization of the free energy of the system. An iterative calculation determines the mole fractions of the components which give the minimum Gibbs free energy, consistent with mass balance constraints. In recent work at Penn State, SOLGASMIX has been used with some success to determine the effects of composition on the growth of strength in slag deposits from pulverized coal firing of low-rank coals (7,8).

Numerous models for calculating viscosity as a function of composition are available in the literature. On the other hand, the surface tension of liquids derived from coal ash has been studied very little. Consequently, our recent work has focused on viscosity. The variety of viscosity models available, and the conflicting results occasionally obtained from them, has led us to develop a master program which incorporates six of the major viscosity models and which calculates the viscosity of a given liquid by all six models. This allows us to make an immediate comparison of the calculated results with the experimental data, and will be of assistance in assessing the applicability of the various viscosity models in our overall program.

PROCEDURE

The objective of the present work was to test the combined SOLGASMIX - viscosity program against available experimental data. The material chosen for the test was Martin Lake (Texas) lignite, for which good slag viscosity data and x-ray fluorescence and diffraction analyses of the solidified slag were available. The experimental data derived from an earlier viscosity project, of which the methods and results have already been published (9,10).

The current version of SOLGASMIX used for this work is written in FORTRAN and is running on the Penn State IBM mainframe computer. The viscosity model program is written in FORTRAN and is also running on the mainframe. The input data for SOLGASMIX was the composition determined by x-ray fluorescence analysis of the ash produced by the ASTM ashing procedure. The liquid phase composition was calculated at 25°C intervals in the range 1200 - 1700°C. At each temperature interval, the calculated liquid phase composition was then used as the input data for the viscosity model.

RESULTS AND DISCUSSION

Viscosity

The viscosity was calculated using the six-model program described above. The results for this lignite showed that the best accuracy (agreement between calculated and experimental viscosities) was obtained from the S^2 viscosity model of Hoy et al. (11). These results are summarized in Table 1.

TABLE 1. Comparison of calculated and experimental viscosity data (S^2 model (11); viscosity units are poises)

Temp. °C	Calcd.	Exptl.
1350	321	220
1375	203	160
1400	131	110
1425	89	77
1450	64	55
1475	50	38*

*Extrapolated; experimental data end at 1471°.

When comparing the calculated and experimental results shown in Table 1, it should be borne in mind that these results were obtained with absolutely no a priori assumptions about what the composition of the liquid "should be." The liquid phase composition used as input data for the viscosity model was obtained directly from the minimization of the free energy of a system having the composition of the lignite ash.

As is the case with virtually all viscosity calculation models, the work we have done so far does not provide a prediction of the temperature of critical viscosity, T_{cv}, nor of the viscosity vs. temperature behavior in the non-Newtonian flow region below T_{cv}. However, it would seem that the ability to calculate the amount and composition of the liquid and solid phases afforded by SOLGASMIX may provide the key to development of a means for calculating both of these important slag properties. Efforts to develop T_{cv} and non-Newtonian viscosity predictions are planned for the future.

Liquid composition

The predicted liquid phase composition changes slightly with temperature, over the range 1350 - 1475°C for which we compared calculated and experimental viscosity data. Nevertheless, the agreement between the SOLGASMIX predictions and the x-ray fluorescence analysis of the solidified slag after a viscosity test are remarkably good, as shown in Table 2, which is given on the next page. The normal SOLGASMIX calculation determines mole fractions of elements and various compounds; however, since the x-ray analysis data are customarily reported as weight percents of the oxides, we have converted the SOLGASMIX output to the same basis for ease of comparison. (In addition, this conversion is necessary to use the SOLGASMIX results as input data for several of the viscosity calculation models.)

Although the reporting of analytical results as oxides and the use of such results as input data for viscosity models are traditions of long standing, in fact a list of oxides does not by itself convey much information about the molecular species actually present in the melt. It is extremely unlikely that very

TABLE 2. Comparison of predicted and determined compositions of Martin Lake lignite ash slag. (Data in weight percent.)

Component	Calcd. 1350°	Calcd. 1475°	Exptl.
SiO_2	50.9	48.5	48.3
Al_2O_3	15.9	15.0	14.9
Fe_2O_3	7.1	11.9	11.8
TiO_2	1.0	1.0	1.0
P_2O_5	0.0	0.0	0.0
CaO	11.7	10.6	10.5
MgO	3.6	3.5	3.5
Na_2O	1.0	0.9	0.9
K_2O	0.5	1.1	1.1
SO_3	8.3	7.5	7.5

reactive oxide donors such as the alkali and alkaline earth oxides would coexist in a melt, as oxides, with oxide acceptors such as silica or alumina. In fact, the species in the melt are most likely aluminosilicate polymers (12,13). Therefore a real test of the SOLGASMIX predictions is a comparison of the liquid phase molecular species with those found by analysis.

Information on the species in the melt was obtained by x-ray diffraction analysis of the solidified slag after a viscosity test. There are of course limitations to this method, most notably the potential for changes to occur as the melt is cooled, the presence of amorphous phases not detected by diffraction analysis, and the presence of materials in quantities below the detection limits of the equipment. Furthermore, x-ray diffraction analysis is not quantitative. These limitations notwithstanding, the comparison of x-ray diffraction results with SOLGASMIX predictions, shown in Table 3, is encouraging.

TABLE 3. Comparison of predicted (SOLGASMIX) and observed (x-ray diffraction) species in liquid phase of Martin Lake lignite ash.

Predicted (a)	Observed	
$CaAl_2Si_2O_8$	$CaAl_2Si_2O_8$	(c)
SiO_2	SiO_2	(b)
$MgSiO_3$	$MgSiO_3$	(c)
$CaSO_4$	$CaSO_4$	(b)
FeO	Fe_2O_3	(c)
Fe_3O_4		

Notes: (a) Species predicted by SOLGASMIX are listed in decreasing order of abundance; (b) identified as a "major" phase by XRD; (c) identified as a "minor" phase by XRD.

Regarding these results, it should be noted that the calcium aluminum silicate observed by x-ray diffraction was reported as "plagioclase" (14). The term plagioclase refers to a series of

general formula $(Ca,Na)(Al,Si)AlSi_2O_8$ of which the compound listed, $CaAl_2Si_2O_8$ (anorthite), is an end member (15,16). We are not yet certain of the reason for the discrepancy between the predicted and observed iron-containing species.

At the present stage of development of the model, SOLGASMIX itself is not without difficulties. Problems have been encountered in obtaining convergence in the SOLGASMIX calculations for some systems. In particular, the calculations seem extremely sensitive to the amounts of CaO and SO_3 in the ash composition used as input data.

In the context of the development of the unified model of ash behavior, the work reported here indicates that, at least for some ashes, it is possible to obtain useful predictions of the liquid phase composition and viscosity over a range of temperatures using only the initial ash composition as the necessary data. Much work remains to be done. As mentioned, a problem exists with the convergence of the SOLGASMIX calculation for some compositions. The prediction of T_{cv} and the viscosity - temperature curve in the non-Newtonian region remains a target for future investigations. The measurement of surface tension of ash-derived liquids and the development of a method for calculating surface tension vs. temperature from composition are research areas that are woefully under-explored. When these hurdles have all been crossed, there still remains the task of synthesizing the overall model from these components. Of course, any model at any stage of development needs continual testing against available experimental data.

ACKNOWLEDGEMENTS

This research has been supported by the Department of the Interior's Mineral Institutes program administered by the Bureau of Mines under allotment grant number G1164142. In particular, the support of the Pennsylvania Mining and Mineral Research Institute is hereby acknowledged. The authors are also pleased to acknowledge the financial support provided by The Pennsylvania State University Research Initiation Grant Program.

LITERATURE CITED

1. Schobert, H. H.; Conn, R. E.; Jung, B-J. Proc. 4th Annual Pittsburgh Coal Conf. 1987, 423.

2. Falcone, S. K.; Schobert, H. H. In "Mineral Matter and Ash in Coal"; Vorres, K. S., Ed.; American Chemical Society: Washington, 1986; Chapter 9.

3. Frenkel, J. J. J. Physics USSR 1945, 9, 385.

4. Eriksson, G. Acta Chem. Scand. 1971, 25, 7.

5. Eriksson, G. Chem. Script. 1975, 8, 100.

6. Eriksson, G.; Rosen, E. Chem. Script. 1973, 4, 193.

7. Benson, S. A. Ph.D. Dissertation, The Pennsylvania State University, University Park, PA, 1986.

8. Austin, L. G.; Benson, S. A.; Schobert, H. H.; Tangsathitkulchai, M. U.S. DOE Report 1987, No. DOE/FE-70770.

9. Streeter, R. C.; Diehl, E. K.; Schobert, H. H. In "Chemistry of Low-Rank Coals"; Schobert, H. H., Ed.; American Chemical Society: Washington, 1984; Chapter 12.

10. Schobert, H. H.; Streeter, R. C.; Diehl, E. K. Fuel 1985, 64, 1611.

11. Hoy, H. R.; Roberts, A. G.; Wilkins, D. M. Inst. Gas Engineers Pubn. 1964, No. 672.

12. Vorres, K. S. ACS Div. Fuel Chem. Preprints 1977, 22(4), 118.

13. Schobert, H. H. ACS Div. Fuel Chem. Preprints 1977, 22(4), 143.

14. Rindt, D. K. Grand Forks Energy Technology Center, personal communication, 1981.

15. Bowen, N. L. "The Evolution of the Igneous Rocks"; Dover Publications: New York, 1956; p. 45 ff.

16. Berry, L. G.; Mason, B. "Mineralogy"; W. H. Freeman: San Francisco, 1959; Chapter 15.

FORMATION AND GROWTH OF COAL ASH AGGLOMERATES

R. H. Carty, D. M. Mason, S. D. Kline, and S. P. Babu

Institute of Gas Technology
3424 South State Street
Chicago, Illinois 60616

BACKGROUND

The behavior of the mineral matter of coal and its reaction product, ash, is of concern in gasification processes because it governs deposition on gasifier and downstream surfaces as well as agglomeration in ash-agglomerating gasifiers. In general, fluidized-bed coal gasifiers operate under backmixed conditions. Consequently, the gasifier solids drain stream could carry with it some unconverted carbon. In contrast, in the KRW and U-GAS processes, the high-velocity jet in the gasifier effectively agglomerates the ash, thereby facilitating its selective removal from the fluidized-bed, and thus achieving carbon conversion in excess of 98%.

The minerals in high-sulfur bituminous coal are predominantly pyrite, quartz, and clay minerals. The reactions of most importance in the formation of ash agglomerates are 1) the oxidation of the ferrous sulfide produced by the decomposition of the pyrite and 2) the subsequent or simultaneous reaction of the resulting iron oxide with the clay minerals and quartz to produce relatively low-melting iron aluminosilicates that form the matrix material for the ash agglomerates. For the ash-agglomerating fluidized-bed gasifier, the iron oxidation and iron aluminosilicate formation occur in the jet region of the reactor due to its oxidizing atmosphere and elevated temperature.

In a fluidized-bed gasifier, the char particles that contain mineral matter may be divided into two groups. One group contains a combination of clays and quartz (the acids) and pyrite or other fluxing agents such as CaO, MgO, Na_2O, and K_2O (the bases) that will form a low-melting aluminosilicate agglomerate as the carbon in the particle is gasified. The second group of particles contain either a single type of mineral matter or very small amounts of pyrite or the other fluxing agents and lead to the formation of "free ash" that does not melt as the char is gasified. Agglomerate growth occurs both by combination of the smaller molten agglomerates and by capture of the free ash by the molten agglomerates. Therefore, the tendency of a coal to form ash agglomerates should be dependent on both the distribution of the mineral matter as well as its average composition.

Coal Mineral Matter: The overall aim of the IGT ash chemistry studies is to predict the behavior of the coal ash in a fluidized-bed gasifier on the basis of a minimum analysis of the characteristics of the feed coal mineral matter and the operating conditions of the gasifier. In this study the objective was to correlate the composition and distribution of the mineral matter for five eastern and two western coals to the behavior of their ash in a laboratory gasifier. The choice of the eastern coals was limited to washed products to concentrate on the initial phases of ash reactions — those of the ash brought into juxtaposition for reaction by the gasification of the carbon of individual particles.

Coals were sought whose ash composition would reflect the full range of the most important variable for agglomeration, the average concentration of pyrite relative to the siliceous minerals. The concentration of calcium minerals — typically calcite — is probably next most important variable. Accordingly, we selected four U.S. bituminous coals covering a wide range of iron oxide and only

small amounts of calcium oxide in the ash. An Illinois No. 6 Seam coal with high calcium oxide and low iron oxide, a western bituminous (York Seam), and a subbituminous coal (Rosebud Seam) were also selected for testing.

The mineral matter in each coal was characterized by: determination of the concentration of major and minor oxides in the ash; Mossbauer analyses to measure the concentration by type of the iron compounds present; and mineralogical analyses by computer-assisted scanning electron microscopy (SEM).[1,2] Typically, in the eastern bituminous coals, iron is present as pyrite and its oxidation products, namely sulfates. In the York coal, the iron is mainly present in chamosite and in siderite.

MINERAL MATTER DISTRIBUTION

For this study, a method of characterizing the distribution of the mineral matter of coal was developed. Of interest here is a practical method of determining how much of the ash of the coal yield slag of viscosity low enough for agglomeration as the char of single particles becomes completely gasified. Most important are the iron and calcium oxide contents of the ash in relation to silica plus alumina. For this investigation, the ash compositions of 32 single particles of the coals were determined chemically. Particles from the -10+12 mesh fraction of the coal were taken for analysis; this size furnishes enough ash for the chemical analysis and is about the average size, by weight, of the coal feed to a pilot plant or commercial fluidized-bed gasifier. Particle weight, ash content, and iron oxide and calcium oxide in the ash were determined. Also, the concentration of basic constituents (BC) was estimated for each particle. The estimation, which included a correction for sulfate in the particle ash, was deemed to be satisfactory on particle ashes containing less than about 20% CaO.

The agreement, or lack thereof, of the average calcium oxide and iron oxide contents of the ash of the particles with those found by the conventional analyses (Table 1) was significant in the behavior of the mineral matter in agglomeration. For example, although the average iron oxide in the ash of the 32 particles of Kentucky No. 9 coal agrees well with the conventional analysis, less than half as much calcium oxide was present in the -10+12 mesh particles as in the conventional analysis. Evidence indicates that the missing calcium oxide occurs as calcite in the cleat of the coal, along which fracture occurs in crushing, and that loss of the calcite by attrition from coal particles occurs in crushing and sieving, resulting in its concentration in the finer sieve fractions. The presence of plates of calcite, about 10 μm thick, in the cleat fractures of the Kentucky No. 9 coal was found by macroscopic examination of LTA-etched coal sections oriented perpendicular to the bedding.[1]

A loss of almost 90% of the calcium oxide from the -10+12 mesh particles is evident with the Indiana VI and Illinois No. 6 coals. No loss, or only a marginal one, is evident from the Pittsburgh No. 8 or Kentucky No. 13 coals. Nor did it occur with the subbituminous B Rosebud coal, in which the calcium occurs dispersed in the organic matter, partly as carboxylate and (probably) partly as calcite from decomposition of calcium carboxylates. However, about 90% of the average amount of iron oxide is abaent from the -10+12 mesh particles of this coal because of a similar occurrence of pyrite in the cleat.[3,4]

The distributions in particles larger and smaller than the -10+12 mesh also should be considered. In general, the distribution is expected to become wider (greater deviation from the average) as particle size decreases, and, for example, the number of particles with a single layer, whether attrital coal or vitrain, increases. The opposite may be true of larger particles, but not if the size of

particles is less than that of the predominant width of the layers. The appearance of the ashes of individual -4+5 mesh particles of the Kentucky No. 9 coal suggested that the distribution of iron in these particles does not differ much from that of the -10+12 mesh particles.[1]

At present, it is estimated that, in the absence of more than about 2 weight percent of calcium oxide, single-particle ash with iron oxide contents of between 15 and 80 weight percent may form a low-melting agglomerate after carbon burn-off without the need for combination with the ash of a different particle. A summary of the distribution of iron oxide in the ash of the -10+12 mesh particles is presented in Table 2 for the eastern bituminous coals, together with the bulk average iron oxide content. Ash of Kentucky No. 9 coal, from the same mine as that used here, agglomerated without difficulty in U-GAS pilot-plant tests with bed temperatures at about 1870°F and substantially higher temperatures in the jet. The particle analyses of this coal show 44% of the ash to have 0 to 15 weight percent Fe_2O_3 and 53% to have 15 to 80 weight percent Fe_2O_3. Although the ash of the Pittsburgh No. 8 coal has an average Fe_2O_3 content of 31.7 weight percent, much higher than that of the ash of the Kentucky No. 9; its fraction of ash in the 15 to 80 weight percent Fe_2O_3 range is much lower, only 12%. This indicates that the ash of the Pittsburgh coal should agglomerate more slowly. The same is true of the Indiana VI coal, whose ash has overall sufficient iron, 15.7 weight percent Fe_2O_3, for agglomeration, although very little falls in the 15% to 80% range. The Kentucky No. 13 and Illinois No. 6 coals probably have insufficient iron for agglomeration of their ash, but if so, the ash content of the bed in a gasifier can be allowed to rise to such an extent that almost all of the carbon is gasified.

EXPERIMENTAL

In the batch gasification tests used in this work, chars rather than coals were used to prevent caking of the coal particles. The preparation of the chars for the gasification tests is described in detail elsewhere.[2] The preparation of char from each coal was identical except for a sample of the Kentucky No. 9 coal that was prepared as a test of the effect of uniformity of distribution of the coal mineral matter on ash agglomeration. This sample of coal was first ground to -200 mesh to more uniformly distribute the coal mineral matter, and then it was devolatilized. During devolatilization, the coal agglomerated to form a bulk sample of char. This char was then ground and sized similar to the other char samples used in the agglomeration tests.

For the ash agglomeration tests of these coals, a previously constructed 2-inch-diameter fluidized-bed gasifier with a center jet configuration was used. A fluidizing gas of nitrogen and steam was introduced through a perforated metal disk at the bottom of the reactor and air was fed through the center jet to produce a hot region within the fluidized-bed where the temperature may be as much as 200° to 300°F higher than the temperature of the bed. Each test used a charge to the reactor of 100 g of coal char. The testing was standardized at a steam-to-oxygen molar ratio of 2:1, a bed temperature of 1950°F, and a superficial gas velocity of between 1.3 and 2.0 ft/s.

Before preparation of aliquots of the residues of the gasification tests, any clinker obtained was crushed to pass an 8-mesh sieve and was mixed with other residue. One portion of the residue was riffled and used for estimation of agglomerate content. This portion was ashed at 900° to 1100°F in a muffle furnace for at least 20 hours to remove carbon and achieve better visibility of the mineral matter. The temperature of ashing is high enough to burn off the carbon but low enough to avoid further reactions of the mineral matter, other than oxidation of the ferrous sulfide. The agglomerates, free ash, and pieces of clinker that are

isolated by the combustion of the carbon in the reactor residue were then sieved and each sieve fraction examined visually under a low-power microscope to estimate the amount of agglomerates.

A point-count analysis was also performed on the residues. Fractions of the ash coarser than 325 mesh were combined for this purpose, mounted in epoxy resin containing a yellow pigment, and polished. Removal of most of the material resulting from ashing of the char, consisting of fine grains, was essential to facilitate the point-count. Particles containing any matrix material, identified by occurrence of vesicles and usually by low reflectance, were counted as agglomerates; all others were counted as free ash, which was then augmented by the addition of the -325 mesh fraction. For the present purposes, the point-count was taken to be proportional to weight percent. Other details of the procedure are reported elsewhere.[2]

RESULTS AND DISCUSSION

A summary of results obtained for the agglomerate content of the ashed residues is presented in Table 3; this table includes agglomerate contents of ash from completely gasified char, calculated on the assumption that the quantity of this ash is proportional to the carbon conversion. In Table 3, excellent agreement is shown between agglomerate contents of the ash by inspection of sieve fractions and by point-count for tests on the Kentucky No. 9, Pittsburgh No. 8, and Illinois No. 6 chars in which no clinkers were produced, and also in tests on the fine-ground Kentucky No. 9, Indiana VI, and Illinois No. 6 in which clinkers were produced.

A comparison of agglomerate contents of ash from completely gasified chars for the tests on the Pittsburgh No. 8 and Illinois No. 6 chars, with and without clinkering, indicates that clinkering increases the agglomerate content. The average percent of agglomerate content obtained without clinkering is 65% to 71% of the agglomerate content obtained with clinkering; depending on the inclusion or not of the low value for agglomerates found by examination of sieve fractions in the test on the Pittsburgh No. 8 char in which clinkering occurred. With application of the correction, the "best" estimate of agglomerates obtained from the fine-ground Kentucky No. 9 is 60% to 66%, and from the Indiana VI is 61% to 67%.

An important step in the agglomeration of ash is the reaction of iron compounds with siliceous ones to form iron aluminosilicates. In a U-GAS pilot-plant test, conversion amounted to as much as 82% of the total iron, according to a Mossbauer analysis of the ash discharge. In the gasification tests reported under the previous program in which a central jet was not used, only a minor amount of iron aluminosilicate was formed.[4,5] With the addition of a central jet tube through which the oxygen is introduced, the tests on bituminous coal chars reported here show formation of iron aluminosilicate mostly in the range of 50% to 80% of the iron, as shown by the Mossbauer analyses.[1]

In the present series, the low conversion of iron to aluminosilicate in the Rosebud char can be attributed to the occurrence of pyrite both in the cleat and as large particles. Both of these factors can be expected to make conversion of iron to aluminosilicate less likely.

For the eastern coals, the best estimate of the agglomerate content of ashed residues in Table 3 gives an overall indication of their initial agglomeration potentials. It is noteworthy that these agglomerate amounts from completely gasified char range from only 38% to 66%, whereas the iron oxide of the ash of these coals ranges from 8% to 32%. An explanation is that the agglomerates from the coals with low iron oxide (the Kentucky No. 13 and the Illinois No. 6) in comparison to

the Kentucky No. 9, contain a substantially greater proportion of clay-derived material engulfed in or attached to the iron aluminosilicate matrix material.

It is also noteworthy that the agglomerate content of the ashed residue from the fine-ground Kentucky No. 9 coal was greater than that of the residues from the usual preparation. In the usual preparation, 1/4-in. top size coal was devolatilized and the resulting char was crushed to pass an 8-mesh sieve, whereas for the fine-ground tests the same coal was ground to pass a 200-mesh sieve before charring. The particle-by-particle distribution of iron in the char made by the usual preparation is probably well-represented by the data of Table 2, according to which 53% of the ash had from 15% to 80% Fe_2O_3. The expected effect of the fine grinding is to cluster the iron content of the ash of the particles of char more closely around the average 20% of Fe_2O_3 in the ash of this coal (Table 2). The test results indicate that this distribution is better for agglomeration than that of the original Kentucky No. 9 coal. These results and those on the Kentucky No. 13 coal indicate that ash containing as little as 10% Fe_2O_3 contributes to agglomeration. However, the resulting iron aluminosilicate may have a higher iron content because reaction with the siliceous minerals is incomplete.

The agglomerate content of the ashed residue from the Pittsburgh No. 8 char was only equal to that of the Kentucky No. 9, in spite of the substantially higher average iron oxide content of its ash — 31.7 versus 19.9 weight percent. This is attributed to the isolation from siliceous minerals of much of its pyrite, as shown by the iron oxide distribution where only 12 weight percent of the ash had between 15% and 80% Fe_2O_3; the effect is substantiated by a detailed point count analysis of the residue from Run 1744-30, in which no clinker was formed and in which 40% of the unagglomerated ash was in the form of iron oxide.

Three residues were analyzed by computer-assisted SEM to investigate the effect of large amounts of calcium oxide in the ash: the low calcium Kentucky No. 9 for reference; the Illinois No. 6, a high-calcium eastern bituminous; and the Rosebud, a western subbituminous with about the same amount of iron oxide and calcium oxide in the ash as the Illinois No. 6. In the residues of the gasification tests, the ratio of weight of iron-containing silicate compounds to that of other iron compounds (oxide and sulfide) is roughly equal (10:1) for the Kentucky No. 9 and Illinois No. 6 tests, and is significantly lower (about 6:1) for the Rosebud char test. This trend agrees with the Mossbauer results, which were attributed to the large size of pyrite particles and its occurrence in the cleat of the Rosebud coal. The opposite is true of the calcium; all of it in the Rosebud char has reacted to form silicates, whereas a substantial part of the calcium in the Illinois No. 6 char has not reacted, as shown by a weight ratio of about 3:1 of calcium silicates to other calcium compounds. The ratio of calcium reacted with silica to unreacted calcium would be even lower. Here again, a mineral in the cleat — calcite of the Illinois No. 6 coal — has reacted with siliceous minerals to a lesser extent than the well-distributed calcium — calcite and carboxylate — of the Rosebud coal.

The analyses for agglomerates in the residues from the Rosebud char show poor agreement, for which no explanation is apparent; no clinker was formed in either of two tests. According to the SEM analysis, the calcium oxide did react to form silicates and aluminosilicates, which should yield slag of about the same viscosity as a slag that would result if the calcium oxide had been iron oxide. As noted previously, the pyrite in this coal has been reported to occur in relatively large grains and, at the 30 mesh level of crushing, to be unattached to coal. Hence, the small amount of iron in the ash (7.0 weight percent Fe_2O_3) may also be less reactive than usual, similar to part of the iron in the Pittsburgh No. 8 coal.

Iron and calcium oxides in the York coal were each slightly higher than in the Rosebud, but the iron is mostly in a clay mineral and thus probably evenly distributed among all the siliceous minerals; as a result, the formation of iron calcium aluminosilicates of higher than average iron and calcium content would be much less favorable than when the iron is present as a discrete phase, as in the other coals.

In summary, the following conclusions have been made based on these results:

- A particle-by-particle method of chemical analysis can be used to determine the distribution and association of minerals in the coal feed to fluidized-bed gasifiers.

- With few exceptions, in gasification tests in which oxygen was introduced through a central jet and the fluidized bed was maintained at 1950°F, a major part of the iron was converted to iron aluminosilicates irrespective of a wide range of iron content from 10 to 32 weight percent Fe_2O_3 in the ash.

- Consistently low conversion of iron to aluminosilicate in the case of the subbituminous Rosebud char can be attributed to the large size of the pyrite and its occurrence in the cleat of this coal. A greater fraction of the calcium of the Rosebud coal, in which the calcium is uniformly distributed, was converted to silicates than was that of the Illinois No. 6 coal, most of which occurs in the cleat. Analyses also confirmed that a greater fraction of the iron of the Kentucky No. 9 and Illinois No. 6 coals was converted to silicates than was that of the Rosebud, most of which occurs in the cleat. This shows that calcite and pyrite that occur in the cleat and separate as free ash during grinding are less likely to form ash agglomerates.

- The results of the gasification tests performed in this study indicate that in individual coal particles Fe_2O_3 concentrations between 15 and 80 weight percent of the ash promote the formation of ash agglomerates, whereas ash outside this range tends to form free ash rather than agglomerates.

- In the gasification of coals of low-iron-content ash, significant formation of ash agglomerates can occur by the joining of unmelted mineral matter with relatively small amounts of the iron aluminosilicate matrix material.

- Characterization of the composition and distribution of the coal ash using the techniques developed in this study could be of assistance in setting the operating conditions of fluidized-bed, ash-agglomerating gasifiers.

ACKNOWLEDGEMENT

The funds for this research were provided by the Morgantown Energy Technology Center, United States Department of Energy under Contract No.: DE-AC21-84MC21313

REFERENCES

1. Mason, D. M. and Chao, S. S., "Determination of the Distribution of Ash, Pyrite and Basic Constituents in Coal Particles," Am. Chem. Soc. Div. Fuel Chem. Prepr. 32 (4), 203-13 (1987) Aug.-Sept.

2. Carty R. H., Mason, D. M. and Babu, S. P., Reaction Kinetics and Physical Mechanisms of Ash Agglomeration. Washington, D.C., U.S. Department of Energy, DOE/MC/21313 (To be published).

3. Kuhn, J. K., Fiene, F. and Harvey, R., "Geochemical Evaluation and Characterization of a Pittsburgh No. 8 and a Rosebud Seam Coal," Report METC/CR-78/8, 1978.

4. Chadwick, R. A., Rice, R. C., Bennett, C. M. and Woodriff, R. A., "Sulfur and Trace Elements in the Rosebud and McKay Coal Seams, Colstrip Field, Montana," Mont. Geol. Soc. Ann. Field Conf. Guide, 22, 167-75 (1975)

5. Mason, D. M., Carty, R. H., Babu, S. P., Ghate, M. R. and Lai, H. Y., "Mineral Matter Behavior in High Carbon Conversion Coal Gasifiers." Paper presented at the 1985 International Conference on Coal Science, Sydney, Australia, October 28-November 1, 1985; published in Proceedings: 1985 International Conference on Coal Science.

Table 1. SUMMARY OF AVERAGES OF SINGLE-PARTICLE ANALYSES

	Ash (Moist Basis)		Fe_2O_3 in Ash		CaO in Ash	
	Avg. of Particles (Range)	Bulk Avg.	Avg. of Particles (Range)	Bulk Avg.	Avg. of Particles (Range)	Bulk Avg.
	wt %					
Kentucky No. 9	6.3 (0.4-32.8)	7.6	22.3 (3.3-98.1)	19.9	1.10 (0.41-19.2)	2.29
Pittsburgh No. 8	10.9 (1.0-42.1)	7.5	34.2 (0.7-91.0)	31.7	1.14 (0.25-28.2)	0.90
Kentucky No. 13	8.2 (0.3-21.2)	7.3	8.6 (0.8-52.8)	8.1	0.69 (0.17-11.5)	0.90
Illinois No. 6	10.3 (1.1-32.5)	11.9	12.1 (1.8-91.7)	10.7	0.83 (0.21-14.0)	8.34
Indiana VI	16.4 (0.6-56.6)	13.4	6.9 (2.0-81.7)	15.7	0.36 (0.10-20.3)	2.48
Rosebud	10.3 (2.1-45.8)	11.3	0.55 (0.1-6.14)	7.0	9.4 (1.95-45.3)	7.2

Table 2. SUMMARY OF DISTRIBUTION OF Fe_2O_3 IN -10+12 MESH PARTICLES OF EASTERN BITUMINOUS COALS

Coal	Fe_2O_3 Content Bulk Avg.	Fe_2O_3 Content Particle Avg.	Distribution of Fe_2O_3 Concentration in All Particle Ashes: 0-15% Fe_2O_3	15-80% Fe_2O_3	80-100% Fe_2O_3
	wt%		% of all particle ashes		
Kentucky No. 9	19.9	22.3	44	53	3
Pittsburgh No. 8	31.7	34.2	59	12	29
Kentucky No. 13	8.1	8.6	89	11	0
Illinois No. 6	10.7	12.1	82	16	2
Indiana VI	15.7	6.9	91	9	0

Table 3. SUMMARY OF AGGLOMERATE CONTENT OF ASHED RESIDUES FROM 2-INCH-ID GASIFICATION TESTS BY POINT-COUNT AND SIEVE ANALYSIS

Coal	Basic Constituents, wt %	Dolomite Ratio	Test No.	Carbon Conversion, wt %	Clinker Formed	Agglomerate Content of Ashed Residue, wt %: In Total Ash, By Point-Count	In Total Ash, On Sieve Fractions	In Ash From Completely Gasified Char, By Point-Count	In Ash From Completely Gasified Char, On Sieve Fractions	Best Estimate
Kentucky No. 9	26	12	1744-06	63	None	36	35	57	56	} 57
			1744-07	73	Small amt.	--	46	--	63	}
Kentucky No. 9 Fine-Ground	26	12	1744-14	83	1.2 g	76	77	92	93	60-66[a]
Pittsburgh No. 8	35	4	1744-08	74	1.35 g	62	48	84	65	} 57
			1744-30	51	None	26	29	56	57	}
Kentucky No. 13	13	16	1744-12	78	2.8	36[b]	19	53[b]	24	~38[a,b]
			1744-15	46	1.2	33[b]	24	61[b]	45	
Illinois No. 6	24	41	1744-17	61	Yes	38	40	62	65	} 41
			1744-20	55	None	22	23	39	42	}
Indiana VI	24	16	1744-21	53	3.4 g	55	50	100	94	61-67[a]
York	23	50	1744-23	64	None	22	8	34	13	} ~23
			1744-29	64	None	--	14	--	22	}
Rosebud	19	57	1744-26	75	None	--	40	--	53	--
			1744-27	67	None	23	10	31	15	

[a]Corrected for the effect of clinkering as shown by the tests on the Pittsburgh No. 8 and Illinois No. 6 coals.

[b] Includes much clay with small amounts of attached iron aluminosilicate.

rhcpap-ta

Relation of Slag Viscosity and Surface Tension to Sintering Potential

S.Falcone Miller* and D.P. Kalmanovitch**

*The Pennsylvania State University
Department of Material Sciences, Fuel Science
University Park, PA 16802

**University of North Dakota Energy and Mineral Research Center
Box 8213, University Station
Grand Forks, ND 58202

The purpose of this paper is to discuss the relative effect of viscosity and surface tension on sintering potential or agglomeration in coal utilization systems. Of specific interest is the effect of composition and atmosphere on viscosity and surface tension.

BACKGROUND

Sintering is the process by which individual particles or ash particles and slag bind together to form a compact mass. The mechanisms by which sintering occurs are: viscous flow, vapor condensation, diffusion, and surface tension (1,2). Raask (3) has shown that, for coal utilization systems, the major mechanism is that of viscous flow with a reactive liquid phase. The extent of sintering, given by the square of the radius of the contact area (x^2) for a given time, t, is defined by the Frenkel model (3):

$$x^2 = \frac{3\gamma rt}{2\eta} \qquad (1)$$

where r is the initial particle radius, γ is the surface tension of the liquid phase, and η is the viscosity of the liquid phase. According to the Frenkel model, the extent of sintering is inversely proportional to the viscosity of the liquid phase and proportional to the surface tension. It is known that viscosity and surface tension are dependent on composition and atmosphere. Figure 1 (after Raask) shows the variation of surface tension , viscosity, and the rate of sintering with respect to temperature.

It must be noted that the Frenkel model is based on studies in which particles are in intimate contact with one another prior to heating. Sintering then occurs, in the case of ash species, with the formation of a liquid phase on the particle surface. In coal utilization systems, the particles are not in intimate contact with one another but are in constant relative motion. Therefore, the process of sintering or agglomeration only begins when particles collide and adhere to each other or to a slag layer. During initial contact the surface tension of the respective surfaces can play a rate-limiting role as it affects the adhesion of ash particles. The lower the surface tension of the liquid phase on the particle surface the greater the degree of adhesion and sintering resulting in either a fairly strong or large agglomerate. If the surface tension of the molten phase is sufficiently high initial adhesion may be limited. This would also be the case for particles with low viscosity liquid phases. If two particles collide, each having liquid phases of relatively high viscosity and low surface tension, initial adhesion can occur which could lead to some degree of agglomeration. However, the extent of sintering would be limited resulting in a relatively weak agglomerate (4).

To account for the non-static condition of ash particles relative to one another a modification of the Frenkel model is used (4):

$$x^2 = f\left[\frac{1}{\gamma}, t_1, r, \frac{1}{\eta}\right]\frac{3\gamma t_2 4}{2\eta} \qquad (2)$$

where t_1 refers to the contact time and t_2 refers to time after the initial contact. The function term indicates that as the probability and extent of initial adhesion approaches zero (high surface tension) then the degree of sintering will approach zero. However, after t_1, the degree of sintering will follow the Frenkel model

(Equation 1). In the probability function surface tension is inversely related to rate, whereas, in the Frenkel model the rate is proportional to the surface tension. The reason for this is that at initial contact the higher the surface tension the less the liquid "wets" the adjacent surface. After the formation of a "neck" or liquid bridge between particles (after t_1) surface tension pulls the liquid material from the convex surface to the concave surface at the region of the neck. With increasing surface tension the force with which adhesion of the particles occurs increases. So the case is made that surface tension does initially affect the critical adhesion of particles in the agglomeration process. However, after adhesion, the rate of sintering is governed by the viscosity of the molten phases present on the particle surface.

EXPERIMENTAL

Ash samples used in both viscosity and surface tension determinations were produced from coal samples pulverized to -60 mesh and then ashed for three hours at 1000°C. Each sample was ashed in an oxidizing atmosphere and a reducing atmosphere of 8% hydrogen in nitrogen. The ash samples were then analyzed by X-ray fluorescence to determine bulk chemical composition.

A Haake RV-2 Rotovisco (rotating bob viscometer) unit was used for viscosity determinations. Each sample was heated to 1450°C and soaked for several to ensure complete melting. A cool down cycle was then initiated with readings taken every 10°C. The sample was equilibrated for 20 to 30 minutes at each temperature when viscosity measurements were made.

To determine surface tension a sessile drop method was used. A sample of ash was pressed into a pellet, weighed, and centered on a plaque of relatively nonreactive vitreous carbon. During heating a slag bead is formed upon melting of the ash pellet. The bead shape is determined by the surface tension forces between the liquid, gas, and solid phases. Therefore, the sessile drop technique requires geometric definition of the bead at any one temperature. The pellet image was photographed at 1000°C and 1200°C and then at 5°C intervals until the ash pellet was completely melted or a temperature of 1400°C was reached.

The computer method used to calculate surface tension was proposed by Maze and Burnet (5,6). The advantage of this technique is that a series of measurements from photographs are used to define the bead shape to calculate surface tension rather than relying on one measurement, as in the case of contact angle, thereby reducing measurement error. For a more detailed discussion of this technique refer to Miller (4) or Maze and Burnet (5,6).

RESULTS AND DISCUSSION

Relation of Viscosity to Atmosphere and Composition

Work conducted at the Bituminous Coal Research National Laboratory and the University of North Dakota Energy and Mineral Research Center (UNDEMRC) has shown that there are differences in slag behavior in oxidizing, reducing, and inert atmospheres (4). The results show that slag viscosity is decreased under reducing conditions and increases under oxidizing conditions as in the case of the Baukol-Noonan coal slag in Figure 2.

In general, ash melts can be classified as silicate melts. The compositional components can be described as follows: glass formers (SiO_2 and P_2O_5), modifiers (CaO, MgO, Na_2O, and K_2O), and amphoterics (Al_2O_3 and Fe_2O_3). Glass formers tend to enhance polymerization of the melt while modifiers tend to disrupt polymerization. The amphoterics can act either as glass formers or modifiers (4). For high-silica slags the important factor in determining viscosity is the ratio of SiO_2 to modifiers. Large amounts of network formers (silica) result in a higher degree of polymerization, a rapid rate of nucleation and crystallization. This behavior produces liquid phases having higher viscosities resulting in a decreased potential for sintering.

The viscosity behavior of low-silica slags is governed by the ratio of CaO to modifiers or alkalies. Alkalies tend to inhibit silica polymerization by weakening the bonds between silica tetrahedra. Alkalies, as modifiers, also increase the rate of crystal growth by reducing viscosity thereby permitting more rapid diffusion of ions to the crystal front. Such liquid phases of low viscosity present during the ash phase would increase the potential of sintering.

Viscosity tests where additions of calcium and sodium were made to intermediate to high-silica slags show a decrease in the viscosity at all temperatures. The result of decreasing viscosity of a liquid phase is to enhance the rate of sintering or potential for agglomeration of ash particles producing a liquid phase of high alkali composition.

Effect of Atmosphere on Surface Tension

Results from three different coal slag surface tension tests conducted under oxidizing and reducing atmospheres are illustrated in Figure 3. Each point is labeled to identify the coal slag and the atmosphere under which the test was performed: Gascoyne Red (GRR, GRO), Gascoyne Blue (GBR, GBO) and Beulah (BSR, BSO) where "O" refers to oxidizing and "R" refers to reducing conditions. The oxidizing and reducing tests for each slag are connected with a straight line. In general, the surface tension of a slag is greater in a reducing atmosphere versus an oxidizing atmosphere. In addition, the temperature at which the ash pellet becomes completely liquid is higher in oxidizing atmospheres than in reducing atmospheres. Assuming a constant composition, viscosity decreases under reducing environments while surface tension increases. Given these facts the potential for sintering is enhanced in reducing versus oxidizing environments.

Relation of Surface Tension to Composition and Viscosity and Its Effect on Sintering

As previously discussed, surface tension and viscosity are important in governing the rate of sintering and the tendency of particles to agglomerate. Both surface tension and viscosity decrease with temperature while the rate of sintering increases (Figure 1). However, the rate of sintering shows an inverse relationship with viscosity and direct relationship with surface tension (Equation 2). Therefore, it is necessary to determine how viscosity and surface tension change relative to one another with changes in temperature and composition.

A series of fifteen low-rank coal slags were studied as to viscosity, surface tension, and bulk composition as shown in Table 1. Of particular interest is the relationship of silica and sodium oxide to surface tension because of their prevalence in coals, agglomerates, and ash deposits, and their effect on viscosity. While fouling tendency may not be considered to be a rigorous measure of sintering it has some merit in this study. The adhesion and sintering of ash particles in a fouling deposit is produced under dynamic conditions where the relative motion of ash particles occurs along with impaction. As discussed earlier, the process of sintering begins when particles collide and adhere to each other. Therefore the initial adhesion of particles is an important step in initiating sintering. In a standard sintering test, the ash particles are packed and heated in a static conditions where no consideration of relative motion or impaction of ash particles occurs. Ashes which tend to agglomerate are designated with an "-H" or "-M" for high or moderate agglomerating tendency, respectively. Ashes which displayed a low tendency to foul or agglomerate are designated with an "-L". The classification is qualitative and determined by pilot-scale combustion and deposition results.

In general, slags having higher silica content tend to have higher surface tension while slags high in sodium content have lower surface tensions. Figure 4 is a plot of the ratio of the mole fraction of SiO_2 to Na_2O as a function of surface tension. There is a separation between those ashes which have a lower tendency to agglomerate and those ashes which tend to agglomerate. This data along with viscosity data suggests that increased silica oxide content increases both surface tension and viscosity. An increase in sodium oxide content decreases both viscosity and surface tension. Figure 4 shows those coals characterized as low agglomerating ashes having increased silica content and higher surface tensions. Conversely, coals with increased sodium content have lower surface tension but have increased fouling and agglomerating tendency. These results seem to be contrary to the relations in Equation 1. Therefore the effect on sintering due to compositional variations must be due to the relative change in surface tension and viscosity with composition.

To determine the relationship of surface tension and viscosity as it varies with composition it was decided to use a combination of experimental surface tension data with calculated viscosity values. The following assumptions were made in the Frenkel model:

- The particle radius (r) and time (t_2) were assumed to be constant. Therefore x^2 is proportional to $\gamma\eta$.
- A modified version of the Urbain equation developed by Kalmanovitch (7) was used to calculate the viscosity of the molten phases at the temperature at which each surface tension measurement was taken. The equation used was based on its successful application in predicting viscosities in previous studies (4).

In Figure 5 a plot of the calculated viscosities versus surface tension reveals some separation of low- and high-fouling coals. In general, the ratio of surface tension to viscosity is related to sintering potential (Equation 2). Those ashes observed to have low agglomerating behavior have low surface tension to viscosity ratios. Those ashes which tend to exhibit agglomeration have larger surface tension to viscosity ratios.

CONCLUDING REMARKS

The discussion here suggests the following relationships:

- Slag viscosity decreases while surface tension increases under a reducing atmosphere. The net result is increased sintering potential of an ash in a reducing versus oxidizing environment
- An increased silicon dioxide content increases the viscosity of a slag at a greater rate than the surface tension of the slag. The net result is reduced sintering.
- An increased sodium oxide content (possibly total alkali content) decreases the viscosity of a slag at a greater rate than the slag surface tension. The net result is an increase in sintering.
- Those ashes which tend not to sinter or agglomerate form molten phases which have higher viscosities relative to their surface tension at a given temperature and those ashes which tend to agglomerate form molten phases which have lower viscosities relative to their surface tension at a given temperature.

REFERENCES

1. Kuczynski, G.C. 1949. J. Metals, 169.
2. Kuczynski, G.C. 1977. J. Science Sintering, 243.
3. Raask, Erich. 1985. Mineral Impurities in Coal Combustion. Hemisphere Pub. Corp., Washington, 484pp.
4. Miller, S.F. 1987. Ash and Slag Characterization Final Technical Report (1986-1987), University of North Dakota Energy and Mineral Research Center to the U.S. Department of Energy, Cooperative Agreement No. DE-FC21-85MC10637, 53pp.
5. Maze, C. and G. Burnet. 1969. Surface Science, 13, 451.
6. Maze, C. and G. Burnet. 1971. Surface Science, 24, 335.
7. Kalmanovitch, D.P. and M. Frank. 1988. Engineering Foundation Conference on Mineral Matter and Ash in Coal, Santa Barbara, February 1988.

ACKNOWLEDGEMENTS

This work is funded under DOE Cooperative Agreement No. DE-FC21-85MC10637 at the University of North Dakota Energy and Mineral Research Center (UNDEMRC). The authors wish to thank Dr. Steve Benson, Research Supervisor, Combustion Studies, UNDEMRC Combustion and Environmental Research Institute for his comments and Julie Weinmann for conducting surface tension tests.

Table 1. Chemical Composition of Sample Coal Slags (Analysis by X-Ray Fluorescence)

Coal	ID	Oxide Weight Percent									
		SiO_2	Al_2O_3	Fe_2O_3	TiO_2	P_2O_5	CaO	MgO	Na_2O	K_2O	SO_3
Beulah High Sodium	BH	16.4	12.7	12.9	1.3	1.7	27.0	8.6	19.4	0.0	0.0
Beulah Low Sodium	BL	24.3	16.4	21.2	1.1	1.2	21.2	10.1	4.0	0.3	0.0
Gascoyne Blue	GB	28.8	16.5	5.3	0.0	0.0	22.5	10.7	8.9	0.5	0.0
Gascoyne Red	GR	37.0	12.5	9.6	0.0	0.0	27.0	9.9	3.5	0.6	0.0
Indianhead	IH	33.8	20.9	10.0	0.9	0.3	20.2	4.9	2.8	0.9	5.2
Indianhead	IHO	36.0	22.1	2.8	1.2	0.1	24.0	5.8	1.9	0.9	5.2
Martin Lake	ML	32.9	17.2	7.5	1.7	0.0	25.8	6.2	4.5	0.4	3.8
Martin Lake	MLO	33.3	19.0	10.4	1.2	0.0	24.9	5.9	1.5	0.4	3.3
Pittsburgh 8	P8	46.0	21.8	20.3	1.2	0.3	5.4	1.1	0.0	2.4	1.5
Pittsburgh 8	P8O	49.4	20.6	17.8	1.3	0.2	5.1	1.1	0.0	2.7	1.7
Rosebud McKay	RM	41.3	24.3	6.4	1.5	0.8	18.2	6.7	0.8	0.0	0.0
Velva	VE	23.6	11.4	7.9	0.9	0.4	35.9	9.8	1.6	0.2	8.4
Velva	VEO	24.7	22.8	7.4	0.7	1.1	20.2	5.1	3.2	0.6	14.3
Wyodak	WY	46.8	23.4	3.3	1.6	0.5	15.0	3.4	1.0	0.4	4.5
Wyodak	WYO	41.2	20.0	4.6	2.0	0.8	24.1	5.3	1.0	0.5	0.5

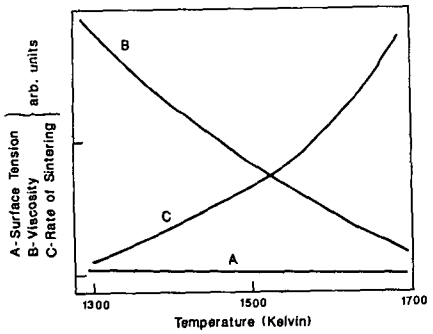

$$x^2 = \frac{3r\gamma t}{2\eta}$$

where x = radius of the interface assumed to be circular
r = radius of the spherical particles
γ = surface tension
t = time
η = viscosity

Figure 1. Relation of Surface Tension and Viscosity to Sintering as a Function of Temperature

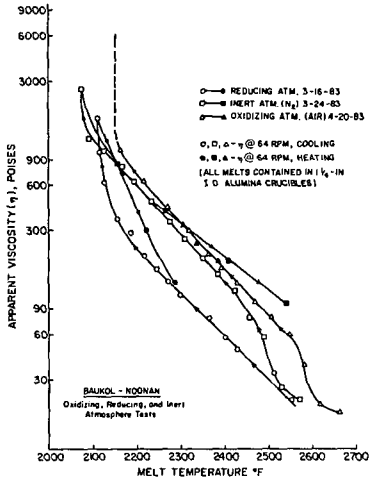

Figure 2. Effect of Atmosphere on Boukol-Noonan Slag Viscosity

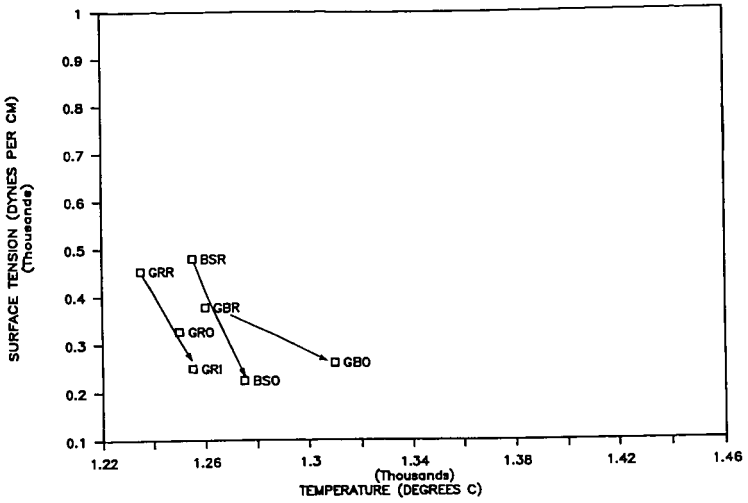

Figure 3. Effect of Atmosphere on Slag Surface Tension

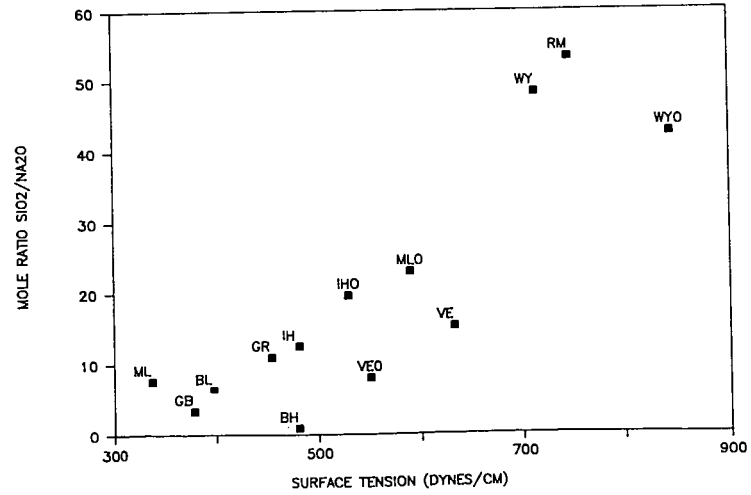

Figure 4. Coal Slag Surface Tension Versus Mole Ratio SiO_2/Na_2O.

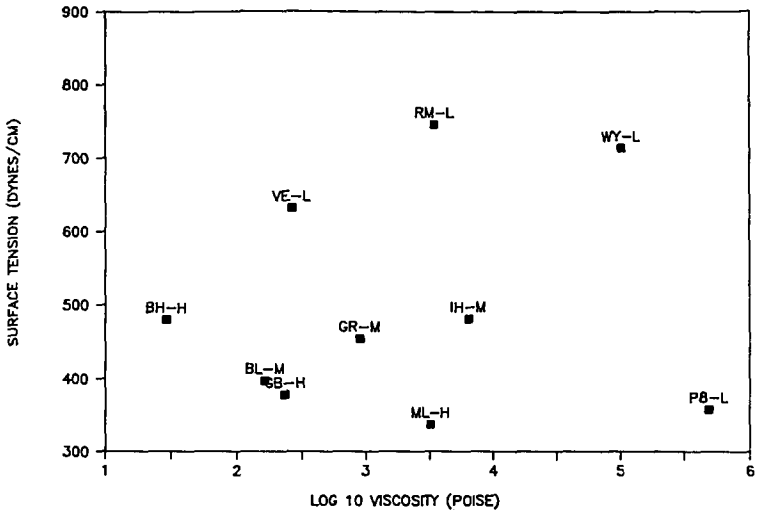

Figure 5. Calculated Viscosity (Log 10 η) Versus Measured Surface Tension

Crystallization in Coal Ash Slags and Its Effect on Slag Strength

Steven A. Benson* and Leonard G. Austin

The Pennsylvania State University
108 Steidle Building
University Park, PA

INTRODUCTION

An understanding of the crystallization behavior of coal ash melts can provide insight into slag flow behavior and the development of ash deposit strength. Past studies have shown that both the strength and crystallization behavior of coal ash pellets during sintering experiment varies dramatically from one coal to another (1). Tangsathitkulchai (1) showed that the development of strength for selected bituminous ash pellets increased to a maximum and then decreased with increasing temperature. The decrease in strength was attributed to a high degree of crystallization. The formation of the crystals was thought to change the physical properties of the pellet, thereby lowering the strength. Tangsathitkulchai found that lower ranked coal ashes exhibited a quite different behavior. These ashes exhibited a high degree of crystallization at lower temperatures and the strength appeared to increase with the degree of crystallization. In addition, no maximum in strength with temperature was found.

Kalmanovitch (2) has shown the crystallization of specific components from coal ash melts changes the composition of the residual liquid phase. Therefore, the residual liquid phase in the deposit is more ilkely to be responsible for the sintering of the ash components. This may explain the differences in ash behavior noted by Tangsathitkulchai. Kalmanovitch was able to estimate the slagging propensities of coal ashes based on the nature of the residual liquid phases as a result of crystallization of the primary components.

The formation of tenacious deposits during the combustion of western U.S. coals has been correlated with the formation of crystalline alkali and alkaline earth aluminosilicates (3,4,5). It was suggested by these investigators that the key in understanding the depositional processes related to these coals is to determine the mechanism of formation of these phases.

In this paper, low-rank coals from the U.S. were combusted and deposits were formed in a laboratory scale laminar flow tube furnace. This system has been used to evaluate the fundamentals of coal ash deposition relative to utility boilers (6,7,8,9,10). In this test a thin ray of pulverized coal is burned in a tube furnace heated to simulate the temperature history of a utility boiler. To form a deposit, the fly ash is accelerated through a simple ceramic nozzle to a velocity similar to that in a boiler. The resultant fly ash is then impacted on an oxidized steel substrate held at a controlled temperature similar to that of a boiler steel surface. A coal feed rate of about one-third of a gram per minute is sufficient to

* Presently at the University of North Dakota Energy & Mineral Research Center, Box 8213, University Station, Grand Forks, ND 58202

build a deposit within 30 minutes. The resulting deposits were examined to determine rate of growth, strength, and microstructural features.

The results presented in this paper are for deposits formed from selected western U.S. coals under simulated slagging conditions. The deposits were characterized in detail using x-ray diffraction and scanning electron microscopy and electron microprobe analysis (SEM-EDS) to determine the distribution of crystalline and amorphous phases. The distribution of these phases are compared to the strength of the deposits formed.

EQUIPMENT AND PROCEDURES

The test apparatus is shown in detail in Figure 1. The main furnace tube of 99.8 % fused alumina (6.35 cm internal diameter and 90 cm long) has a maximum heated length of 50 cm. The tube is heated by three tangentially-fired natural gas-air burners and the temperature is controlled by adjusting the air-to-fuel ratio. The injector and secondary air preheat section is located at the top of the furnace. The secondary air is preheated to approximately 900^{o}C before entering the main furnace which was at 1500^{o}C for these tests. In addition, the preheat/injector system is equipped with a flow straightener which evenly distributes the secondary air across the muffle tube cross-section. Depending upon the coal, the total air flow is between 3-4 L/min with a coal feed rate of 0.25-0.40 g/min. Estimated particle residence times within the furnace are between 1 and 2 seconds. At the exit of the furnace the gas stream and fly ash are accelerated by a ceramic nozzle to approximately 4 m/sec prior to impingement on a boiler steel substrate held at a controlled temperature as shown in Figure 2. The gas temperature at the ceramic nozzle was approximately 1260^{o}C. The temperature of the boiler steel substrate was held at 500^{o}C.

A device was developed to measure the strength of deposits after they were removed from the test furnace. It consists of two primary components as shown in Figure 3, a miniature horizontal translator and a miniature pressure transducer. The output of the transducer is read from a strain and transducer indicator and has maximum value of 5.5 MPa (750 psi). The strength of ash deposits was determined by compressing them between the end of a steel rod and a stationary aluminum block. The deposits from the tube furnace are quite small (approximately 20 mm high and 5 mm in diameter) and strength measurements can be made at 3 mm intervals.

The deposits were examined to determine the variations in crystalline and amorphous phases. Bulk deposits were sectioned and ground for x-ray diffraction analysis to identify the crystalline phases. Deposits were also mounted in epoxy, allowed to harden, cross-sectioned, and polished for scanning electron microscopic examination. Both secondary and backscattered electron imaging were used to examine the morphology of the deposit cross-sections. Quantitative elemental analysis of specific regions within the deposits were performed with an energy dispersive x-ray detector.

RESULTS AND DISCUSSION

The coals combusted included two lignites from the Gascoyne mine of North Dakota and a subbituminous from the Wyodak mine of Wyoming. The analysis of these coals are summarized in Table 1.

The deposits formed from these coals were lightly sintered near the base of the deposit at the deposit substrate interface. As the deposit grew in the direction of the oncoming gas stream more sintering and fusing occurred as a result of higher temperatures. In some instances the tops of the deposits appeared to have been molten.

The compressive strength of the deposits were measured from the base to the top of the deposit. Figure 4 illustrates the deposit strength versus height measured for the ash deposits produced from the three coals. The Gascoyne Blue deposit exhibited the greatest strength lower in the deposit as compared to the others. The Gascoyne White and the Wyodak deposits had very similar strengths but were weaker than the Gascoyne Blue.

The crystalline phases common to these deposits and their chemistries are listed in Table 2. The crystalline phases identified in the deposit sections are summarized in Table 3. The distribution of phases are listed in order of decreasing abundance based on the intensity of the x-ray peaks. The abundance designation is only an estimate.

The crystalline phases identified in the top portions of the Gascoyne Blue and Wyodak deposits consist mainly of complex alkali and alkaline earth aluminosilicates such as melilite and pyroxene. The top portion of the Gascoyne White deposit contained mostly amorphous material or glass. This may be due to the lower relative calcium content found in the ash of this coal. The calcium will act as a network modifier that can break up the glass network and aid in crystallization. In general, the base layer of the deposits, closest to the cooled steel substrate, contain lower quantities of the crystalline alkali and alkaline earth elements. The crystalline phases present in the base layers consist mostly of simple oxides such as quartz, lime, periclase and hematite. The silicates and aluminosilicates are in an amorphous form. The distribution of crystalline phases found in the base layer is similar to those found in fly ash.

SEM-EDS analysis was used to examine the microstructure of polished deposit cross-sections. Backscatterd electron imaging was used to distinguish between the crystalline and glassy phases. Analysis of points and areas were performed to determine the composition of the glass and crystalline phases in the melts.

Figure 5 is a backscattered electron image of a region near the top of the Gascoyne White deposit. The important features of the figure to note are the following: the deposit contains abundant glass material with small crystals growing within the glassy matrix, numerous partially reacted quartz grains, and that the crystals appear to nucleate from regions that appear bright. These bright regions contain high levels of iron as shown by the analysis of point 1 in Table 4. Point 2 has slightly lower iron content. These crystals are probably melilite based on their morphology and the x-ray diffraction analysis. The region that appears to be glass is quite homogeneous. A typical analysis of this region is point 3 in Table 4. The glass phase is very rich in sodium as compared to the crystalline phases.

SEM-EDS examination of the Gascoyne Blue deposit cross-section indicated more crystalline phases than glass material near the top. Figure 6 is a backscattered electron image of a selected area. The area is highly crystalline consisting mostly of melilite and some pyroxene crystalline phases. The materials surrounding the crystals appear to be the glass phase. The crystals found in this deposit were about twice the size of those found in the Gascoyne White deposit. Point analyses

were performed on the crystals and glass material shown in Table 5 by analysis 1 and 2, respectively. As can be seen by the analysis sodium was found to be concentrated in the glass and not in the crystals.

Figure 7 is a backscattered electron image of region near the top of the Wyodak deposit polished cross-section. The deposit appears to very dense and crystalline. There are several types of crystalline phases present in the deposit. The darker crystals have lower concentrations of iron and calcium. These may be plagioclase crystals. The brighter crystals observed are probably melilite. The crystal growth was very dense and a good analysis of the glass phase was difficult. The composition of these crystals are listed in Table 6. This coal was very low in sodium content, but formed a strong highly-crystalline ash deposit. Besides the low-sodium content, the only difference between the Wyodak and Gascoyne coals is the Si/Al molar ratio. The high strength exhibited by this deposit may be due to the interaction of calcium with the aluminosilicates to form a low melting-point phase.

The characteristics of the residual liquid phase after crystallization of the primary phases may influence the strength of these deposits. This is evident by the high concentrations of sodium in the glass or amorphous phase. Sodium containing phases have been identified as one of the primary causes of ash deposition in utility boilers firing Western coals (5). The sodium in the amorphous phase probably decreases its viscosity allowing continued sintering after crystallization has taken place.

SUMMARY AND CONCLUSIONS

The melting and sintering of deposited ash material rich in alkali and alkaline earth elements results in the formation of highly crystalline deposits. The crystalline phases identified include melilite, plagioclase, and pyroxene.

The crystallization of components appears to be most pronounced when the ash is rich in sodium and calcium. Detailed characterization of deposit cross-sections indicates a partitioning of elements between the crystalline and glass phases. In both deposits from the Gascoyne lignite sodium was found to be concentrated in the glass phase.

The deposit formed from the Wyodak coal was highly crystalline and developed a high strength. This coal did not contain very high sodium content. The only other difference between this coal and the lignites is the Si/Al molar ratio. The available calcium in the ash may have interacted with the aluminosilicate to form a low-melting point phase that allowed sintering to take place.

The residual liquid phase after crystallization may be responsible for the development of deposit strength, and deposit growth. Therefore, the relative amounts of glass and crystalline phases formed in deposits are important parameters that affect deposit strength and growth.

REFERENCES

1. Tangsathikulchai, M., "Studies of the Initiation, Growth and Sintering in the Formation of Utility Boiler Deposits," Ph.D. Thesis, The Pennsylvania State University, 1986.

2. Kalmanovitch, D.P., "Reactions in Coal Ash Melts," Ph.D. Thesis, Imperial College University of London, 1983.

3. Sondreal, E.A., Tufte, P.H., and Beckering, W., "Ash Fouling in the Combustion of Low-Rank Western U.S. Coals," Combustion Science and Technology, 16, 95, 1977.

4. Rindt, D.K., Selle, S.J., and Beckering, W., "Investigations of Ash Fouling Mechanisms for Western Coals using Microscopic and x-ray Diffraction Techniques," ASME, Paper No. 79-WA/CD-5, 1979.

5. Rindt, D.K., Jones, M.L., and Schobert, H.H., "Investigations of the Mechanism of Ash Fouling in Low-Rank Coal Combustion," in Fouling and Slagging from Mineral Impurities in Combustion Gases, R.W. Bryers, Ed., p17-36, 1983.

6. Abbott, M.F., and Austin, L.G., "A Study of Slag Deposit Initiation in a Drop Tube Type Furnace," in Mineral Matter and Ash in Coal, K.S. Vorres, Ed., ACS Symposium Series, No. 301, American Chemical Society, Washington, D.C., p325-352, 1986.

7. Tangsathitkulchai, M. and Austin, L.G., "Studies of Boiler Slag Deposit Formation Using a Laboratory Furnace: Part 1. Preliminary Results," ASME Paper No. 85-JPGC-Pwr-45, 1985.

8. Benson, S.A., Tangsathitkulchai, M. and Austin, L.G., "Studies of Ash Deposit Formation Using A Laboratory Furnace," Second Annual Pittsburgh Coal Conference, 689-694, 1985.

9. Austin, L.G., Benson, S.A., and Schobert, H.H., "Description of the Growth of Slag Deposits in an Accelerated Laboratory Test," Sixth International Coal Liquids and Alternative Fuels Technology Workshop, Halifax, Nova Scotia, September 1986.

10. Conn, R.E., Benson, S.A., and Austin, L.G., "Laboratory Coal Ash Slagging and Fouling Studies at Simulated Utility Boiler Conditions," ASME Paper No. 87-JPGC-FACT-6, 1987.

Table 1. Coal and ash analysis (all data on a dry basis except for the moisture determination).

	Gascoyne White	Gascoyne Blue	Wyodak
Proximate, wt %			
Moisture	30.0	24.6	30.4
Volatile Matter	41.6	47.5	43.8
Fixed Carbon	41.3	42.3	47.7
Ash	17.2	10.2	8.3
Ultimate, wt %			
Carbon	57.0	63.1	67.4
Hydrogen	3.8	4.2	4.8
Nitrogen	0.9	1.0	1.0
Oxygen (diff.)	19.7	20.1	17.8
Sulfur	1.3	1.2	0.7
Calorific Value (BTU/lb)	9649	10484	11818
Ash Composition, wt % as equivalent oxide			
SiO_2	49.9	22.5	23.8
Al_2O_3	12.0	9.7	14.8
Fe_2O_3	3.0	5.0	6.6
TiO_2	1.4	5.0	1.2
P_2O_5	0.8	0.7	1.5
CaO	12.4	24.3	22.8
MgO	4.1	8.2	5.9
Na_2O	3.5	6.9	0.7
K_2O	0.8	0.1	0.3
SO_3	12.2	21.9	22.4
Si/Al Molar Ratio	3.5	2.0	1.4

Table 2. Chemistry of crystalline phases identified by x-ray diffraction.

Phase	Chemistry
Melilite (solid solution series)	
Gehlenite	$Ca_2Al_2SiO_7$
Soda melilite	$NaCaAlSi_2O_7$
Akermanite	$Ca_2MgSi_2O_7$
Pyroxene (solid solution series)	
Augite	$(Ca,Na)(Mg,Fe,Al)(Si,Al)_2O_6$
Diopside	$CaMgSi_2O_6$
Plagioclase (solid solution series)	
Albite	$NaAlSi_3O_8$
Anorthite	$CaAl_2Si_2O_8$
Spinel	Fe_3O_4 - $MgFe_2O_4$
Hematite	Fe_2O_3
Lime	CaO
Periclase	MgO
Quartz	SiO_2
Anhydrite	$CaSO_4$

Table 3. Crystalline phases identified in the deposits using x-ray diffraction (phases listed in order of decreasing abundance).

Deposit location	Gascoyne White	Gascoyne Blue	Wyodak
Top half	major: quartz amorphous	major: melilite minor: pyroxene trace: quartz	major: melilite quartz trace: plag* pyroxene spinel hematite periclase
Lower half	major: quartz melilite pyroxene minor: spinel	major: melilite quartz minor: periclase hematite pyroxene	major: melilite quartz trace: $Ca_3Al_2O_6$ periclase lime
Base	major: quartz minor: melilite periclase hematite	major: periclase hematite lime minor: melilite quartz amorphous	major: lime periclase quartz minor: $Ca_3Al_2O_6$ trace: anhydrite melilite

* plag -- plagioclase (anorthite).

Table 4 EDS analyses of selected points located in Figure 5. (Wt. % as equivalent oxide)

Oxide	1	2	3 (Glass)
SiO_2	23.9	26.9	59.7
Al_2O_3	10.5	13.5	10.2
Fe_2O_3	44.6	34.5	0.9
TiO_2	0.6	2.6	3.1
P_2O_5	0.0	0.0	0.0
CaO	12.6	13.9	16.4
MgO	6.5	6.0	2.5
Na_2O	0.9	1.1	5.3
K_2O	0.1	0.1	0.5
SO_3	0.2	0.3	0.2
Si/Al molar ratio	1.9	1.7	5.0

Table 5 EDS analyses of selected points in Figure 6. (Wt. % as equivalent oxide)

Oxide	1 (Crystal)	2 (Glass)
SiO_2	47.5	54.3
Al_2O_3	9.8	13.0
Fe_2O_3	8.9	3.7
TiO_2	1.0	0.5
P_2O_5	0.0	0.0
CaO	25.4	21.4
MgO	6.1	0.9
Na_2O	0.8	5.2
K_2O	0.3	0.1
SO_3	0.1	0.0
Si/Al molar ratio	4.1	3.6

Table 6 EDS analyses of selected points in Figure 7.
(Wt. % as equivalent oxide)

Oxide	Bright Crystals	Darker Crystals
SiO_2	41.8	50.8
Al_2O_3	17.2	27.5
Fe_2O_3	7.8	1.4
TiO_2	2.0	0.0
P_2O_5	1.4	0.0
CaO	24.9	18.6
MgO	4.1	0.4
Na_2O	0.4	0.6
K_2O	0.1	0.2
SO_3	0.3	0.2
BaO	0.0	0.4
Si/Al molar ratio	2.1	1.6

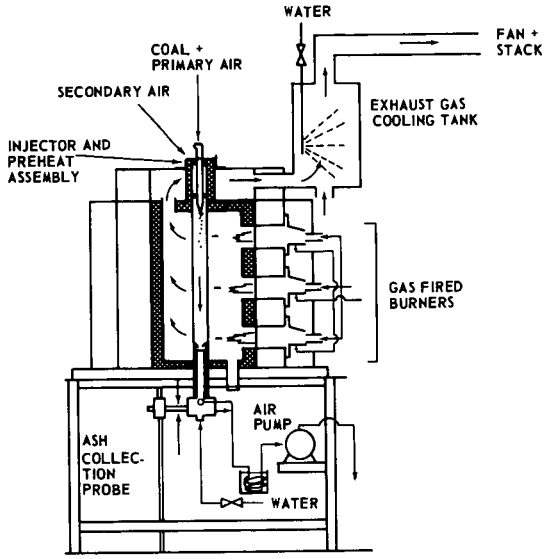

Figure 1. Laminar flow tube furnace system.

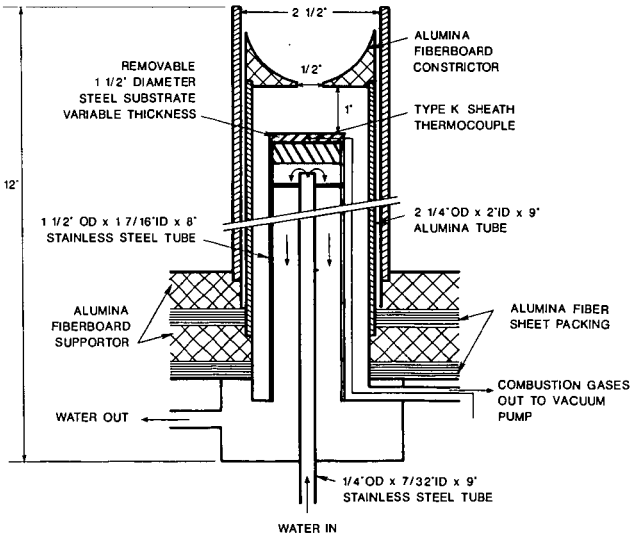

Figure 2. Base of main furnace containing the ceramic nozzle (constrictor) and ash deposition probe.

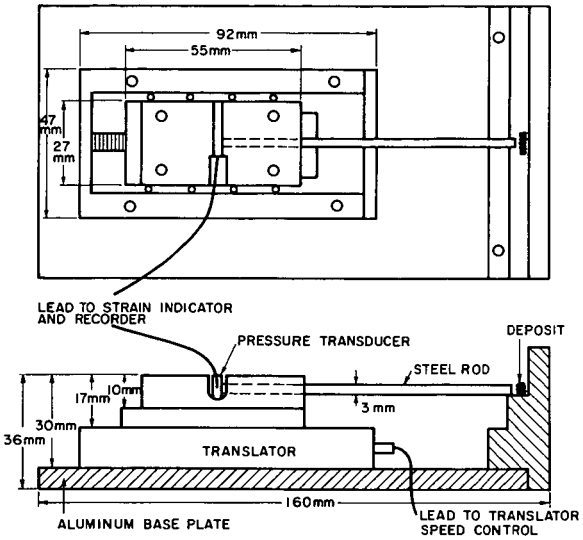

Figure 3. Deposit strength measuring device.

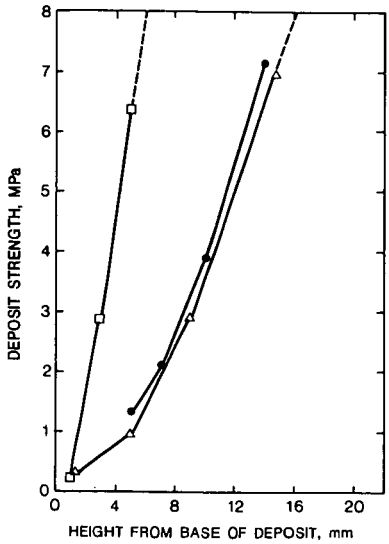

Figure 4. Deposit strength versus height for deposits formed in the laboratory scale furnace (◻ Gascoyne Blue, △ Gascoyne white, and ● Wyodak).

Figure 5. Backscatter electron image of a polished section of Gascoyne White lignite deposit at 8.1 mm from the base of the deposit.

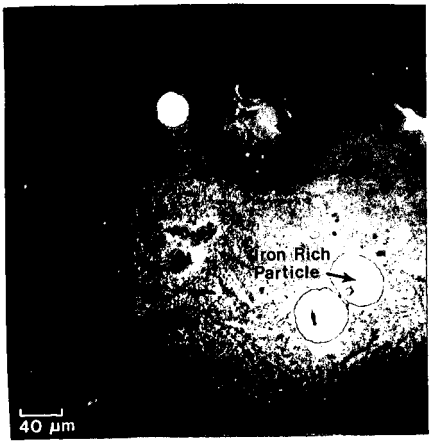

Figure 6. Backscatter electron image of a polished section of a Gascoyne Blue lignite deposit at 14 mm from the base.

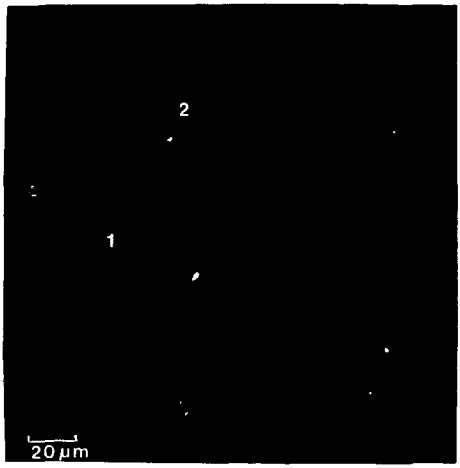

Figure 7. Backscatter electron image of polished sections of subbituminous coal deposits. A) Rosebud, B) Wyodak.

EVALUATION OF COAL-MINERAL ASSOCIATION AND COAL CLEANABILITY BY USING SEM-BASED AUTOMATED IMAGE ANALYSIS

W. E. Straszheim, K. A. Younkin, R. Markuszewski and F. J. Smit[1]

Ames Laboratory, Iowa State University, Ames, Iowa 50011 and
[1]AMAX Research and Development Center, Golden, Colorado, 80403

ABSTRACT

A technique employing SEM-based automated image analysis (AIA) has been developed for assessing the association of mineral particles with coal, and thus the cleanability of that coal, when the characteristics of the separation process are known. Data resulting from AIA include the mineral distribution by particle size, mineral phase, and extent of association with coal. This AIA technique was applied to samples of -325 mesh (-44 μm) coal from the Indiana No. 3, Upper Freeport, and Sunnyside (UT) seams. The coals were subjected to cleaning by float-sink separations at 1.3, 1.4, 1.6, and 1.9 specific gravity and by froth flotation. For the three coals, the float-sink procedure at a given specific gravity produced different amounts of clean coal, but with similar ash content. Froth flotation removed much less ash, yielding a product ash content of ~8% for the Upper Freeport coal, regardless of recovery, while reducing the ash content to less than 5% for the other two coals. The AIA results documented significantly more association of minerals with the Upper Freeport coal, which thus led to the poor ash reduction.

INTRODUCTION

The task of removing mineral matter from coal is greatly aided by a thorough characterization of the distribution and/or association of mineral and coal particles. Conventional characterization, based on laboratory float-sink and froth flotation tests at different sizes and conditions, is cumbersome and does not generally lead to any clear understanding of coal-mineral matter associations.

SEM-based automated image analysis (AIA) has unique capabilities for analyzing mineral particles in-situ for the important characteristics of size, phase, and association with the coal matrix. These AIA techniques have previously been applied to the determination of mineral matter size and phase distributions in coal (1-3) and are now being extended to the measurement of association. This work describes our application of AIA to characterize the association of minerals with coal and to correlate the AIA results with those of conventional tests such as float-sink separation and froth flotation.

EXPERIMENTAL

Coals

The characteristics of the three coals used in this study are presented in Table 1. The coals had been precleaned and ground to pass a 325 mesh screen. Since the conventional analyses give values for ash, whereas AIA provides results in terms of mineral matter, low temperature ash values were also obtained for easier comparison with AIA measurements.

Table 1. Characteristics of the three coals used (results are expressed as % of dry coal)

	Indiana No.3	Upper Freeport	Sunnyside
Proximate Analysis			
Ash	7.35	9.88	5.19
Volatile Matter	40.67	26.02	38.54
Fixed Carbon	51.98	64.10	56.19
Forms of Sulfur			
Total	4.26	1.56	0.61
Pyrite	2.23	0.95	0.05
Sulfate	0.07	0.01	0.00
Low Temperature Ash	10.5	12.5	6.1

Cleaning tests at AMAX

The coals were subjected to float-sink separations at the specific gravities (sp. gr.) of 1.3, 1.4, 1.6, and 1.9, and samples from each incremental sp. gr. range were weighed and analyzed. Another set of samples was subjected to froth flotation in an automated Denver batch cell, using 28 ppm MIBC and 0.54-1.92 ml kerosene per kg of coal. Froth was collected after 1.5, 3, 6, 12, and 24 minutes, and the remaining unfloatable material (tailings) was also collected for analysis.

SEM-based image analyses at Ames Lab

Samples of coal were embedded in carnauba wax, and a cross section was prepared for analysis as described previously (4). The AIA system included a JEOL JSM-U3 electron microscope, a Tracor-Northern TN-2000 energy-dispersive x-ray analyzer, and a LeMont Scientific DB-10 image analyzer. Samples were examined at magnifications of 300-400 diameters using an accelerating voltage of 25 kV and a beam current of 1-2 nA.

Software from LeMont Scientific was used to distinguish coal and mineral features from the background and from each other based on the brightness of their backscattered electron signal. Area and perimeter were measured for each feature, along with the fraction of perimeter in contact with each of the adjoining phases. Mineral particles were identified from the relative intensities of the characteristic x-ray emissions. X-rays were collected for 4 seconds per particle at a nominal rate of 500 counts per second. Data for contiguous features (i.e., with shared boundaries between coal and mineral matter) were grouped together so that the characteristics of the composite features could be determined.

RESULTS AND DISCUSSION

Conventional cleaning studies

The results of the float-sink separations are presented in Table 2. Data are presented for both the incremental fractions and for the cumulative fraction lighter than the indicated specific gravity. Plots of recovery and cumulative ash content are shown in Figure 1.

Table 2. Float-sink results for three coals (results are expressed as % of dry coal)

Sp. Gr.		Incremental			Cumulative		
Sink	Float	Weight	Ash	S(tot)	Weight	Ash	S(tot)
			Indiana No. 3 Coal				
	1.30	24.0	1.09	2.31	24.0	1.09	2.31
1.30	1.40	64.5	3.23	2.45	88.5	2.65	2.41
1.40	1.60	4.7	15.86	4.52	93.2	3.32	2.52
1.60	1.90	1.5	29.14	7.34	94.7	3.72	2.59
1.90		5.3	64.32	32.47	100.0	6.95	4.18
			Upper Freeport Coal				
	1.30	7.1	0.98	0.71	7.1	0.98	0.71
1.30	1.40	70.1	2.60	0.75	77.2	2.45	0.75
1.40	1.60	12.9	12.21	1.03	90.1	3.85	0.79
1.60	1.90	3.8	31.77	1.49	93.9	4.98	0.82
1.90		6.1	70.94	10.78	100.00	8.99	1.42
			Sunnyside Coal				
	1.30	23.6	0.57	0.57	23.6	0.57	0.57
1.30	1.40	67.1	1.66	0.57	90.7	1.38	0.57
1.40	1.60	5.4	13.82	0.54	96.1	2.07	0.57
1.60	1.90	0.8	38.26	0.48	96.9	2.37	0.57
1.90		3.1	81.10	0.67	100.0	4.85	0.57

As expected, the ash contents were relatively similar for the three coals for the same incremental specific gravity fraction. However, since the weight distribution among the fractions varied between the coals, the ash content of the cumulative fractions also varied somewhat between the coals.

The curves in Figure 1 indicate that the recoveries were similar for the Indiana No. 3 and Sunnyside coals. This suggests comparable coal-mineral association for these coals, provided that their mineralogical properties are similar. The recovery was notably lower for the Upper Freeport coal. Much more sample was found in the 1.4-1.9 specific gravity range (as seen from Table 2). This resulted in a higher ash content for the 1.6 and 1.9 sp. gr. float product.

Results of the froth flotation tests are shown in Table 3 and Figure 2. The recovery curves for all three coals flattened out after about 6 minutes collection time. The Upper Freeport coal appears to have been more responsive to the froth flotation, showing more recovery at shorter times. However, this reflects more the hydrophobicity of the coal than the degree of association of the mineral matter with the coal.

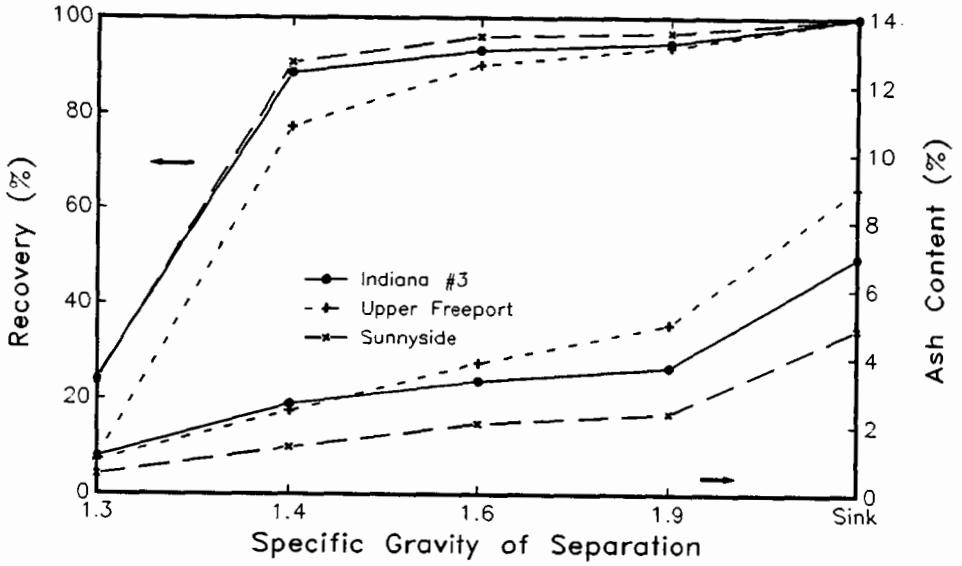

Figure 1. Recovery and ash content as a function of the specific gravity of float-sink separations

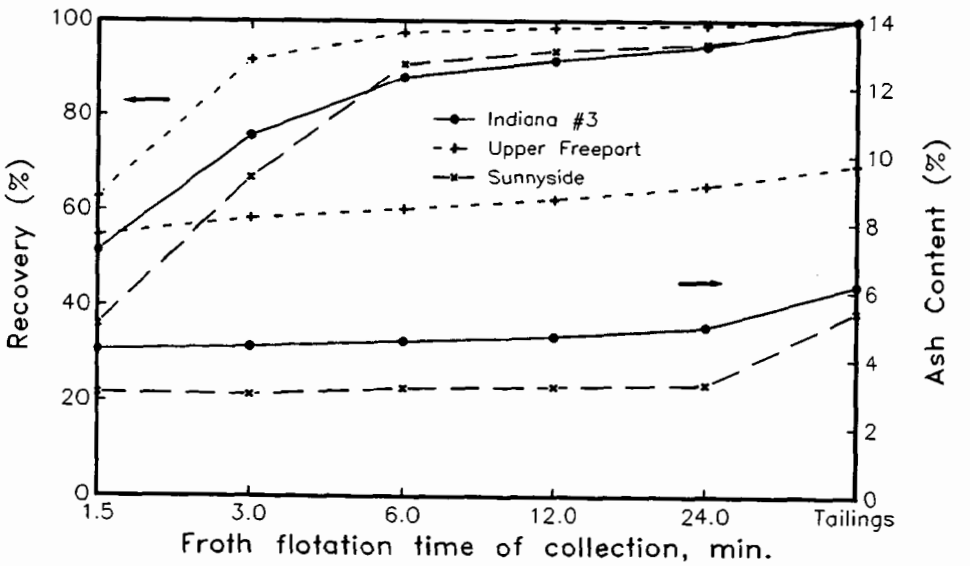

Figure 2. Recovery and ash content as a function of flotation time

Table 3. Froth flotation results for all three coals using 28 ppm MIBC and differing ml of kerosene per kg of coal (results are expressed as % of dry coal)

Flotation Time, Total Minutes	Incremental Float Product			Cumulative Float Product		
	Weight	Ash	S(tot)	Weight	Ash	S(tot)
Indiana No. 3 coal(using 1.92 ml kerosene)						
1.5	51.5	4.30	3.34	51.5	4.30	3.34
3.0	24.2	4.58	3.26	75.7	4.39	3.31
6.0	12.3	5.53	3.49	88.0	4.55	3.34
12.0	3.6	8.27	4.04	91.6	4.69	3.37
24.0	3.0	13.23	5.06	94.6	4.97	3.42
Tailings	5.4	27.62	8.78	100.0	6.19	3.71
Upper Freeport coal (using 0.54 ml kerosene)						
1.5	62.8	7.66	1.36	62.8	7.66	1.36
3.0	28.9	9.29	1.53	91.7	8.17	1.41
6.0	5.9	12.59	1.83	97.6	8.44	1.44
12.0	1.0	36.25	4.27	98.6	8.73	1.47
24.0	0.6	77.86	8.46	99.2	9.12	1.51
Tailings	0.8	85.65	9.17	100.0	9.74	1.57
Sunnyside coal (using 0.55 ml kerosene)						
1.5	36.0	3.03	0.56	36.0	3.03	0.56
3.0	30.9	2.95	0.58	66.9	2.99	0.57
6.0	23.9	3.67	0.57	90.8	3.17	0.57
12.0	2.8	4.59	0.59	93.6	3.21	0.57
24.0	1.5	7.37	0.58	95.1	3.28	0.57
Tailings	4.9	46.93	0.63	100.0	5.41	0.57

From Figures 1 and 2, it is also evident that much less ash reduction was achieved by froth flotation than by float-sink separation for all three coals. Since froth flotation is a surface-sensitive process, small amounts of coal attached to mineral particles can result in these mineral particles being carried along to the froth. This effect appears to be especially significant for the Upper Freeport coal, for which minimal ash reduction was observed, apparently due to its great hydrophobicity. Examination of ash content of the incremental fractions in Table 3 indicates that after 6 minutes, the ash content of the incrementally recovered material rises dramatically, nullifying the small amount of ash reduction achieved previously. For the Upper Freeport coal, practically all of the mineral matter could float if given enough time. For the Indiana No. 3 and Sunnyside coals, on the other hand, some mineral matter simply would not float at all.

AIA results compared to float-sink results

The association results for the three coals, included in Table 4, show the incremental and cumulative percent distributions of coal, mineral matter, and coal+mineral matter as a function of the amount of mineral matter apparent in the particle cross sections. The cumulative distribution relates how much of the original sample (i.e., coal plus mineral matter) could be recovered by collecting particles of a certain mineral matter content.

The mineral matter content in a particle, listed in column 1 of Table 4, can be translated to a specific gravity estimate, assuming a coal density of 1.30 and an average mineral density of 2.60. Thus, a specific gravity of 1.3 corresponds to 0% mineral matter, 1.4 to 20%, 1.6 to 40%, 1.9 to 60%, and a specific gravity of more than 1.9 corresponds to 100%. In this manner, the distributions of Table 4 may be correlated with float-sink results. Such AIA results are plotted in Figure 3, and they can be used for comparison with the float-sink separation results in Figure 1.

Several parallel trends may be noted between the AIA and float-sink results in Figures 3 and 1, respectively. The recovery curves for the three coals generally appear in the same order in both figures. The recovery of the Sunnyside coal is greater than that of the other two coals, and the Indiana No. 3 coal generally shows higher recovery than the Upper Freeport coal for separations at specific gravities greater than 1.4. Likewise, the ash (or mineral) content curve for the Sunnyside coal is consistently below those of the other two coals. Unfortunately, the influence of stereological effects on the AIA results prevents a completely quantitative comparison of the AIA and float-sink results.

However, because the same qualitative trends appear in both figures, AIA results can be more useful since they can be obtained much faster than the float-sink results. During routine operation, sample preparation for AIA requires about 2 hours and the analysis less than 20 hours per sample. At least one sample per day can be analyzed with our equipment, but allowance for sample preparation and data reduction could result in a two-day sample turnaround. Such throughput is better that what can be achieved by testing with float-sink separation followed by ash analysis.

AIA results compared to froth flotation results

It is more difficult to relate the AIA results to froth flotation results. No comparable set of curves can be produced using the AIA results as they appear in Table 4. However, some useful information can still be obtained. The AIA results in Table 4 do show more association of minerals with the Upper Freeport coal. The plots in Figure 4 show the distribution of coal and mineral matter for the mixed (i.e., coal plus mineral matter) particles of the three coals taken from Table 4; free coal has been excluded. It can now be seen graphically that the Upper Freeport coal contains more mineral matter in this type of particle. In fact, the average mineral content of the mixed particles (i.e., the associated coal-mineral fraction) of the Upper Freeport coal is 45%, compared to only 26% and 29% for the Indiana No. 3 and Sunnyside coals, respectively.

However, even with these coal-mineral association insights, the previously stated tendency for the Upper Freeport coal to respond more to froth flotation than the other two coals appears to be the determining factor in the poor mineral removal for this coal. Apparently, the mineral matter in the Upper Freeport coal can float, even with very little coal associated with it. However, this issue cannot be answered by AIA alone and requires further study by other analytical techniques.

Table 4. Distributions (in %, dry basis) of coal and mineral matter for all three coals, as a function of particle mineral matter (MM) content

MM Content	Incremental			Cumulative			% MM in Cumulative Total
	Coal	MM	Total	Coal	MM	Total	
Indiana No. 3 coal							
0	61.61	0.00	61.61	61.61	0.00	61.61	0.00
0-10	14.32	0.58	14.90	75.93	0.58	76.50	0.75
10-20	5.51	1.04	6.55	81.44	1.61	83.05	1.94
20-30	2.86	0.96	3.82	84.30	2.57	86.88	2.96
30-40	2.34	1.27	3.61	86.64	3.85	90.49	4.25
40-50	0.87	0.72	1.59	87.51	4.57	92.08	4.96
50-60	0.96	1.17	2.13	88.47	5.73	94.21	6.09
60-70	0.65	1.27	1.92	89.12	7.00	96.12	7.28
70-80	0.53	1.62	2.15	89.65	8.62	98.28	8.78
80-90	0.20	1.14	1.34	89.85	9.77	99.62	9.80
90-100	0.01	0.36	0.38	89.87	10.13	100.00	10.13
Total	89.87	10.13	100.00				
Upper Freeport coal							
0	73.35	0.00	73.35	73.35	0.00	73.35	0.00
0-10	4.62	0.20	4.82	77.97	0.20	78.17	0.26
10-20	3.32	0.57	3.88	81.28	0.77	82.06	0.94
20-30	1.25	0.43	1.68	82.53	1.20	83.73	1.43
30-40	1.24	0.64	1.88	83.77	1.84	85.61	2.15
40-50	0.95	0.75	1.70	84.72	2.59	87.32	2.97
50-60	1.14	1.30	2.44	85.86	3.89	89.75	4.34
60-70	0.94	1.79	2.73	86.81	5.68	92.48	6.14
70-80	0.31	0.88	1.19	87.11	6.56	93.68	7.01
80-90	0.67	3.83	4.50	87.78	10.39	98.17	10.59
90-100	0.11	1.71	1.82	87.89	12.11	100.00	12.11
Total	87.89	12.11	100.00				
Sunnyside coal							
0	84.28	0.00	84.28	84.28	0.00	84.28	0.00
0-10	6.06	0.32	6.38	90.34	0.32	90.66	0.35
10-20	1.88	0.31	2.19	92.22	0.63	92.85	0.68
20-30	0.86	0.27	1.13	93.08	0.90	93.97	0.95
30-40	0.66	0.37	1.04	93.74	1.27	95.01	1.34
40-50	0.85	0.71	1.56	94.59	1.98	96.57	2.05
50-60	0.27	0.32	0.59	94.86	2.30	97.16	2.37
60-70	0.25	0.46	0.71	95.11	2.77	97.88	2.83
70-80	0.25	0.74	0.99	95.36	3.51	98.87	3.55
80-90	0.10	0.55	0.65	95.46	4.06	99.52	4.08
90-100	0.04	0.44	0.48	95.49	4.51	100.00	4.51
Total	95.49	4.51	100.00				

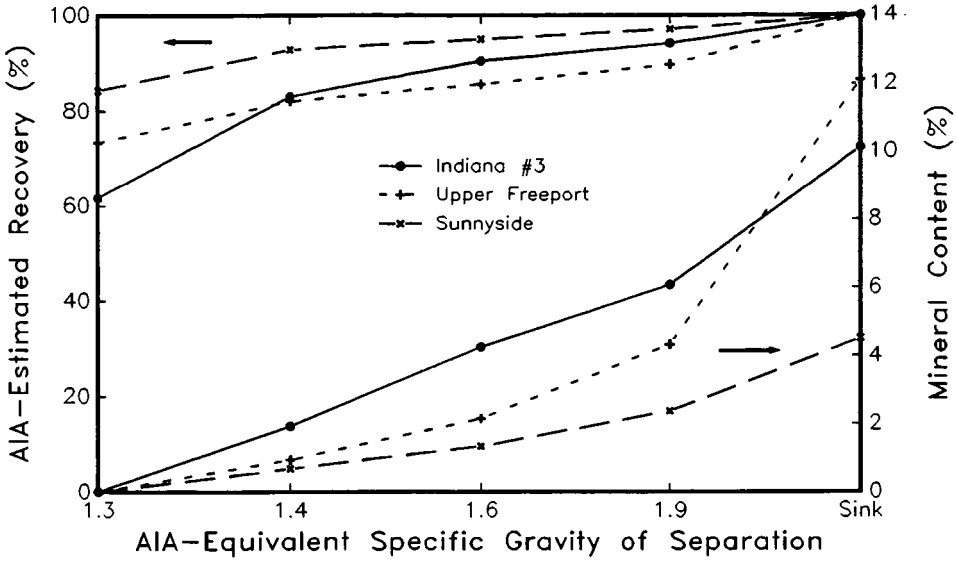

Figure 3. AIA-estimated recovery and mineral content as a function of AIA-equivalent specific gravity

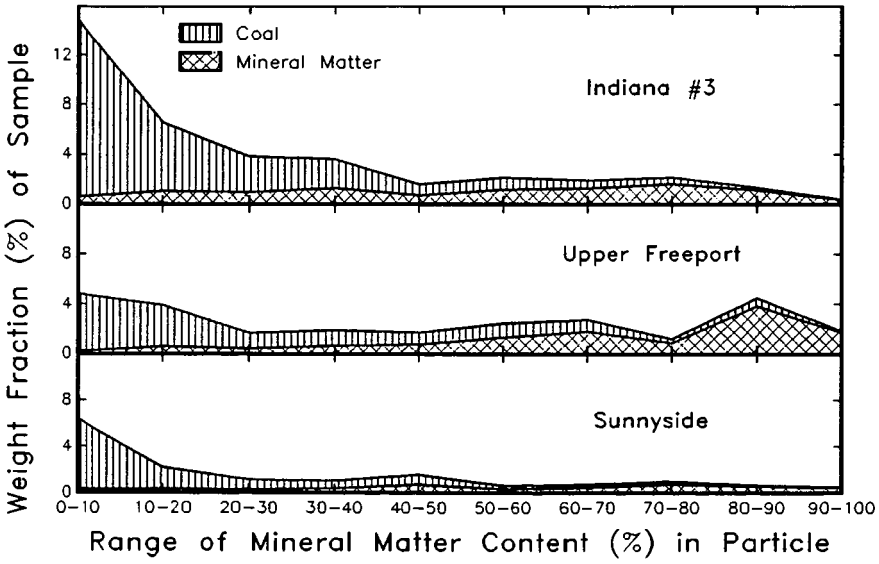

Figure 4. Distribution of coal and mineral matter as a function of weight fraction of mineral matter in the particles

CONCLUSIONS

Automated image analysis was used to determine the association of mineral features with coal, and the results were expressed in a format that provided insight into the float-sink response of the sample. Qualitatively similar trends were observed for the conventional float-sink and the AIA results; however, quantitative comparisons are currently limited by stereological effects on the AIA results.

The AIA results, as developed and presented in this work, provide less direct insight into the froth flotation behavior. However, there did appear to be a correlation between the large amount of mineral matter in the mixed particles of the associated coal and mineral fraction measured by AIA and the poor ash rejection from the Upper Freeport coal during froth flotation. Work is continuing on other AIA reporting formats which could be more directly related to froth flotation.

AIA results can be obtained considerably quicker than results from either of the conventional cleaning tests. This suggests that AIA may be useful in monitoring the character of feed to a preparation plant, particularly since AIA is able to detect differences in the association of coal and mineral matter particles.

ACKNOWLEDGEMENT

Ames Laboratory is operated for the U. S. Department of Energy by Iowa State University under Contract No. W-7405-Eng-82. The work at Ames was supported by the Assistant Secretary for Fossil Energy through the Pittsburgh Energy Technology Center and by a grant from AMAX through the Iowa State Mining and Mineral Resources Research Institute. The work at AMAX was supported by DOE Contract No. DE-AC22-84PC72007.

LITERATURE CITED

1) W.E. Straszheim, J.G. Yousling, K.A. Younkin, and R. Markuszewski, "Mineralogical Characterization of Lower Rank Coals by SEM-based Automated Image Analysis and Energy-Dispersive X-ray Spectrometry", Fuel, in press, 1988.

2) W.E. Straszheim, K.A. Younkin, and R. Markuszewski, "Determination of Pyrite Association with Coal Particles by Automated Image Analysis", Processing and Utilization of High Sulfur Coals-II, Y.P. Chugh and R.D. Caudle, eds., Elsevier, New York, 1987, pp. 41-48.

3) W. E. Straszheim, J. G. Yousling, and R. Markuszewski, "Analysis of Ash-Forming Mineral Matter in Raw and Supercleaned Coals by Automated Image Analysis-Scanning Electron Microscopy", in Mineral Matter and Ash in Coal (ACS Symp. Series No. 301), K. S. Vorres, ed., Am. Chem. Soc., Washington, D. C., 1986, pp. 449-461.

4) W.E. Straszheim, K.A. Younkin, R.T. Greer, and R. Markuszewski, "Mounting Materials for SEM-based Automated Image Analysis of Coals", submitted to Scanning Microscopy, 1988.

COMPARISON OF COMBUSTION DEPOSITS FROM BITUMINOUS COALS AND A LIGNITE

F. E. Huggins[1], G. P. Huffman[2],

Departments of Geological Sciences[1] and Chemical Engineering[2],
University of Kentucky,
Lexington, KY 40506

and A. A. Levasseur

Kreisinger Development Laboratory,
Combustion Engineering, Inc.,
P.O. Box 500,
Windsor, CT 06095

INTRODUCTION

Deposits generated during combustion of pulverized coals are determined to a large extent by the type, relative amounts, size, and association of the different inorganic species present in the coal. In this investigation, we examine and compare the inorganic constituents in various samples of two bituminous coals and of a Texas lignite and the deposits generated from these coals in the same test furnace. Whereas the principal basic mineral in the bituminous coals is pyrite, which is found in these coals in relatively coarse particle form, the principal component in the lignite is carboxyl-bound calcium, which is highly dispersed throughout the lignite macerals. These situations can be considered to represent different ends of the spectrum with respect to the size and distribution of the major basic component of the inorganic species.

The mineral matter of the coals was characterized using a combination of computer-controlled SEM (CCSEM) and Mössbauer spectroscopic methods. Similar techniques were used to examine deposits.

EXPERIMENTAL

(a) Samples:

The Illinois #6 coal was obtained as a combustion product (Il#6-Base) and as a cleaned metallurgical product (Il#6 - Met). The other two coals, a Kentucky #9 coal and a Texas Lignite, were subjected to cleaning at the EPRI Coal Cleaning Test Facility, near Homer City, PA. A medium-cleaned product (Ky#9 - MCln) and a deep-cleaned product (Ky#9 - DCln) were prepared from the original Kentucky #9 coal (Ky#9-Raw) and a cleaned product (TexL - Cln) was prepared from the original lignite (TexL - Raw). Pulverized coal samples were prepared from the original coals and the cleaned products. These coals were then burnt in the Fireside Performance Test Facility (FPTF) at Combustion Engineering and a variety of deposit samples were collected, including in-flame solids, superheater deposits and waterwall deposits.

(b) Techniques:

The combination of Mössbauer spectroscopy and CCSEM for the determination of coal mineralogies has been described in detail elsewhere (1). Basically, the CCSEM technique determines quantitatively the types, relative amounts, and size distributions of the major discrete minerals in the coal, whereas Mössbauer spectroscopy provides more detailed complementary information regarding the iron-bearing minerals, in particular pyrite. For lignites, however, the CCSEM method does not determine the carboxyl-bound inorganics dispersed in the lignite macerals. These components were semi-quantitatively

estimated from a comparison of the discrete mineralogy and the overall inorganic composition as revealed by wide area energy dispersive X-ray scans or the chemical analysis of the high-temperature ash.

For samples generated in the FPTF, Mössbauer spectroscopy was used to document the behavior of iron in the various deposits and optical and electron microscopic techniques were used to examine the microstructure and mineralogy in polished sections of the deposit mounted in epoxy. Much reliance was placed on elemental X-ray and backscattered electron intensity mapping techniques in the CCSEM to document element distributions and associations.

Some exploratory extended X-ray absorption fine-structure (EXAFS) spectroscopy measurements were made at the calcium K-edge to investigate the form of occurrence of Ca in the Texas lignite and Illinois #6 coal and in deposits generated from the coals. These measurements will be discussed in detail elsewhere and will merely be mentioned here in passing where information from the EXAFS technique corroborates or supplements data from the other techniques.

RESULTS

(a) Coal Mineralogies:

The mineralogies of the various coal samples are summarized in Table 1. The samples from the Illinois #6 and Kentucky #9 bituminous coals exhibit somewhat similar mineralogies: pyrite, along with its oxidation products, is the principal basic mineral, although both raw coals also contain significant amounts of calcium minerals: gypsum in Kentucky #9, calcite in Illinois #6. However, the combination of quartz and clay minerals dominates the mineralogies. The Texas lignite discrete mineralogy is dominated by quartz; pyrite and other basic minerals are very minor components. Cleaning does effect some differences in mineralogy: both bituminous coals become relatively poorer in pyrite with cleaning. However, for the Kentucky #9 coals, the decrease in pyrite is compensated by an increase in magnetite, which was introduced into the cleaned coals from the heavy media used for cleaning. This contamination is best revealed by the Mössbauer data and spectrum (Fig. 1). The discrete mineralogy of the Texas lignite is little affected by cleaning; however, the ratio of the discrete mineral matter to the dispersed maceral inorganics changes from approximately 2:1 to less than 1:1 based on changes in the overall energy-dispersive X-ray composition. The major dispersed inorganic elements were calcium and sulfur. EXAFS spectroscopy confirmed that calcium was present as carboxyl-bound Ca in macerals, based on the similarity of the Ca EXAFS spectrum to previously published data on Ca in lignites (2).

Some data are presented on mineral size distributions in Table 2. As can be seen from Table 2 and more clearly for the Kentucky #9 coals shown plotted on a wt% coal basis in Fig. 2, cleaning has the effect of preferentially removing the coarser mineral matter (>20μm). Hence, specific minerals with a coarser size distribution are removed more completely than those with size distributions biased to smaller size ranges. It is clear that the relative size distributions explains why pyrite and not quartz is removed by the cleaning of the Kentucky #9 coal. Although less dramatic, there is also a significant reduction in the coarse quartz content of the Texas lignite upon cleaning; however, there is little change in the discrete mineralogy (Table 1), implying that all minerals are, on average, similarly affected.

It should be noted, however, that cleaning reduces the basic mineral content of the bituminous coals, but increases the proportion of basic inorganics for the Texas lignite.

TABLE 1a: COAL MINERALOGIES BY CCSEM+

	Kentucky #9			Illinois #6		Texas Lignite	
Mineral	Raw	MCln	DCln	Base	Met.	Raw	Cln
Quartz	14	16	24	17	20	47	36
Kaolinite	2	4	5	8	9	3	12
Illite	3	6	9	10	17	3	3
Misc. Sil.	22	26	21	28	31	34	28
Pyrite	29	19	16	22	11	3	9
Gypsum	8	3	3	2	2	--	--
Fe sulfate	2	5	4	1	2	--	--
Misc. Sulf.	5	3	3	2	2	--	--
Fe-rich	1	6	6	<1	2	1	2
Ca-rich	--	--	--	8	<1	2	1
Misc., mixed	14	12	9	2	4	6	8

+Data expressed as percentage of mineral matter

TABLE 1b: MÖSSBAUER DATA ON DISTRIBUTION OF IRON

	Kentucky #9			Illinois #6		Texas Lignite	
%Fe in	Raw	MCln	DCln	Base	Met.	Raw	Cln
Pyrite	65	60	48	87	84	71*	67*
Clay	3	4	3	--	5	--	--
Szomolnokite	1	--	--	7	--	14	8
Jarosite	32	26	33	5	11	15*	25*
Magnetite	--	11	16	--	--	--	--
Wt% Pyr. S	1.30	0.81	0.34	1.05	0.48	0.32	0.17

*Absorptions are broad; may include minor FeOOH

(b) Deposits:

(i) In-flame Solids: The samples of in-flame solids collected from in or near the flame region during the burning of the bituminous coals consisted, for the most part, of very loose aggregates of fly-ash cenospheres. Compositions of the individual cenospheres as revealed by EDX spectra and CCSEM mapping were highly variable reflecting the different associations of minerals in the coal particles. As might be expected, the fly ash particles were smaller and more uniform in size for the cleaned coals compared to the raw coals. Occasionally, these aggregates had nuclei of more highly agglomerated material or of large pieces of incompletely burnt char. Iron in all the samples was distributed among glass (both ferric and ferrous components), magnetite, and minor hematite. No iron sulfide or crystalline iron silicate phase could be discerned from the Mössbauer spectra. Typically over 50% of the iron was present in glass and the cleaned lignite had the most Fe in this form, up to 90%. Extensive reaction between silicates and pyrite must occur very rapidly in the initial combustion process in the flame.

TABLE 2: MINERAL SIZE DISTRIBUTION DATA FOR COALS

Coal	Size Distribution Data - All Minerals					
	<2.5μm	2.5-5μm	5-10μm	10-20μm	20-40μm	>40μm
Ky#9 - Raw	20	14	21	25	14	7
- MCln	27	21	23	16	11	1
- DCln	27	29	26	12	4	2
Il#6 - Base	21	16	19	21	11	12
- Met.	30	17	22	17	6	7
TexL - Raw	21	7	13	14	21	23
- Cln	21	15	20	16	13	16

Coal	Size Distribution Data - Pyrite					
	<2.5μm	2.5-5μm	5-10μm	10-20μm	20-40μm	>40μm
Ky#9 - Raw	9	6	25	22	21	17
- MCln	10	15	24	21	30	0
- DCln	14	16	35	26	9	0
Il#6 - Base	9	6	18	31	20	16
- Met.	16	11	29	27	14	4
TexL - Raw	--	--	--	--	--	--
- Cln	--	--	--	--	--	--

Coal	Size Distribution Data - Quartz					
	<2.5μm	2.5-5μm	5-10μm	10-20μm	20-40μm	>40μm
Ky#9 - Raw	15	22	33	24	4	3
- MCln	22	25	38	13	2	0
- DCln	17	31	36	8	2	6
Il#6 - Base	13	22	38	16	3	8
- Met.	21	18	24	13	1	24
TexL - Raw	10	5	10	13	31	31
- Cln	16	16	20	19	17	12

(ii)a Superheater Deposits - Initial: The initial superheater deposits from the bituminous coals are composed of largely undeformed silica and aluminosilicate cenospheres, less regular spherical particles rich in Fe and Si or Ca and S, and highly deformed Fe-rich particles. The latter particles often appear to be molded around the more rigid spheres, probably as a result of collision, and to be the "glue" that cements the deposit together. The interparticle contacts are quite sharp, indicating that little, if any, chemical reaction has taken place. Mössbauer data indicate a significant enrichment in iron by more than 50% for this type of deposit (Fig. 3), which also reinforces the importance of the iron particulate matter in the

cohesion of the deposit. In contrast to the in-flame solid samples, only 5-15% of the iron is present in glass, with the other 85-95% in the form of iron oxides, predominantly hematite.

Mössbauer data for the lignite superheater deposits, however, show no such enrichment in iron and less than 20% of the iron is present in magnetic oxides. For these deposits, iron does not appear to play a similar role to that in the bituminous coals. In this case the "glue" material may be calcium sulfate as this phase was shown by EXAFS spectroscopy to be very abundant in the initial deposit.

(ii)b Superheater Deposits - Outer: The structure of the outer superheater deposit is derived from the initial superheater structure by partial fusion and blending of the different fly-ash particulate matter. Many larger Fe-rich and Si-rich particles, however, persist unassimilated in the matrix so that the aluminosilicate particles become important at this stage as the major bonding phase. Partial fusion of these particles coupled with incorporation of all potassium and calcium phases and an appreciable fraction of the iron particles into this partial melt creates an extensive continuous framework. When frozen, these deposits were extremely tough and resistant to fracture because of this structure. For the bituminous deposits, Mössbauer data indicate that there is only a very minor enrichment of iron in these deposits compared to the in-flame solids and that there is a significantly higher percentage of iron in glass compared to the initial deposit.

The lignite outer superheater deposits varied from lightly sintered fly-ash to highly agglomerated amber-brown vitreous material. Fly-ash relicts, mostly large quartz particles and a few Fe-rich cenospheres, persist in less agglomerated areas and diminish in abundance with increasing agglomeration. The matrix is rich in calcium, aluminum and silicon and appears to have formed by reaction between Ca-rich and aluminosilicate particles. The matrix is quite highly crystallized with melilite ($Ca_2(Al,Mg,Fe,Si)_2SiO_7$) and anorthite ($CaAl_2Si_2O_8$) being the most common phases. Melilite tended to occur in the less agglomerated areas whereas anorthite was found in the more highly agglomerated areas.

(iii) Waterwall Deposits: An initial and outer waterwall deposit was collected for each coal. The initial deposit consisted of thin deposit whereas the outer deposit was considerably thicker and often collected in large masses. Mössbauer data showed some differences between the initial and outer deposits in that the initial deposits always contained more iron as oxides (except for the lignite), had a higher Fe^{3+}/Fe^{2+} ratio for the glass, and had less Al substituted for Fe in hematite, based on the magnetic hyperfine splitting parameter for this phase. However, there was little difference in the amount of iron between corresponding samples of waterwall deposit (Fig. 3).

The microstructure of the outer waterwall deposits from the bituminous coals varies significantly from the wallside to the fireside. At the immediate wallside is a thin layer that resembles the outer superheater deposit in that considerable fly-ash structure is present in a partially fused matrix. This layer is typically discontinuous towards the wall and offers a somewhat tenuous connection between the wall and the main body of the waterwall deposit. The continuous part of the deposit nearest the wallside exhibits a similar structure. Upon moving away from the wall, the relict Si-rich cenospheres are quickly assimilated into the matrix whereas the Fe-rich cenospheres fragment as the iron oxide equilibrates with the matrix. Upon moving further into the middle of the deposit, the Fe-rich fragments become increasingly angular and are eventually superseded by well crystallized, often skeletal, crystals of iron oxides. At the same time the glassy matrix becomes more

uniform in composition and appearance. On moving closer to the fireside, the iron oxides become less frequent and mullite laths begin to appear. At the immediate fireside, mullite occurs along with glass and the iron oxides occur as extremely fine scale dendrites. This latter phase probably developed upon cooling and was not present at temperature.

Similar microstructural changes are seen for the outer waterwall deposits from the lignite, but with different phases. In the adhesive layer, the fly-ash material is very calcium rich and contains appreciable sulfur and some Fe-rich particles. Large relict quartz particles are found near the wall and these appear to be only very slowly assimilated into the matrix. The matrix structure near the wall is fine-grained and chaotic, but coarsens considerably towards the center of the deposit as melilite crystallizes. Upon moving further towards the fireside, fewer quartz relicts are observed and the melilite crystallization is replaced by anorthite. In addition, crystallization of some minor phases such as calcium ferrites occurs in the outer waterwall samples.

For the raw Texas lignite sample, relict quartz was significantly more abundant than for the cleaned lignite sample. Furthermore, it appeared that the quartz was not so easily incorporated into the matrix of the raw lignite waterwall deposits. Occasionally, it was noted that a mantle of immiscible liquid was formed around the quartz particles that hindered the assimilation of this mineral into the Ca-rich matrix.

CONCLUSIONS

Despite significant differences in chemical composition, the microstructures of the lignite and bituminous deposits were quite similar and it would be difficult to identify a particular deposit as coming from a given coal in the absence of compositional information. However, this implies that similar structures can be brought about by quite different chemical interactions. In particular, the role of iron oxides in the initial formation of the superheater deposits and possibly also for the waterwall deposits from the bituminous coals is not evident for the lignite deposits. For these latter deposits, calcium sulfate may play a similar critical role, but this remains to be demonstrated. Partial fusion of the aluminosilicates accompanied by assimilation of basic cations into the matrix appears to be the principal cementing mechanism of both types of deposit, once they are established. As the deposits thicken and are subject to higher temperatures, the melts become more homogeneous and their mineralogy and behavior are largely governed by phase equilibria considerations.

In both types of deposits, relict Fe-rich and quartz fly-ash particles resist assimilation into the aluminosilicate matrix. In the case of the bituminous deposits, the abundance of iron oxide is such that it is either the liquidus phase or close to it. Hence, the aluminosilicate melts, except at very high temperatures, are effectively saturated with iron. In the case of the lignite deposits, quartz particles are generally quite large and assimilation in the melt is probably retarded because of sluggish reaction kinetics and also perhaps liquid immiscibility. This effectively makes the melt more basic than it should be and enables the crystallization of basic phases such as melilite. However, as quartz is absorbed into the melt and the composition becomes more acidic, anorthite takes over as the major crystallizing phase, as would be predicted from the CaO-Al_2O_3-SiO_2 phase equilibria diagram.

ACKNOWLEDGEMENTS

This work was supported by the Electric Power Research Institute by means of a contract to Combustion Engineering, Inc.

REFERENCES

(1) F.E. Huggins, G.P. Huffman, and R.J. Lee, in: Coal and Coal Products: Analytical Characterization Techniques, ACS Symposium Series 205 239-258, (1982).
(2) G.P. Huffman, and F.E. Huggins, in: Chemistry of Low-Rank Coals, ACS Symposium Series 264 158-174, (1984).

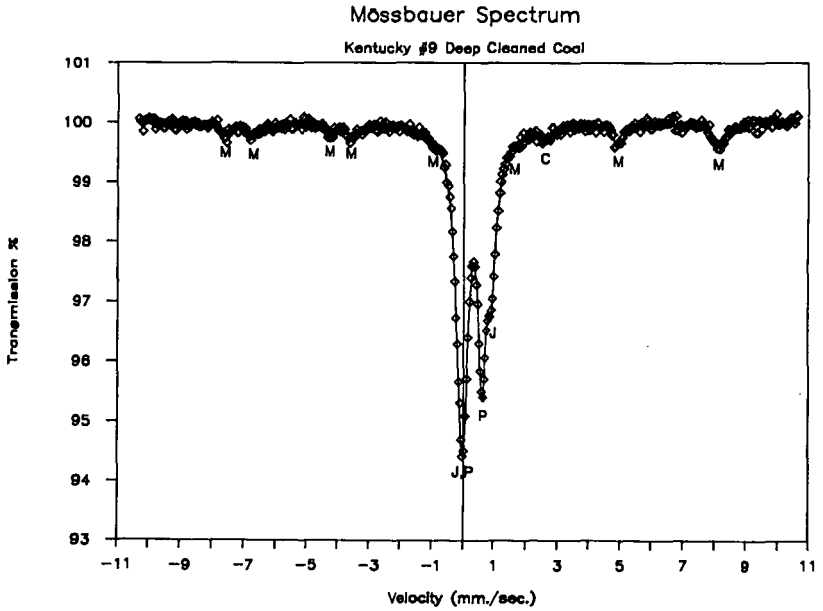

Figure 1: Mössbauer spectrum of the deep-cleaned Kentucky #9 coal showing the contamination by magnetite (M) from heavy-media cleaning. Other iron-bearing minerals present in the spectrum are pyrite (P), jarosite, (J) and ferrous-bearing clay (C).

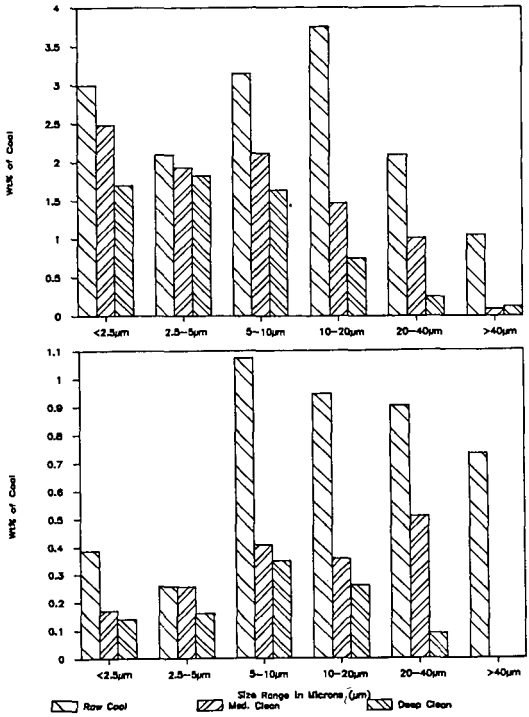

Figure 2: Size distribution data for all minerals (upper) and pyrite (lower) in Kentucky #9 coals. Data are expressed as wt% of the coal.

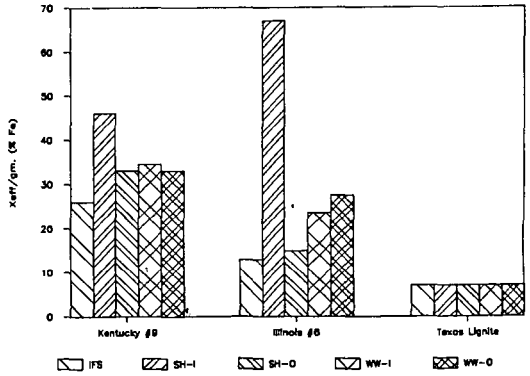

Figure 3: Histogram showing the significant enrichment in iron (based on the Mössbauer effective thickness parameter, X_{eff}/gm) for the initial superheater deposits from the raw bituminous coals and the lack of iron segregation exhibited by the lignite.
Key: IFS - in-flame solids; SH-I - initial superheater; SH-O - outer superheater; WW-I - initial waterwall; WW-O - outer waterwall.

PHYSICAL AND CHEMICAL TRANSFORMATIONS DURING PULVERIZED COAL COMBUSTION -- OPTICAL SYSTEMS FOR MEASUREMENTS

D. K. Ottesen and D. R. Hardesty
Sandia National Laboratories
Combustion Research Facility
Livermore, CA 94550

L. J. Radziemski
Physics Department
New Mexico State University
Las Cruces, NM 88003

INTRODUCTION

One of the most difficult problems in developing diagnostic methods for coal combustion research is that of determining the composition of entrained coal, char, and mineral matter particles in the combustion zone. We have employed two laser-based techniques for the simultaneous measurement of the size, velocity, and elemental composition of particles in combustion flows. Laser spark spectroscopy [1,2], also called laser induced breakdown spectroscopy (LIBS) [3], is used to determine the elemental composition of coal particles. Sizing measurements are done using two-color laser light scattering [4].

Laser spark spectroscopy is a variation of conventional emission spectroscopy which uses a focused pulsed laser beam to generate an optical breakdown, commonly called a laser spark or a laser induced plasma. The origin and uses of this technique are well summarized [5]. Many of its properties are similar to those of conventional arc or spark plasmas as discussed in standard texts on spectrochemistry [6]. As with conventional techniques, the laser spark allows simultaneous multi-element detection. An important advantage is the ability to obtain information in hostile environments, in situ, where electrodes cannot be introduced.

Two principal applications for this technique are proposed. The first is the simultaneous measurement of size, velocity, and composition of single particles and is primarily an analytical research tool for coal combustion studies. The second is the measurement of bulk properties before, during, and after combustion by coaddition of hundreds or thousands of individual spectra. This can be envisioned as an on-line monitor in an operating combustor. Our experiments have elucidated the advantages and difficulties which will be encountered in these applications.

INSTRUMENTATION

The apparatus was arranged so that sizing and spectroscopic information could be obtained simultaneously. A general apparatus diagram for all experiments is shown in a top view in Figure 1. Measurement of particle size and velocity using a two-color colinear beam has been more fully described elsewhere [4].

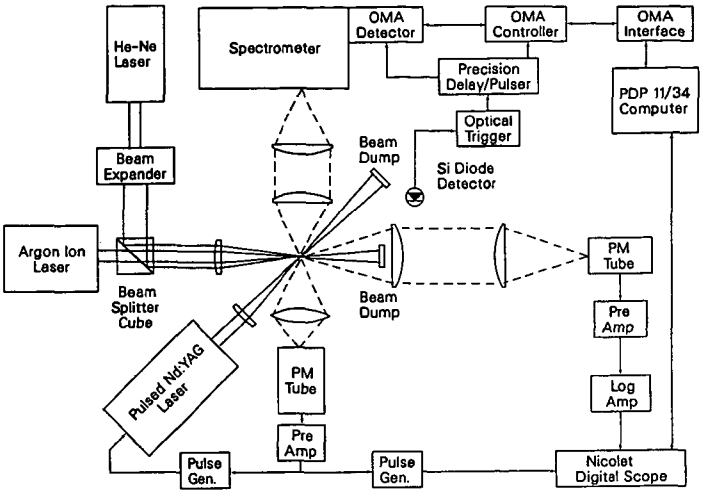

Figure 1. Top view of laser sizing and spark spectroscopy system.

Light Scattering Instrumentation

The two-color scattering technique permits an accurate estimate of particle size and velocity. Beams from He-Ne and Ar-ion lasers were combined using a beam splitter cube. Scattered light from particles passing vertically through the common focal volume was viewed with two photomultiplier tubes: one in the near-forward direction, and the other at 90 degrees to the laser beam axis. Particle scattering signals were used to fire a pulsed Nd:YAG laser, creating a high temperature laser spark from the particle.

This technique can be very satisfactorily calibrated to measure particle size by using regularly shaped particles and orifices. Particle velocity was calculated from a knowledge of the Ar-ion laser beam waist diameter and the transit time of a particle determined from the 1/e points in the measured near-forward scattered light intensity.

Laser Spark Instrumentation

Spectra were generated from the plasma formed by the focused Nd:YAG laser beam (Quanta Ray DCR-2, Q-switched, oscillator only). Laser energy was a nominal 110 mJ per pulse at 5320 Å. Important parameters for the acquisition of spectra were timing, optical alignment, and temporal resolution. The irradiance at the focus of the Nd:YAG laser beam was adjusted to ensure breakdown would occur only in the presence of a particle in the focal volume. This eliminated spurious data from a triggered breakdown of the entrainment gases.

The operation of the Nd:YAG laser Q-switch introduced a 250 μs delay between the arrival of the trigger pulse and firing of the laser. Because the particles under investigation were moving, the optimum focal volume for the Nd:YAG

laser beam was displaced from that of the sizing laser beams. The mean particle velocity could be maintained at a fairly constant value (± 10%) in the range of 1 - 5 m/s. We found that with proper experimental alignment of the three beams, about 90% of the particles which triggered the Nd:YAG laser actually formed a plasma due to laser induced breakdown.

Light from a laser spark was imaged on a silicon diode detector to generate a trigger pulse which initiated collection of the spectrum (Figure 1). The laser spark was imaged on the entrance slit of the spectrometer (Spex Model 1870) with a nominal 20 μm slit width and a gated, intensified diode array (PAR Model 1420). The emission spectrum was then digitized and stored on hard disc for subsequent analysis.

Previous investigators [2,7] have shown that time resolution is essential for analytical uses of laser plasmas. For times less than 1 μs following laser induced breakdown the emission spectrum was dominated by continua and lines due to ionized species. Time delays of at least 2 μs were necessary to discriminate against the continuum and to restrict the observed species to neutral and singly ionized atoms. Molecular spectra were observed but were due to recombination of atoms in the plasma, not from molecules originally in the sample. Integration times depended primarily on the intensity of lines observed in a given spectral region, and ranged from 1 to 10 μs for this study.

Particle entrainment system and reactor

Samples investigated were of two forms, liquid droplets or solids of various composition. Liquid droplets of pure substances or solutions were produced using a vibrating orifice generator and were dropped through the optical focal region under ambient conditions. They were used primarily to calibrate the scattering signal.

The entrainment of solid particles into a stream of purified dry nitrogen was done with a particle feeder. The fluidized solid particles were introduced along the vertical centerline of a circular premixed burner through a central tube. This was aligned below the intersection of the three laser beams as shown in Figure 1. The combustion region of the burner was 50 mm in diameter and was surrounded by a co-flow region for flow regulation and to prevent mixing with the laboratory atmosphere.

A flat flame above the burner surface produced a hot, vertically flowing column of gases into which the particulates were entrained. By varying the amounts of the fuel, oxidizer and diluent gases, one could control the combustion temperature and residual oxygen partial pressure in the hot environment. Methane and oxygen were used in this study, with nitrogen added as a diluent. Gas flows were controlled with mass flowmeters. Temperatures 50 mm above the burner surface measured with a Pt-Rh thermocouple in the absence of particles were on the order of 1500° C.

CALIBRATION

Calibration of the sizing apparatus

Calibration of the particle sizing apparatus was done by the measurement of near-forward scattering intensities of uniform liquid droplets and precision

pinholes. Once the calibration scale was established, the daily measurement of scattering intensity from a single reference pinhole was used to establish a current working curve. This is more fully described elsewhere [4].

Calibration of and factors affecting the spectroscopic signal

To be useful, the observed emission intensities had to be related to relative and absolute elemental compositions. There were several variables with which to deal: (1) incident laser power, (2) particle size, (3) particle composition and associated matrix effects, (4) location of the particle in the laser focal volume, (5) amount of the particle material removed and ionized, (6) plasma temperature and possible self-absorption, (7) image location on the spectrometer entrance slit, and (8) the lack of "standard reference materials" for coals on a particle-by-particle basis.

It was first necessary to establish the level of reproducibility of the emission signal for well-characterized, monodispersed, homogenous samples. The use of pure solid particles was not found to be particularly valuable for this purpose. Analytical lines for most metallic species found in coal were strongly self-absorbed in laser spark emissions from target particles consisting of the pure oxides or simple salts.

Calibration experiments were undertaken using homogenous solid particles composed of an ion exchange resin, Amberlite, loaded with calcium at 10 wt %. A typical spark emission spectrum is shown in Figure 2. A small magnesium impurity was present in the ion-exchange material, and additional lines due to Mg I and Mg II were also observed in this spectrum.

These multiple line spectra (and others discussed below) were fit by a non-linear least squares computer program using Lorentzian line shapes and reference intensities from the NBS collections [8,9]. The calculated reference intensities for each species were multiplied by a coefficient to fit the experimental data. Because the reference intensities were determined for standard concentrations [8,9], the ratio of the coefficients for different elements should be closely related to the relative elemental concentrations.

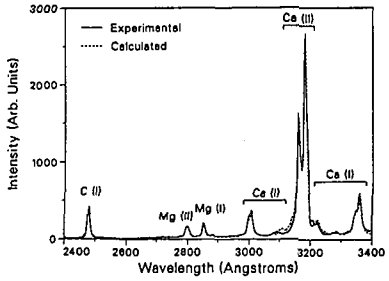

Figure 2. Laser spark spectrum of a single ion-exchange resin particle.

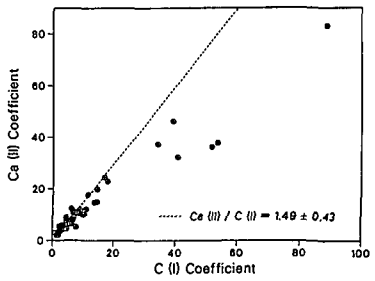

Figure 3. Least-squares fitting coefficients for Ca II and C I in 80 spark spectra.

About 80 particles were analyzed for the various C, Ca, and Mg transitions. Ratios of metal/carbon coefficients were calculated in order to assess the reproducibility of emission intensities on a shot-to-shot basis. The intensities for Ca II and C I (Figure 3) are clearly correlated and show an initial linear relationship. Points corresponding to higher counts show a gradual saturation. Within the linear regime the scatter may be due to particle heterogeneity and shot-to-shot variations of the excitation within the plasma. The latter can be caused by variations in the coupling of the energy into the plasma, or the size or morphology of the particle. Even so, the existence of a linear regime is evidence of significant shot-to-shot reproducibility.

Previous studies [10] have shown that matrix effects exist for different atomic species included in a solid material using laser spark spectroscopy. This is typical of conventional emission spectroscopy techniques also. For a given matrix composition of a bulk phase the most volatile atomic species were preferentially removed in the high temperature plasma, and the observed elemental composition of the ionized material was found to differ from the bulk composition accordingly. We might also expect such effects in our study.

Measurements on solid particles will always have to contend with incomplete vaporization. Calculations based on the heat of vaporization of carbon indicated that the coupling of 1% of the available incident laser energy into a solid particle would completely vaporize particles no larger than 10 μm in diameter. For incomplete vaporization, particle heterogeneity could be a serious problem. However, it appears impractical to use a laser with sufficient energy to vaporize large particles.

Coupling of the laser energy into the target particle is complicated by the complexities of hitting a moving particle with a pulsed laser beam at a stationary focal point. Careful control of particle feeding conditions and laminar flow of the gases above the reactor surface helped to minimize variations in particle velocity. Light scattering data indicated an axial velocity distribution of ± 10% about a mean velocity of 2 m/s for pulverized coal particles. For a Q-switch delay of 250 μs, this would yield an axial variation of ± 50 μm in particle position. This is quite large compared to the calculated beam waist of 100 μm for our Nd:YAG laser, and is probably the dominant experimental variable for the coupling of incident laser light with the plasma.

RESULTS

Pulverized coal particles were entrained in the reactor system and spark emission spectra were collected with and without sizing data for single particles under different conditions. Three bituminous coals were studied: an Illinois #6, a Pittsburgh #8, and a Kentucky #11 coal. All had high temperature ash contents of 13 to 14% with varying amounts of inorganic constituents. Particles were size classified and the 63-75 μm diameter fraction for the first two coals, and the 30-50 μm diameter fraction for the third coal, were used here.

Qualitative Results

Extensive spectra were taken from 1900 to 7700 Å to assign emission lines and determine sensitivity to trace components. Representative spectra of single particles for the same coal sample are shown in Figures 4a and 4b. Two of the

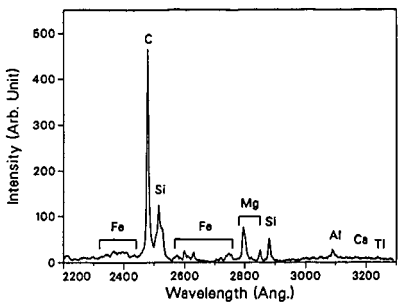

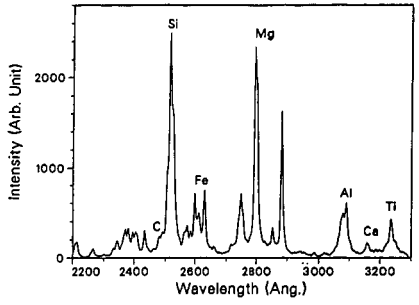

Figures 4a - 4b. Representative laser spark spectra of single coal particles.

most useful aspects of laser spark spectroscopy in the study of coal combustion are seen: the sensitivity to inorganic constituents in the organic material, and the capability for simultaneous multi-element detection.

The following elements were identified in these survey spectra at room temperature: C, H, O, N, Li, Na, K, Mg, Ca, Sr, Ba, Al, Si, Ti, Mn and Fe. Major species were silicon, aluminum, calcium, magnesium, iron, sodium, potassium and titanium. The rest were trace constituents. All the identifications were made from spectra of individual particles.

We also searched for sulfur and phosphorous lines. The array-spectrometeter system was not sensitive at the sulfur resonance lines (1800-1900 Å), and phosphorous was simply not seen. Other trace metallic elements at lower concentrations, such as chromium and vanadium (with average bulk concentrations of 3-30 ppm), were not detected with our current instrumentation. Sensitivity to these elements may be improved by coaddition of many single particle shots. An ultimate detection limit for most metallic species in single coal particles is likely to be below 100 ppm. Molecular species originally in the coal are dissociated by the plasma and not observed. Recombination of hot atoms gave rise to strong CN bands, however, which obscured the regions from 3750- 3900 Å and 4150-4220 Å. No other excited molecular or radical spectra were observed.

Experiments were also performed at combustion temperatures. While the residence time was quite short, the coal particles had ignited and were undergoing vigorous devolitalization at this point. Data of high quality, similar to Figures 4a and 4b, were collected in situ without significant degradation in the signal/noise ratio for ambient conditions.

Semi-quantitative results

The absolute mass sensitivity of the technique may be illustrated by considering the spectrum in Figure 5. Sizing data indicated that this particle was of 29.5 μm diameter. Based on a density of 1.5 g/cc for coal, this yielded a total particle mass of 20 ng. We assumed a plasma temperature of 1 eV (11,600 K) and calculated relative intensities for transitions of C and Fe. With an average carbon content of 83% (dry basis), the observed relative intensities

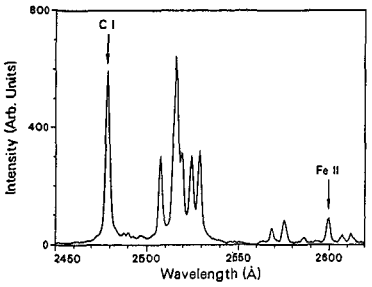

Figure 5. Laser spark spectrum of a single, 20 ng coal particle showing detection of 700 fg of iron.

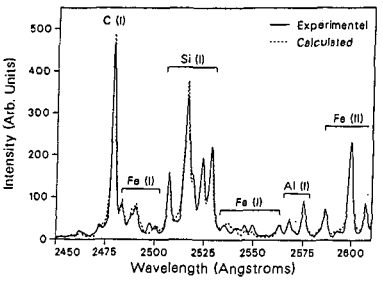

Figure 6. Comparison of experimental and calculated spectra for a single coal particle.

corresponded to detected quantities of 0.7 pg of iron. The actual absolute amount of material in the plasma was probably less due to incomplete vaporization of the particle during the excitation process.

Since coal is a very heterogeneous material, one expects a large variation in emission intensity for the observed constituents on a particle-by-particle basis. A convenient and systematic way of studying these variations is to examine the relative intensity for two elements for a large number of particles. If this is done over a narrow spectral bandwidth, then the optical system response will be reasonably constant and the observed intensity ratios can be semi-quantitatively related to reference intensities [8,9] for a given average plasma temperature.

For particles at ambient temperature and those examined after short residence times at combustion temperatures, we observed the spectral region from 2400 to 2650 Å and chose the ubiquitous C I transition at 2478 Å as the reference line. This region also contained several transitions due to Si I, Al I, Fe I and Fe II. Even though carbon is a major species, the C I line at 2478 Å is not likely to saturate since the lower level of the transition is at 2.68 eV.

In our first attempt at quantitative analysis, we obtained spectra from eighty particles of Kentucky #11 coal entrained at room temperature in nitrogen. Synthetic spectra were computed rapidly and produced a good fit to each individual spectrum as illustrated in Figure 6. Deviations between calculated and observed intensities for several Fe I and II transitions were probably due to a difference in plasma temperatures for our experiment and the reference intensity data. The least-squares analysis yielded fitting coefficients which we related to the relative concentration of the element.

Matrix effects also will alter these relative elemental line intensities with respect to the reference data [8,9]. While these variations may be most directly accounted for by calibration with suitable homogeneous reference particles, difficulties in making such standards may necessitate their evaluation

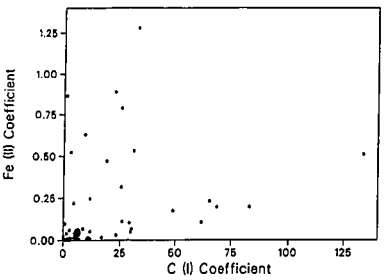

Figure 7. Relative amounts of Fe and C for 80 single coal particles.

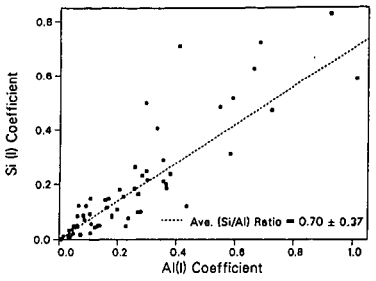

Figure 8. Relative amounts of Si and Al for 80 single coal particles.

through a detailed statistical comparison of bulk chemical analyses with a large number of laser spark spectra.

A plot of C I and Fe II fitting coefficients obtained from these spectra is shown in Figure 7 and illustrates the heterogeneity of the coal particles. Particles rich in iron show a random distribution of points with high Fe II coefficients, and are attributed to inclusions of iron-bearing minerals (predominantly pyrite). On the other hand, a second population of points is seen near the x-axis with low values of Fe II coefficients. These appear to be highly correlated with carbon content, and may be due to iron distributed homogeneously throughout the organic matrix. Scanning electron microscopy results on a sample of this coal substantiated that these two distinct iron populations exist [11].

A second example of relative elemental composition is shown in Figure 8 for silicon and aluminum from the same set of 80 spectra. These two elements appear to be correlated and present in comparable amounts. Some of the considerable scatter in the data is due to variations in plasma temperature; however, a much larger effect is that the various clay minerals containing aluminum and silicon may differ significantly in relative elemental composition. Further, another source of silicon in the coal is quartz, which would be completely uncorrelated with the silicon and aluminum present in clays.

In contrast to these two examples, sodium is often quite evenly distributed in bituminous coals, and this is illustrated in Figure 9 for 50 particles of the Kentucky #11 sample. This plot is of experimental intensities for the doublet at 5890 and 5896 Å, and these values have not been normalized against other transitions. The data illustrate the very uniform distribution of sodium in this coal despite differences in plasma conditions mentioned above.

DISCUSSION

Our results demonstrate the potential for laser spark spectroscopy as an in situ analytical technique for particulate composition in ambient and high

temperature environments. An obvious next step is the quantitation of emission intensities. This can take two directions: correlation with available bulk analyses through coaddition of many single particle analyses, and development of appropriate standard materials.

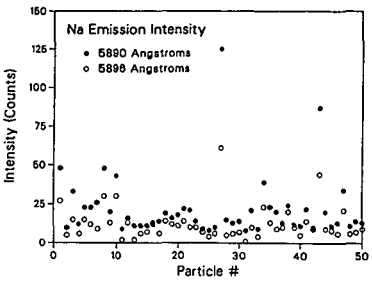

Figure 9. Distribution of sodium in spark spectra of 50 coal particles.

In the present study, the sizing capability was often not employed because sized particles were used. In general, however, simulataneous sizing and spectral analysis will allow an approximate mass analysis on each particle. The addition of hundreds to thousands of these could begin to emulate the bulk analysis. The study of coals with significantly differing composition could verify the sensitivity of the technique, and the likely result would be a semi-quantitative in situ analysis capability.

Experiments with uniform ion exchange resin particles have demonstrated that reproducible results can be obtained with well characterized particles. The difficulty in acquiring adequate calibration standards for quantitative analysis lies not only in their preparation, but also in the certification of their homogeneity on a particle-by-particle basis. A possible approach might be the doping of porous char particles with a given elemental species. The issue of emission intensity dependence on the amount of particle vaporized during excitation may be studied using reference particles with varying levels of incident laser energy.

Another important aspect of particle inhomogeneity is the evolving character of surface composition during combustion, since significant quantities of mineral species may coalesce on the particle surface. Incomplete vaporization of the solid during excitation would yield intensities not representative of the entire particle, and calculated compositions would be biased as a result.

The increase in mineral composition relative to the organic matrix during the combustion process would be expected to show an increasing amount of self-absorption and, finally, line reversal for the strongest transitions. This potential problem may be mitigated in the analysis of post-combustion material since ash particles are smaller than the initial pulverized fuel particles, and might be quantitatively vaporized by the incident pulsed laser beam.

CONCLUSIONS

The experiments described above have demonstrated that qualitative analysis can be performed on single particles, in situ, in hostile environments. The practical level of signal reproducibility has been measured, and the first indication of semi-quantitative results has been established. Problem areas have been identified. Some can be overcome while others will limit the applicability of the technique.

The studies will continue with emphasis on establishing the semi-quantitative capability of the combined techniques for well characterized coals, and for new homegeneous standard materials. The experiment will be integrated with a laboratory bench-scale combustor, and the capability to discern changes in coal composition during burning will be investigated by spectral analysis as a function of coal type, combustion residence time, and gas phase chemistry.

ACKNOWLEDGEMENTS

This work was supported by the U. S. Department of Energy, Office of Fossil Energy, Advanced Research and Technology Development Program, Morgantown Energy and Technology Center. We acknowledge the technical assistance of Bill Kent who assembled and maintained the experimental apparatus, and Don Nissen who kindly provided the SEM analyses.

REFERENCES

1. R. W. Schmieder, "Techniques and Applications of Laser Spark Spectroscopy," Sandia Natl. Laboratories Report, SAND83-8618, Mar., 1983.
2. D. K. Ottesen, "In Situ Real-Time Analysis of Particulates Using Laser Spark Spectroscopy," Proc. Int. Conf. on Coal Science, ed. J. A. Moulijn, Elsevier, NY, p. 777 (1987).
3. L. J. Radziemski and T. R. Loree, J. Plasma Chem. Plasma Proc. 1, 281 (1981).
4. J. C. F. Wang and K. R. Hencken, Applied Opt. 25, 653 (1986).
5. D. A. Cremers and L. J. Radziemski, "Laser Plasmas for Chemical Analysis," Ch. 5 in Laser Spectroscopy and Its Applications, eds. L. J. Radziemski, R. W. Solarz, and J. A. Paisner, Marcel Dekker, NY (1987).
6. J. Mika and T. Torok, Analytical Emission Spectroscopy, Butterworth, London (1974).
7. L. J. Radziemski, T. R. Loree, D. A. Cremers, and N. M. Hoffman, Anal. Chem. 55, 1246 (1983).
8. W. F. Meggers, C. H. Corliss and B. D. Scribner, "Tables of Spectral-Line Intensities, Part I," Natl. Bur. of Stds., NBS-MN-145, May, 1975.
9. W. L. Wiese and G. A. Martin, "Wavelengths and Transition Probabilities for Atoms and Atomic Ions," Natl. Bur. of Stds., NSRDS-NBS 68, Dec., 1980.
10. E. Cerrai, and R. Trucco, Energia Nucleare 15, 581 (1968).
11. D. Nissen, Sandia Natl. Laboratories, private communication, Aug., 1987.

A NEW MODEL FOR PREDICTING THE FOULING DEPOSIT WEIGHT OF COAL

J.D. Yeakel

Exxon Production Research Co.
P.O. Box 2189, Houston, TX 77001

R.B. Finkelman

U.S. Geological Survey, MS 956
Reston, VA 22092

INTRODUCTION

One of the major problems associated with coal combustion is the buildup of sintered ash deposits in the convective passes of boilers. These deposits, referred to as fouling deposits, can drastically reduce heat transfer, cause erosion by channelizing gas flow, and contribute to the corrosion of exposed metal surfaces. Downtime for cleaning fouled commercial boilers can be a multi-million- dollar expense (1).

Utility boilers generally are designed to burn coal that falls within a specific fouling behavior range. Therefore, to minimize the deleterious effects of boiler fouling and to maximize boiler efficiency, it is necessary to anticipate or assess the fouling characteristics of a coal prior to combustion.

This paper introduces a new method for predicting fouling deposit weights by using commonly available coal quality data.

We have developed a modified concept of the coal quality characteristics that influence fouling. This concept evolved from a review of the literature and from the statistical analysis of results from 44 combustion tests.

COAL-FOULING-ASSESSMENT INDICES

Several fouling indices based on ash chemistry have been proposed (2). Most are applicable to coal with eastern, or bituminous, ash.* These indices have met with mixed success. Wall et al. (3) state that "there may be very severe limitations to the applicability of 'fouling indices' based on elemental analysis or even on fusion observations...." Moreover, Wall et al. (3, p. 8) note that at a conference on combustion "a number of speakers stated that fouling indices they had used appeared applicable only to coal from a particular field."

*For technological purposes, coals in which the sum of the calcium oxide and magnesium oxide content is greater than the ferric oxide content are characterized as having "eastern" or "bituminous" ash. The relationship is reversed for coals characterized as having "western" or "lignitic" ash.

One reason for the lack of success in applying the fouling indices is that fouling deposits are formed from a complex series of physical and chemical interactions involving several chemical constituents in the coal. The fouling indices, however, focus on only a few of these constituents and put major emphasis on the sodium content.

METHODS

The data used in this study were supplied by the University of North Dakota Energy Research Center (UNDERC) in Grand Forks, North Dakota. The UNDERC supplied the results from over 200 combustion tests conducted in a pilot-scale test combustor. In addition to the combustion test results, the UNDERC also provided complete characterization of the coal samples tested, and the combustion conditions maintained during the course of each test. Coal characterization included proximate, ultimate, and ash composition information. Table 1 shows the coal composition values and combustion test results used as variables in our study.

We selected a set of 44 samples from the raw data provided by UNDERC. This data set served as the basis for developing the model for fouling deposit prediction. The development data set 1) is representative of the UNDERC data set containing data on lignites and subbituminous coals predominantly from the Northern Great Plains Coal Province, 2) contains at least one observation from each mine or locality represented in the UNDERC file, 3) has no sample duplication, 4) is taken from samples that exhibit a wide range of compositions and fouling behaviors, and 5) had similar combustion test conditions.

Our goal was to use the development data set to model fouling deposit weight in grams per million Btu by using coal quality parameters as independent variables. Coal feed rates and total coal burned in a test could vary from test to test, depending upon the calorific value of the coal. Therefore, conversion of deposit weights to a weight per million Btu basis puts the fouling tendency on a unit energy input basis, a basis frequently used by boiler operators for other purposes such as evaluating sulfur emissions.

The first step in data analysis was to determine if the natural frequency distributions of the variables in the development data set approximate a normal frequency distribution. In all statistical analyses, we assumed the variables to be approximately normally distributed. Therefore, the variables that, in their original form, were not normally distributed were mathematically transformed to yield frequency distributions that approximated normal distribution. The transform functions (Table 1) for each variable were used in all subsequent analysis.

The second step in our study was to conduct bivariate analyses, i.e., calculation and interpretation of correlation coefficients (r-squared values). This analysis determined which variables most closely correlate with fouling deposit weight.

The third and principal step in our analysis was to employ multiple regression analysis to develop a model. We used the STEPWISE, RSQUARE, and REG procedures in SAS (4) to develop and evaluate possible models. All of these

procedures are linear least-squares methods for establishing empirical relationships between one or more independent variables and some response variable. In our case, the independent variables, or regressor variables, are transformed coal-quality parameters. The response variable is the log function of the fouling deposit weight in grams of deposit per million Btu fired.

Models were evaluated on the basis of the improvement in r-squared values, the decrease in the residual sum of squares, the significance of parameter estimates for each variable, and the linkage between fouling behavior and each variable being considered. Statistical significance alone was not enough to include a variable in the model. The final model selected was one that maximized the fit of the predicted values to the actual fouling deposit weight values; thus, maximizing the r-squared value and minimizing the sum of squared residuals.

Finally, we tested the model. For this purpose, we selected a second set of observations from the raw UNDERC data set. This set had the same characteristics as the development data set but contained only 15 samples and had no observations in common with the original data set. We tested the model by calculating a predicted fouling deposit weight using the model and then by comparing the calculated deposit weight with the actual deposit weight.

RESULTS

Bivariate Analysis

In the process of calculating the correlation coefficients for the variables in the development data set we discovered that several coal compositional parameters have significant correlation with fouling deposit weight (Table 2). The amount of ash, total sulfur, titania (TiO_2), potash (K_2O), silicon (Si), sodium (Na), aluminum (Al), and the alkali ratio are significantly related to fouling deposit weight. However, even though the correlations are significant at the 1-percent confidence level, the correlation coefficients are not very high indicating that no one variable is principally responsible for variation in fouling deposit weight. The relationship between fouling and coal composition is too complex to explain with just one variable. This relation is illustrated by means of a few scatter plot diagrams, one showing sodium versus deposit weight (Fig. 1) and the other showing ash yield versus deposit weight (Fig. 2).

Sodium, at present, is the most widely used predictor of fouling tendency; yet, Figure 1 demonstrates that low sodium oxide content in a coal does not guarantee low fouling or that high sodium oxide content equates with severe fouling. Obviously, fouling behavior is dependent upon something other than, or in addition to, the sodium oxide content of coal.

Figure 2 shows the dry ash yield of a coal plotted against the coal's fouling deposit weight. The relationship here is more linear than the one observed for Na_2O, therefore, as ash yield increases so too should fouling deposit weight. This may be thought of as the boiler tubes being exposed to more potential fouling material per unit energy generated. However, the

significant scatter in the relationship of ash yield and deposit weight would preclude the use of only ash as a predictor.

Both sodium (5) and ash yield have been shown to enhance fouling behavior (6). If we plot sodium, ash, and deposit weight on a three-dimensional diagram (Figure 3) we can see the relative influence of the two variables on deposit weight.

Figure 3 indicates that low sodium, low ash coals are low fouling coals. High fouling coals are having with moderate to low amounts of sodium but high ash yields. Deposit weights are more variable when ash yields are low to moderate and sodium values are moderate to high.

The use of ash and sodium together as predictors of fouling may be more reliable than the use of sodium alone, however, we had reliable predictions only in end member situations (low sodium, very high ash). One or two coal composition variables cannot adequately explain or predict fouling behavior. Consequently, we used multiple regression analysis to develop a model to explain the variation of fouling deposit weight values in the development data set.

THE REGRESSION MODEL.

The regression model we found that best fits the fouling deposit weights in the development data set is given in equation 1. The variables incorporated into the model and their basis are listed in Table 3. The model calculates the logarithm of the fouling deposit weight in terms of grams of deposit per million Btu fired and it incorporates TiO_2, total sulfur, ash yield, Ca/S, and a factor called the alkali ratio. This latter term is calculated by using calcium, magnesium, sodium, and potassium oxide values and the ash yield. The fouling prediction equation is:

$$\log_{10}(\mathbf{FDW}) = 1.21 + 0.45\ (\log_{10}\mathrm{Ti}) + 1.46\ (\log_{10}\mathrm{S}) + 0.38\ (\log_{10}\mathbf{ASH}) + 1.14\ (\log_{10}\mathrm{Ca/S}) + 0.63\ (\log_{10}\mathbf{ALK}) \qquad (1)$$

Where: **FDW** = Fouling Deposit Weight (grams/million Btu)
Ti = Titanium Dioxide % (sulfate-free ash)
S = Sulfur % (dry coal)
ASH = Ash Yield % (dry coal)
Ca/S = Calcium/Sulfur (both % wt. of dry coal)

$$**\mathbf{ALK} = \frac{\text{Ash \% (dry} * (Na_2O + .659K_2O)}{CaO + MgO}$$ **(alkali ratio)**

** Na_2O, K_2O, CaO, and MgO are all on a % of sulfate-free ash basis.

To use the model, the coal quality information required is: ash yield (percent dry coal), sulfur (percent dry coal), and titanium, sodium, calcium, potassium, and magnesium oxides (percent sulfate-free ash). The calcium-sulfur ratio and the alkali ratio are then calculated. Then the logarithm of each parameter in Table 3 is calculated and inserted in equation 1. The result of the calculation is the base 10 logarithm of the fouling deposit weight. This can then be converted directly to grams deposit per million Btu, the predicted fouling deposit weight.

In Figure 4, predicted and observed deposit weight values are plotted. The proximity of the points to the parity line indicates that the model and actual data are in good agreement. Also, the r-squared value, 0.84, is high and significant and indicates that a significant amount of the variability in actual fouling deposit weight is explained or accounted for by the model. The sum of the squared residuals is 1.35. This value is low relative to those obtained for other potential models that we tested. In addition, all of the variables included in the model, except the calcium-sulfur ratio, correlate with fouling deposit weight.

TESTING THE MODEL

Our test of the regression model using the smaller test data set shows that the model works well. The actual versus predicted fouling deposit weights for the test samples are plotted in Figure 5. As with the development data set, points are clustered along the parity line. However, for the test data, the r-squared value is lower than that calculated for the development data because the range in values in the test data set is more limited and there are fewer observations.

We recognize that the model is subject to error. The plots are on a logarithmic scale thus small deviations from the parity line could result in errors of several 10's of grams per million Btu. However, a comparison of Figures 4 and 5 with Figure 1 shows that our model is superior to sodium oxide as a predictor of fouling deposit weight.

The error associated with any individual prediction is approximately 20-30 percent of the calculated fouling deposit weight. This figure is based on the range of differences between actual and predicted values for all the observations in both the development and test data sets. We found that 90 percent of the differences were <57 grams per million Btu, 75 percent of the differences were <28 grams per million Btu, and 50 percent of the differences were less than 15 grams per million Btu. Also, the largest errors occurred in samples that had very high actual fouling deposit weights. Large errors in this range are acceptable because, once deposit weights exceed 150 grams per million, a severe fouling problem exists and actual deposit weights are relatively unimportant. Accuracy is required, however, in the lower range of values, below 150 grams per million Btu. Our data indicate that equation 1 can be used to estimate fouling deposit weight to within 15-30 grams per million Btu, or less, an acceptable margin of error.

DISCUSSION

We believe that that fouling behavior of low-rank coal is predictable but that predictions will not be reliable when based on information from only one or two quality variables. Fouling is a complex phenomenon that involves a complex process (combustion) acting on a complex material (the coal). Therefore, predicting the fouling behavior of any coal will to depend on a variety of coal components, their relative amounts, their mode of occurrence, and on furnace conditions.

A variety of components in the coal interact with one another during combustion to form or retard the formation of fouling deposits. These components include the total ash yield of the coal; sulfur content; and the amount of sodium, calcium, magnesium, potassium, and perhaps silica. The ash content, particularly the more siliceous minerals, forms the bulk or aggregate of the fouling deposits. Calcium, sulfur, sodium, etc., interact to influence how much and what types of materials will bind this siliceous/ash aggregate together and to the boiler tubes. Coal that has a low ash yield exhibits low fouling behavior. Coal that has a high ash yield exhibits extreme fouling behavior but only if there is sufficient adhesive material to amalgamate the deposit. Consequently, diluting high-sodium coal with ash material (roof rock for instance) may be inadvisable if ash yields are already very low. The aggregate or bulk phase of the fouling deposit is accounted for in our model by ash, by ash as part of the alkali ratio, and also by the TiO_2 factor, which we believe is indicative of the detrital component of the coal ash.

The binding, or hardening, of the deposits is, in our opinion, the least understood and probably the most complex aspect of the fouling deposit formation. In our view of fouling deposit formation, the sodium and potassium ions released by coal combustion compete with the calcium and magnesium ions for sulfur. There is evidence that potassium and sodium sulfates are present in fouling deposits or play a role in their formation (7). The picture is less clear for calcium and magnesium sulfates. However, in our opinion the calcium and magnesium sulfates do not participate as a binding phase in fouling deposit formation, but may,however, be incorporated into the deposit as inert material.

The sulfur, Ca/S, and alkali ratio factors in equation 1 all relate to this binding phase of the fouling deposit. The sulfur content is obviously important, for, without sulfur, no binding phase could be present. The calcium-sulfur ratio is a measure of how much sulfur will be bound by calcium and is, thus, not available to binding by sodium. The alkali ratio is a measure of the quantity of alkali elements that have been positively linked to deposit formation (sodium and potassium [8, 9]) relative to the elements that may have a negative impact on deposit formation (calcium and magnesium).

Finally, we be stress that the model proposed in equation 1 is based principally on the degree of fit between the modeled data and the actual data, moderated by our perception of how various components in coal may behave during the formation of fouling deposits. The model is redundant because ash yield is represented in two places and the binding phase of the fouling deposits is represented by three terms. Two factors cause this redundancy. First, the mode of occurrence of the elements in the model affects the reactivity of the elements, in fouling deposit formation. Our model does not take mode of occurrence into account. Second, the development and test data sets are heavily biased towards moderate fouling coals. Only a few examples of coal that had extreme fouling behavior were available for inclusion in the data set. Inclusion of more low and high fouling coal samples in the data set might clarify the situation and result in a less redundant and more theoretically sound model. However, given the data currently available, this model does a good job of accurately predicting fouling behavior and it is clearly an improvement over the conventional (sodium) index currently in use.

CONCLUSIONS

1. We have developed a new model for predicting the fouling behavior of low rank coal. The model is based on commonly available coal quality data.

2. The proposed model has the potential to provide accurate quantitative estimates of fouling deposit weight per million Btu.

3. This model is more accurate in predicting fouling behavior than the sodium index.

4. Actual combustion tests of unknown coals need to be conducted to fully test the utility of this model.

5. The fouling potential of a coal cannot be adequately evaluated by using one or two compositional variables. A multivariate approach is more apt to yield reliable evaluations of fouling behavior.

REFERENCES

1. Honea, F.I., Montgomery, G.G., and Jones, M.L., 1982, Recent research on ash fouling in combustion of low rank coals, in W.R. Kube, E.A. Sondreal, and D.M. White, comps., Technology and use of lignites, Vol. 1, Proceedings, Eleventh Biennial Lignite Symposium: Grand Forks Energy Technology Center IC-82/1, p. 504-545.

2. Vaninetti, G.E., and Busch, C.F., 1982, Mineral analysis of ash data--a utility perspective: Coal Quality, Spring, p. 22-31.

3. Wall, R.F., and others, 1980, Pulverized coal-firing--the effects of mineral matter: Energy Work (UK), Vol. 70, p. 7-8.

4. SAS, 1985, SAS Users Guide: Statistics, version 5: SAS Institute Inc., Box 8000, Cary, NC 27511.

5. Reid, W.T., 1981, Coal ash--its effect on combustion systems, in M.A. Elliott, ed., Chemistry of coal utilization, 2nd Suppl. Vol.: New York, John Wiley, p. 1389-1445.

6. Tufte, P.H., and Beckering, W., 1975, A proposed mechanism for ash fouling burning Northern Great Plains lignite: Jour. Eng. Power, Vol. 97A, p. 407-412.

7. Tufte, P.H., Grohnovd, G.H., Sondreal, E.A., and Selle, S.J., 1976, Ash fouling potential of western subbituminous coals as determined in a pilot plant test furnace: Proceedings, American Power Conference, Chicago, IL.

8. Hurley, J.P., Miller, B.G., Jones, M.L., Finkelman, R.B. and Yeakel, J.D., 1985, Correlation of coal characteristics and fouling tendencies of various coals from the Gascoyne mine: Thirteenth Biennial Lignite Symposium: Technology and Utilization of Low Rank Coals; M.L. Jones, editor, DOE/METC/86/6036, p. 76-85.

9. Attig, R.C., and Duzy, A.F., 1969, Coal ash deposition studies and application to boiler design: Proceedings of the American Power Conference, Vol. 31., p. 290-300.

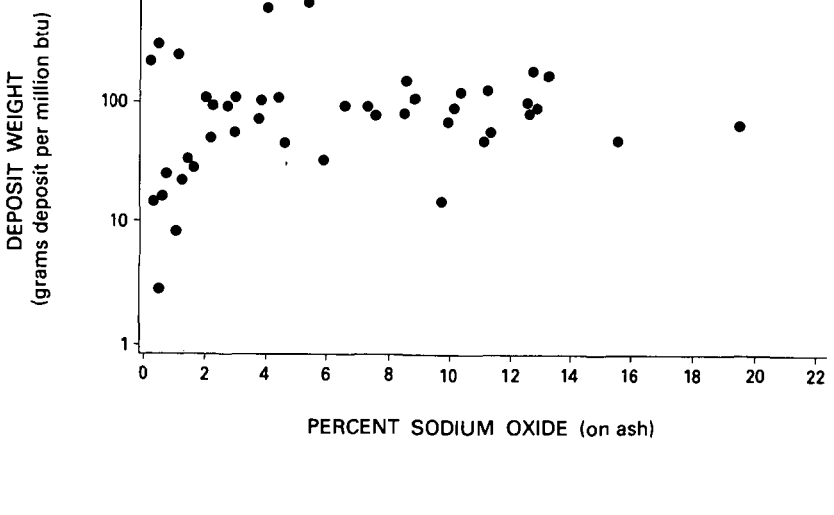

Figure 1.--Relation of sodium content to Fouling Deposit Weight.

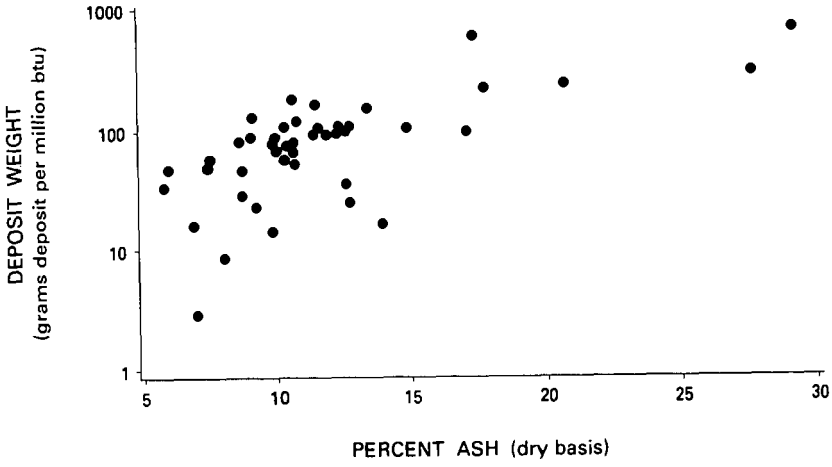

Figure 2.--Relation of coal ash yield to Fouling Deposit Weight.

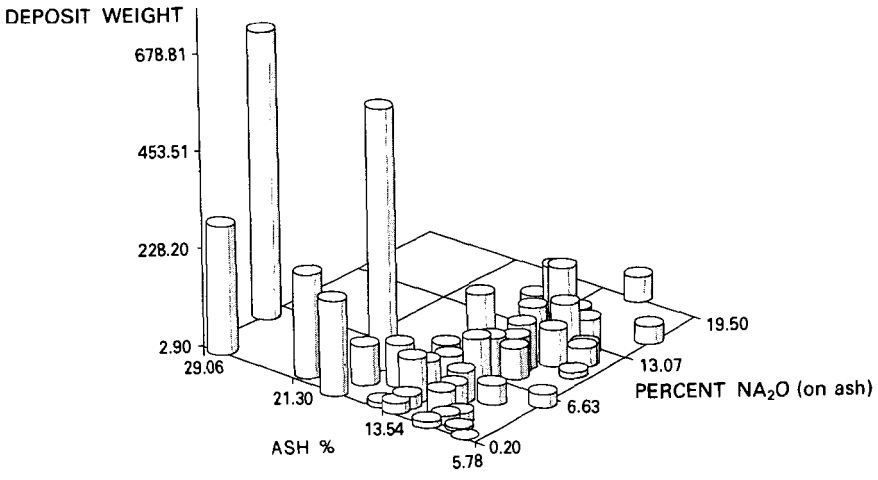

Figure 3.--Relation of ash and sodium contents to Fouling Deposit Weight.

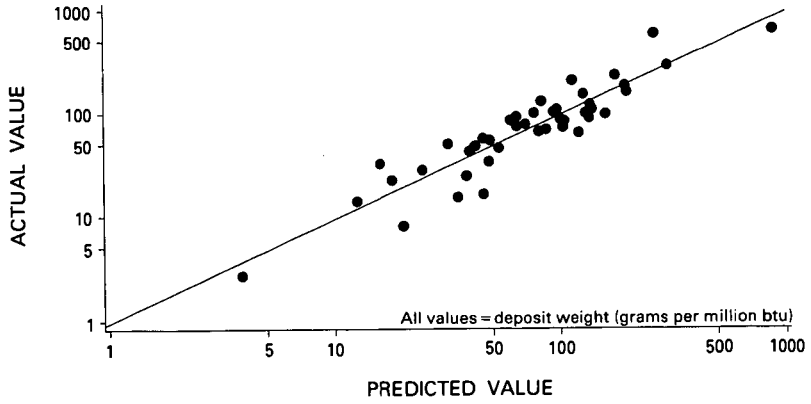

Figure 4.--Log/log plot of actual versus predicted Fouling Deposit Weight using our multivariate model (development data).

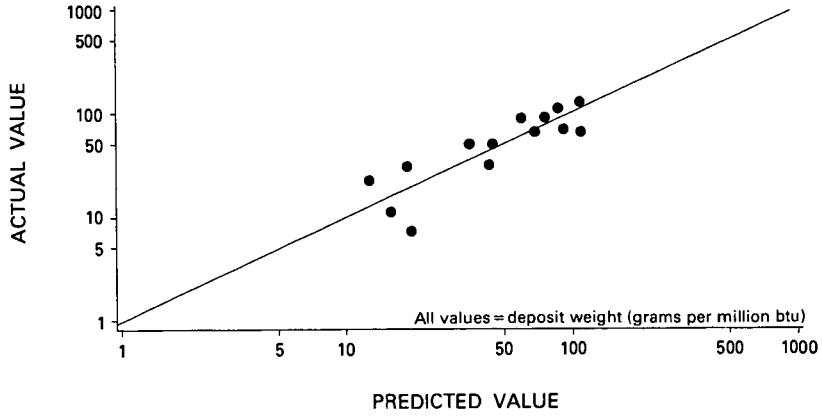

Figure 5.--Log/log plot of actual versus predicted Fouling Deposit Weight using our multivariate model (test data).

Table 1.--List of variables included in multivariate statistical analysis

Variable	Mean	Range	Transform* Function
Ash (dry)	11.73	5.78 - 29.06	Log(10)
Btu (dry)	10634	8400 - 12110	-
Carbon (daf=dry ash-free)	71.89	68.81 - 77.94	-
Hydrogen (daf)	4.75	2.78 - 5.73	Square
Nitrogen (daf)	1.16	0.99 - 1.86	-
Oxygen (daf)	20.68	15.73 - 24.49	-
Volatile Matter (daf)	48.25	42.41 - 55.13	-
Sulfur (dry)	1.29	0.29 - 4.13	Log(10)
SiO_2 (sulfate-free ash)	32.75	15.20 - 61.50	-
Al_2O_3 (sulfate-free ash)	15.02	8.50 - 22.90	-
TiO_2 (sulfate-free ash)	0.68	0.20 - 1.70	Log(10)
Fe_2O_3 (sulfate-free ash)	11.62	1.80 - 24.50	-
CaO (sulfate-free ash)	25.45	6.00 - 45.70	-
MgO (sulfate-free ash)	7.06	0 - 13.00	-
K_2O (sulfate-free ash)	0.61	.10 - 2.50	Log(10)
Na_2O (sulfate-free ash)	6.26	.20 - 19.5	Sq. Root
Silicon (dry coal)	1.64	.43 - 7.71	Log(10)
Aluminum (dry coal)	0.78	.27 - 2.78	Log(10)
Sodium (dry coal)	0.39	.02 - 1.34	Sq. Root
Calcium (dry coal)	1.59	.27 - 2.70	-
SiO_2/Al_2O_3	2.25	1.11 - 5.02	Log(10)
Ca/S (dry coal)	1.83	.27 - 9.26	Log(10)
Base-Acid Ratio	1.21	.22 - 3.15	-
Alkali Ratio	2.75	.14 - 23.48	Log(10)
Deposit Weight ($gm/10^6$ Btu)	112.7	2.90 -678.81	Log(10)

*Function applied to those variables whose natural frequency distribution did not approximate a normal distribution. Transformed values do approximate a normal distribution.

All values except deposit weight, Btu, and ratios are percentages on basis shown.

Table 2.--Coal quality variables that significantly correlate with fouling deposit weight (g/million Btu)

Variable	Correlation Coefficient
Ash (percent wt. of dry coal)	0.67
Sulfur (percent wt. of dry coal)	0.49
Btu/lb (dry coal)	-0.61
TiO_2 (percent wt. of sulfate-free ash)	0.39
K_2O (percent wt. of sulfate-free ash)	0.36
Volatile Matter (daf)	0.52
Si (percent wt. of dry coal)	0.43
Na (percent wt. of dry coal)	0.49
Al (percent wt. of dry coal)	0.44
Alkali Ratio	0.65
Na_2O (percent wt. of sulfate-free ash)	NS*

*NS = not siginficant

Table 3.--List of coal quality variables used in prediction of fouling deposit weight (g/million Btu)

Quality Parameter	Basis
Titanium Oxide (TiO_2)	percent wt. of sulfate-free ash
Ash Yield	percent wt. of dry coal
Total Sulfur	percent wt. of dry coal
Calcium Oxide (CaO)	percent wt. of sulfate-free ash
Sodium Oxide (Na_2O)	percent wt. of sulfate-free ash
Potassium Oxide (K_2O)	percent wt. of sulfate-free ash
Magnesium Oxide (MgO)	percent wt. of sulfate-free ash

A GRANULATION/SINTERING METHOD FOR THE CODISPOSAL OF SOLID RESIDUES FROM COAL CONVERSION PROCESSES

G. Burnet, A. J. Gokhale, and R. F. Meisinger

Ames Laboratory, U.S.D.O.E. and Department of Chemical Engineering
Iowa State University, Ames, IA 50011

ABSTRACT

A stabilization process for coal cleaning and coal combustion-related wastes has been developed that uses the energy derived from the fuel contained in the coal cleaning waste. The wastes are pulverized, when necessary, formed into granules in a rotary pan agglomerator, and then fired to a sintering temperature. The resulting readily disposable product consists of rock-hard granules that are highly resistant to environmental degradation. The green (nondried and nonfired) granules satisfy durability tests that measure the capability to be handled and stored. The sintered granules meet requirements of the standard ASTM and EP leaching tests and a freeze-thaw cycle test. The strength of the sintered granules compares favorably with the strength of natural aggregates. The process has been applied to coal cleaning refuse alone and to refuse/fly ash and refuse/FGD sludge mixtures.

INTRODUCTION

Disposal of coal cleaning and of coal combustion wastes looms as a significant problem for many coal producers and utilities. This has stimulated research on environmentally acceptable alternatives to current disposal practices. About 35% of the nearly 700 million tons of coal consumed by utilities each year receives some cleaning before it is burned (1). Most of the cleaning is performed on eastern and midwestern bituminous coals, resulting in an annual production of coal cleaning wastes in excess of 100 million tons (2). The waste piles are a source of severe air, stream, and ground water pollution (3).

Other environmentally troublesome solid wastes result from coal combustion and are proving to be even more difficult to deal with. For every three tons of coal cleaning refuse, about one ton of ash and one ton of flue gas desulfurization (FGD) solids result from combustion of the clean coal produced. Besides contributing to pollution, the waste disposal sites required mar the landscape and consume large amounts of land area.

The principle combustion-related solid waste today is fly ash from the burning of pulverized coal. In spite of vigorous research and marketing efforts, uses have been found for only about one-fifth of nearly 50 million tons of fly ash produced each year (4). Disposal is the only practical option available today for wet or dry FGD wastes. More than 150 U.S. utility installations generating wet scrubber sludge are operating, under construction or planned, with a total capacity of over 70,000 MWe (5). About 25 million tons (dry basis) of sludge or 50 million tons of wet vacuum filter cake are now generated annually and, as new systems come online, this amount will increase significantly.

A potentially beneficial approach to the disposal of the above wastes could be pretreatment in the form of stabilization or fixation. The research work reported herein deals with development of a stabilization by sintering process for the above wastes that uses the energy derived from fuel contained in the coal cleaning refuse itself. The process calls for pulverizing the wastes when necessary, forming them into granules in a rotary pan agglomerator, and then firing

the granules to a sintering temperature. The resulting, readily disposable product consists of rock-hard granules that are highly resistant to environmental degradation. A flowsheet for the process is shown in Figure 1.

Stabilization results are reported for coal cleaning refuse alone and for refuse/fly ash and refuse/sludge mixtures. The amount of carbon in the granules is critical to their behavior during combustion/sintering. Other investigators (6,7) have found that a carbon content of 5-10%$_w$ is sufficient to achieve the desired level of sintering. If the carbon content is too high, the granules overheat upon combustion of the fuel present and soften, forming a slag. Blending fly ash or FGD sludge with the refuse provides the necessary reduction in carbon content per unit weight of granules and an effective means for disposing of these wastes.

DESCRIPTION OF WASTES USED

Analyses of the coal cleaning and coal combustion wastes used are given in Table 1. The coal cleaning refuse was collected at the Peabody Coal Company River King coal preparation plant in Freeburg, Illinois. The waste was derived from Illinois No.6 coal which is high volatile C, bituminous, medium heating value (24,400 kJ/kg; 10,500 Btu/lb, as received) and medium sulfur (4.5%$_w$). The coal is cleaned of unwanted clay, pyrite, and other impurities by jigging at a rate of up to 800 tons/hr. The major minerals present in the raw refuse are illite, kaolinite, quartz, calcite, and iron pyrite.

Table 1. Analyses of Coal Cleaning and Coal Combustion Wastes

Item	Weight Percent or Value		
	Cleaning Refuse[a]	Fly Ash[b]	FGD Sludge[b]
Constituent			
Al_2O_3	15.1%	19.8%	3.4%
CaO	5.7%	24.9%	33.7%
SiO_2	43.8%	34.4%	15.6%
Fe_2O_3	13.5%	5.1%	6.1%
MgO	n.a.[c]	4.0%	0.6%
Na_2O	n.a.	2.1%	0.2%
K_2O	n.a.	0.3%	n.a.
TiO_2	n.a.	1.5%	n.a.
P_2O_5	n.a.	1.8%	n.a.
C	13.9%	n.a.	n.a.
S (inorganic)	6.0%	n.a.	n.a.
S (total)	7.3%	0.7%	5.4%
H_2O	4.5%	-	-
LOI	24.3%	0.2%	n.a.
Value			
Heating value (gross)	6055 kJ/kg (2610 Btu/lb)		

[a] Air dried from an as-received moisture content of 20%$_w$.
[b] Reported on a dry basis. The sludge contained 26.5%$_w$ total C reported as CO_2.
[c] n.a. denotes not analyzed for.

The as-received refuse contained lumps as large as 8 cm in diameter and had to be ground to a size suitable for granule formation. The refuse was ground using two passes through a Holmes hammer mill equipped first with a screen with 3/16 in. circular holes and then a screen with 1/16 in. circular holes. The weighted average diameter of the product was about 330 microns; 95%$_w$ was retained on a 325 mesh screen.

The fly ash used was obtained from the Ottumwa power station of Iowa Southern Utilities in Ottumwa, Iowa and was from combustion of a subbituminous coal mined near Gillette, Wyoming. The particle size of the ash was such that about 20%$_w$ was retained on a 325 mesh screen. The FGD sludge came from the LaCygne station of the Kansas City Power and Light Company near Kansas City, Missouri. The plant was burning Missouri subbituminous coal and using a wet limestone scrubber that produced a non-oxidized sludge. The limestone was ground to about 70 microns prior to slurrying and the crystals of sulfur-containing compounds formed ranged from 5-200 microns. The S was present 78%$_w$ as $CaSO_3 \cdot \frac{1}{2}H_2O$ and 22%$_w$ as $CaSO_4 \cdot 2H_2O$; 78%$_w$ of the Ca was present as $CaCO_3$.

PREPARATION OF GREEN GRANULES

Granules as formed in the pan agglomerator are referred to as green granules. The parameters controlling green granule formation are the particle size of the wastes, amount of water added as a binder, residence time of the granules in the agglomerator (feed rate), and the angle of inclination and rpm of the agglomerator.

The pan agglomerator (Agglomiser, 36 cm pan, 1/8 hp, Mars Mineral Corp.) was equipped with a vibratory feeder (Syntron, Model FTOC, FMC Corp.). The water to serve as the binding agent was added using an automatic spray system or a manually operated spray bottle. The refuse/ash and refuse/sludge mixtures were prepared by blending the solids in a ball mill before they were added to the agglomerator.

A batch method of operation for small scale testing was developed that gave granules of predictable and reproducible properties. Depending upon the conditions used, each run lasted for 30-80 minutes and consumed about 1500 grams of feed. Granules were removed from the pan during the run as they reached the desired product size of about 12 mm diameter.

Large quantities of green granules (10-12 kg) were subsequently prepared for sintering and testing for resistance to leaching and freeze-thaw degradation. The pan agglomerator was operated continuously at a set of conditions previously determined from the small-scale batch tests.

The green granules formed had to be sufficiently durable to withstand the vibration, attrition, compression, and similar forces that would be encountered in a commercial sintering facility. Durability was measured using the ASTM B440-49 Drop Shatter Test (modified) and a drops-to-fracture test (8). Satisfactory granules would show 95%$_w$ intact or better for the drop shatter test and 15 drops or better for the drops-to-fracture test.

In determining the optimum conditions for green granule formation, the total moisture content in the pan was varied from 15-22%$_w$, the pan angle from 45-55°, and the feedrate from 15-60 g/min. Lower moisture contents resulted in poor particle adhesion and granules that developed breakage planes easily. Higher moisture contents resulted in caking in the pan.

Steeper pan angles resulted in greater granule compaction but a reduced residence time. A pan speed of 19 rpm was found to provide the rolling and cascading action required to promote continuous granule growth. The best granules were obtained at lower feed rates where uniform granule growth occurred and the longer residence time resulted in greater granule compaction.

The best refuse only granules as determined by durability testing were obtained in the 18-20%$_w$ moisture range using a pan angle of 45°. Refuse/fly ash granules showed lower durability and required less moisture as the ash content was increased. Very satisfactory granules containing 25%$_w$ ash were obtained at feed rates of 15-30 g/min, a pan angle of 50°, and a moisture content of 17-18%$_w$, wet basis.

Granule durability for refuse/sludge mixtures decreased as the sludge content increased. Depending upon the amount of sludge present, the optimum moisture content varied from 15-22%$_w$. The best results were obtained with a pan angle of 50° and a feedrate of about 50 g/min.

The amount of refuse in a refuse/ash mixture was determined by carrying out a standard loss on ignition (LOI) test. The ash present had already been ignited when it was formed in the furnace so that the total LOI could be attributed to the refuse present. The amount of sludge in a mixture was determined by analyzing for Ca by xray fluorescence. Knowing the ratio of Ca in the sludge to that in the refuse, it was then possible to calculate the composition of the blend.

COMBUSTION/SINTERING OF THE GREEN GRANULES

To cause sintering to occur, the granules were heated in the presence of air causing the coal in the refuse to burn, thus raising the temperature of the granules to the desired sintering temperature. The green granules used had been produced using the conditions previously found to give optimum granule durability.

The effect on sintered granule properties of different time-temperature treatments was determined using small scale boat tests carried out using an electrically heated laboratory tube furnace (I.D. 3.4 cm). Five to ten granules that had been previously dried in a 100°C oven were placed in an alumina boat which was then inserted into the tube furnace preheated to the test temperature. A carefully measured flow of air (10 L/min at 1 atm. and 20°C) was then introduced into one end of the furnace tube.

Granules were sintered at temperatures ranging from 900-1200°C for 1 hour to approximate the conditions in a traveling grate furnace. The amount of sintering that had taken place was determined by subjecting the cooled sintered granules to an unconfined compressive strength test using an Instron machine. The best of the small scale test results determined the operating conditions for the production of environmental test quantities of sintered granules in a large tube furnace.

Figure 2 gives the force-at-fracture for the sintered refuse only granules as a function of sintering temperature. The granules sintered at 1200°C were very weak due to early slagging on the surface and incomplete sintering inside. Insufficient sintering overall took place at temperatures below about 1075°C. The strongest granules were produced at about 1100°C.

Similar small scale sintering tests were conducted on granules made from refuse/fly ash and from refuse/sludge mixtures. The highest force at fracture (105 lb) for refuse/subbituminous coal fly ash was obtained for a 3:1 refuse/ash mixture sintered at 1000°C. Refuse/sludge mixtures in a ratio of 4:1 gave satis-

factory strength (85-90 lb) at 1050°C and at 1075°C. At 1100°C, granules of both mixtures developed a vitreous melt or slag on the surface that resulted in an undersintered core and low granule strength.

The large-scale boat tests were carried out using a large horizontal, electrically heated tube furnace and a boat (4 cm x 4 cm x 15 cm) custom made from a ceramic brick. The walls of the boat were about 8 mm thick and contained frequent holes about 6 mm in diameter to allow for passage of air and combustion gases. The boat could accommodate up to 180 g of granules.

Using the best of the conditions from the small-scale boat tests, dried green granules were placed in the large boat and introduced into the furnace which had been preheated to 600°C. The flow of combustion air was then started and the furnace temperature controls reset to 1050°C for the duration of the run. A thermocouple placed in the bed of granules indicated that the bed would reach 1050°C in about 45 minutes and a peak temperature of about 1100°C after about 60 minutes. Total residence times of 90 minutes and 120 minutes were investigated.

The individual sintered granules from the large boat tests were either red-brown or black-brown in about a 1:1 ratio. The black-brown granules were found towards the bottom of the bed where the temperature was the highest and the supply of oxygen was limited. These conditions would be similar to those encountered in the granule bed in a traveling grate furnace. The black-brown granules were significantly stronger with the strength influenced by residence time. The black color is thought to result from the presence of Fe_3O_4 and of hersynite, $FeAl_2O_4$, a spinel group that would add to granule strength. The red-brown granules were found at the top of the bed where oxygen was readily available and Fe_2O_3 would form.

For a total residence time of 90 minutes, the refuse only black-brown granules gave a force at fracture of about 120 lb, the 3:1 refuse/subbituminous coal fly ash granules 100 lb, and the 4:1 refuse sludge granules 150 lb. The compounds in the sludge facilitate sintering and increase strength.

EVALUATION OF SINTERED GRANULES

In order to be environmentally disposable, the sintered granules must be very strong, able to resist cycles of freezing and thawing, and essentially non-leachable. The latter two characteristics were measured using a standard freeze-thaw resistance test (9), shake Extraction with Water Test, ASTM D3987-81 (10), and EP Toxicity Test (11).

The concentrations of elements in the leachates from the refuse/sludge granules as determined by mass spectroscopy along with the permissible levels established by RCRA regulations (12) are given in Table 2. The results for all elements are well below the current RCRA standards. Similar satisfactory results were obtained for leachates from the sintered refuse only and refuse/fly ash granules.

The results from the freeze-thaw cycle tests were most encouraging for all three types of sintered granules. The weight loss by degradation was less than $0.5\%_w$. Natural aggregate such as crushed rock will commonly show a degradation in the range of $5\text{-}10\%_w$ (13). None of the sintered granules should offer a problem when disposed of where leaching and/or freezing weather occur.

Table 2. Leachate analysis of sintered refuse/FGD sludge granules

Element	RCRA**	Concentration of metals in leachate, ppm (mg/L)* 10% FGD ASTM	10% FGD EP	20% FGD ASTM	20% FGD EP	30% FGD ASTM	30% FGD EP	Green Granules ASTM	Green Granules EP
Al	-	.68	5.33	.51	3.74	.54	7.72	-	.55
As	5	-	-	-	.03	-	.07	-	-
Ba	100	.16	.05	.22	.05	.16	.08	-	.09
Cd	1	-	-	-	-	-	-	.024	.109
Ca	-	587	303	558	287	626	545	533	2131
Cr	5	-	-	-	-	.05	-	-	-
Fe	-	-	4	-	1.5	-	2.3	-	.1
Pb	5	-	-	.005	-	-	-	-	-
Hg	.02	.0065	.0041	.0071	.0007	.0048	.0031	.008	.0096
Se	1	.007	.009	-	-	.015	-	.34	.072
Si	-	10	23	8	18	9	42	5	4
Ag	5	-	-	-	-	-	-	-	-

* Concentrations not shown were below detection limits.
** RCRA (EPA) limits are 100 times drinking water standards.

EVOLUTION OF SULFUR DURING SINTERING

Combustion/sintering of the green granules results in release of about three-fourths of the S present as SO_2 in the off gases. A microreactor system illustrated in Figures 3 and 4 has been built to obtain a more fundamental understanding of S evolution and the reactions taking place.

The microreactor is made of stainless steel and is equipped with a combustion air distributor and a removable mount for a single granule. This arrangement ensures uniform contact between the combustion air and the granule, and control of the sintering taking place. By analysis of the off gases and the granule, the effects of sintering conditions and of granule composition, diameter, and particle size on the pattern of S evolution can be determined.

Preliminary tests have shown that a surge of SO_2 consisting of about two-thirds of the S present in the granules is released in about the first one-third of the combustion process. The SO_2 concentration in the off gases during this time would be expected to be relatively high because of the limited amount of combustion air required and the recycle of combustion air from windboxes to hoods along the traveling grate furnace. A SO_2 content of 3-5%$_v$ appears to be readily attainable. If it proves to be unattractive to thus process all of the off gases, the more dilute fraction could be recycled to the power station FGD system. Recovery of S from the off gases as S or H_2SO_4 would serve the dual purpose of controlling S emissions and generating a valuable byproduct. Sulfur recovery from waste gas streams is a well proven and well established technology (14).

CONCLUSIONS

The combustion/sintering of granules of coal cleaning refuse or of refuse mixed with fly ash or FGD sludge has been shown to yield a strong and highly vitrified product. Durable green granules were prepared in a pan agglomerator using

water as the binder. A laboratory, bench scale procedure was developed to approximate the combustion/sintering that occurs in a commercial traveling grate furnace. Most of the energy required for the sintering can be derived from the fuel inherently present in the refuse. All three types of sintered granules were found to be environmentally compatible as measured using standard ASTM and EP leaching tests and a freeze-thaw cycle test. The byproduct recovery of S from the combustion/sintering off gases looks promising based on laboratory microreactor studies.

ACKNOWLEDGEMENTS

Ames Laboratory is operated for the U.S. Department of Energy by Iowa State University under Contract No. W-7405-Eng-82. This work was supported by the Assistant Secretary for Fossil Energy through the Morgantown Energy Technology Center.

REFERENCES

1. Shepard, M., EPRI Journal, 14-21, Nov. (1985).
2. Lemon, A.W., G.L. Robinson, S.E. Rogers and P. Van Voris, Environmental Assessment of Coal Cleaning Processes, NTIS EPA-600/7-28-024 (1982).
3. Nriagu, J.O. (Editor), Sulfur in the Environment, Part II: Ecological Impacts, John Wiley and Sons, New York, 316 (1978).
4. American Coal Ash Association, Washington, DC, Ash Production and Ash Utilization-1985 (1986).
5. Gutschick, K.A., Lime for Environmental Uses, STP 931, ASTM, Philadelphia, PA, 52-53 (1985).
6. Gutt, W., P.J. Nixon, R.J. Collins and R. Bollinghaus, Precast Concrete (3), 120-127 (1980).
7. Ball, D.F., J. Dartnell, J. Davison, A. Grieve and R. Wild, Agglomeration of Iron Ores, American Elsevier, New York, 250, 314-319 (1973).
8. Burnet, G. and A.J. Gokhale, Processing and Utilization of High Sulfur Coals II, Y.P. Chugh and R.D. Caudle (Editors), Elsevier Science Publishing Company, New York, 431-443 (1987).
9. Annual Book of ASTM Standards, D3987-81, ASTM, Philadelphia, PA (1977).
10. Federal Register, 43, No. 243, 58956-57, December 18 (1978).
11. Dolar-Mantuani, L., Handbook of Concrete Aggregates, Noyes Publications, Park Ridge, NJ, 216-218 (1983).
12. Federal Register, 45, No. 98, 33122, May 19 (1980).
13. Hockett, P., Personal communication, Iowa Dept. of Transportation, Ames, IA, November (1986).
14. Ford, P.G., Modern Power Systems, 7, No. 6, 37-43 (1987).

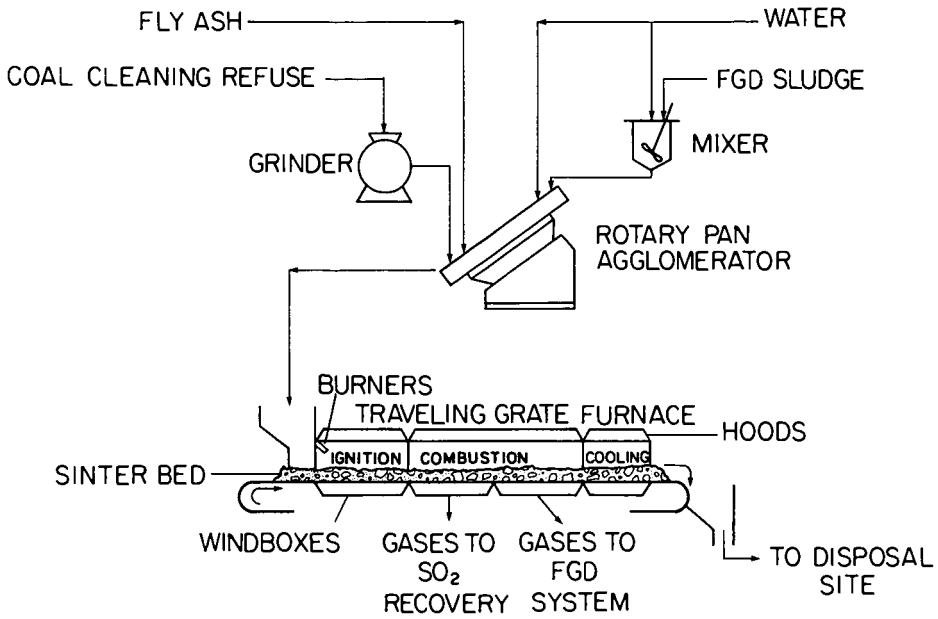

Fig. 1 Schematic flowsheet for the granulation/sintering waste stabilization process.

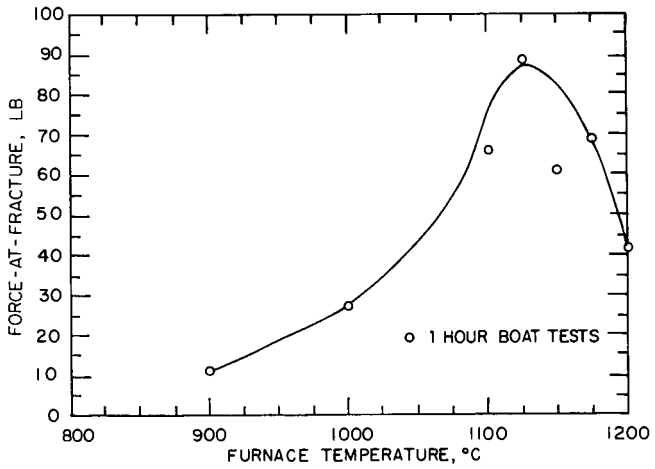

Fig. 2 Force-at-fracture for sintered refuse only granules as a function of small-tube furnace temperature.

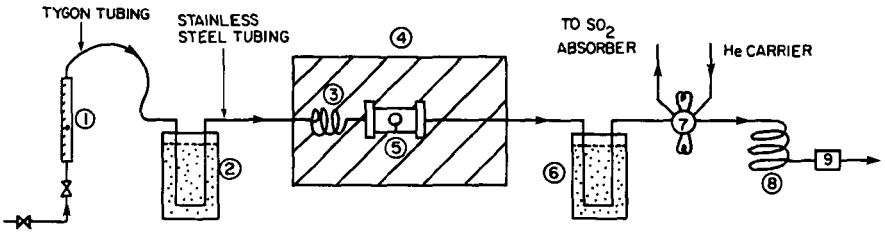

Fig. 3 Schematic flowsheet for the system to measure SO_2 evolution.

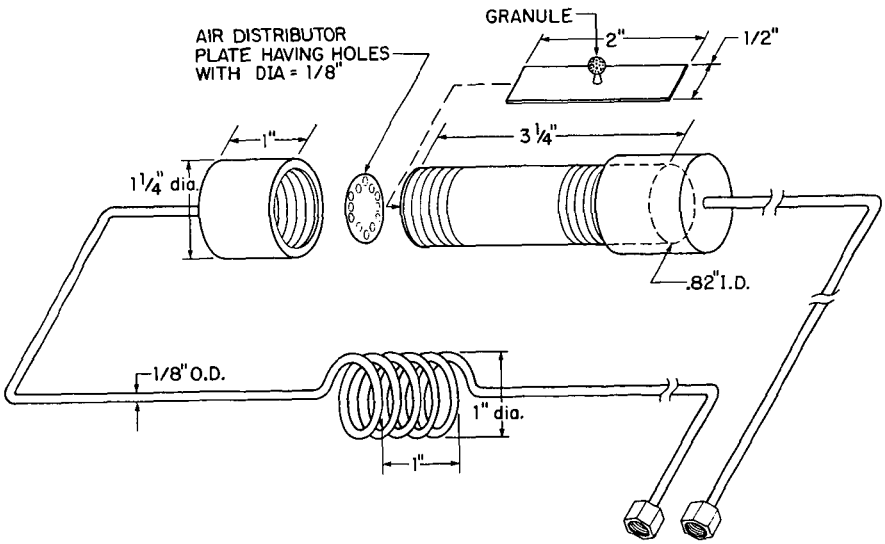

Fig. 4 Microreactor for the combustion/sintering of single granules.